264

.....contributing to man's
understanding of the environment world

SINGLE STATION AND ARRAY METHODS FOR IMPROVED SURFACE WAVE SPECTRAL ESTIMATES

S. S. ALEXANDER
CONSULTANT to the SDL

J. W. LAMBERT
SEISMIC DATA LABORATORY

13 DECEMBER 1971

Prepared for
AIR FORCE TECHNICAL APPLICATIONS CENTER
Washington, D.C.

Under
Project VELA UNIFORM

Sponsored by
ADVANCED RESEARCH PROJECTS AGENCY
Nuclear Monitoring Research Office
ARPA Order No. 1714

TELEDYNE GEOTECH
ALEXANDRIA LABORATORIES

R106

Neither the Advanced Research Projects Agency nor the Air Force Technical Applications Center will be responsible for information contained herein which has been supplied by other organizations or contractors, and this document is subject to later revision as may be necessary. The views and conclusions presented are those of the authors and should not be interpreted as necessarily representing the official policies, either expressed or implied, of the Advanced Research Projects Agency, the Air Force Technical Applications Center, or the U S Government.

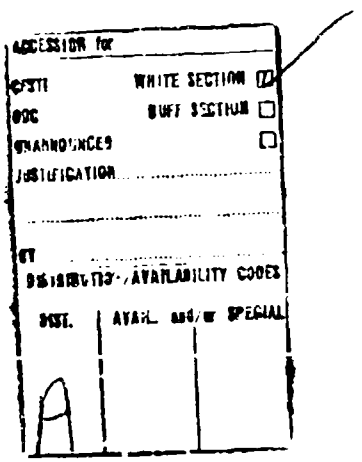

SINGLE STATION AND ARRAY METHODS FOR IMPROVED SURFACE WAVE SPECTRAL ESTIMATES

SEISMIC DATA LABORATORY REPORT NO. 264

AFTAC Project No.:	VELA T/2706
Project Title:	Seismic Data Laboratory
ARPA Order No.:	1714
ARPA Program Code No.:	2F-10
Name of Contractor:	TELEDYNE GEOTECH
Contract No.:	F33657-72-C-0009
Date of Contract:	01 July 1971
Amount of Contract:	$ 1,314,000
Contract Expiration Date:	30 June 1972
Project Manager:	Royal A. Hartenberger (703) 836-7647

P. O. Box 334, Alexandria, Virginia

UNCLASSIFIED
Security Classification

DOCUMENT CONTROL DATA · R&D
(Security classification of title, body of abstract and indexing annotation must be entered when the overall report is classified)

1 ORIGINATING ACTIVITY (Corporate author) TELEDYNE GEOTECH ALEXANDRIA, VIRGINIA	2a REPORT SECURITY CLASSIFICATION Unclassified 2b GROUP

3 REPORT TITLE
SINGLE STATION AND ARRAY METHODS FOR IMPROVED SURFACE WAVE SPECTRAL ESTIMATES

4 DESCRIPTIVE NOTES (Type of report and inclusive dates)
Scientific

5 AUTHOR(S) (Last name, first name, initial)
Alexander, S.S.
Consultant to the Seismic Data Laboratory

Lambert, John W.
Seismic Data Laboratory

6 REPORT DATE 13 December 1971	7a TOTAL NO OF PAGES 104	7b NO OF REFS 3
8a CONTRACT OR GRANT NO. F33657-72-C-0009 b PROJECT NO. VELA T/2706 c ARPA Order No. 1714 d ARPA Program Code No. 2F-10	9a ORIGINATOR'S REPORT NUMBER(S) 264 9b OTHER REPORT NO(S) (Any other numbers that may be assigned this report)	

10 AVAILABILITY/LIMITATION NOTICES
APPROVED FOR PUBLIC RELEASE; DISTRIBUTION UNLIMITED.

11 SUPPLEMENTARY NOTES	12 SPONSORING MILITARY ACTIVITY Advanced Research Projects Agency Nuclear Monitoring Research Office Washington, D.C.

13 ABSTRACT

Combined matched filtering and array summing methods have been developed that yield improved spectral estimates for weak surface waves. Both theoretically and experimentally the best spectral estimates are obtained by first beaming an array of individual matched filtered seismograms and then computing a single noise-corrected spectrum. Spectral results for test cases and actual events are compared using three different techniques. Computer programs implementing these spectral methods have been written which are suitable for routinely processing many events.

14 KEY WORDS

LASA	Surface Waves
Matched Filter	Array Processing
Signal-to-Noise Ratio	

UNCLASSIFIED
Security Classification

ABSTRACT

Combined matched filtering and array summing methods have been developed that yield improved spectral estimates for weak surface waves. Both theoretically and experimentally the best spectral estimates are obtained by first beaming an array of individual matched filtered seismograms and then computing a single noise-corrected spectrum. Spectral results for test cases and actual events are compared using three different techniques. Computer programs implementing these spectral methods have been written which are suitable for routinely processing many events.

TABLE OF CONTENTS

LIST OF FIGURES

LIST OF FIGURES (Cont'd.)

LIST OF FIGURES (Cont'd.)

LIST OF FIGURES (Cont'd.)

LIST OF FIGURES (Cont'd.)

INTRODUCTION

Recent work on surface waves has shown that it is possible to detect weak surface wave signals at teleseismic distances by means of a matched filter operation whereby the long dispersed waveforms are compressed into autocorrelation-like waveforms. In that operation the matched filtered output is the crosscorrelation of a reference signal with the smaller event of interest.

The objective of the present study is to investigate methods for reliably estimating the spectra of weak surface waves in the presence of noise. In particular we attempt to take advantage of the signal enhancement that can be achieved by both matched filtering and array summing. Reliable spectral estimates are important because the spectral differences in surface wave excitation observed for large explosions ($m_b > 5$) and earthquakes of comparable body wave magnitude are expected to exist for very small events also. Moreover, reliable spectral estimates are essential for using the frequency dependence of surface wave radiation patterns as a diagnostic (earthquakes are expected to exhibit frequency dependent radiation patterns while explosions should not).

In this study we have developed new methods of obtaining spectra using both single channel and multichannel processing. For both test cases and actual events we compare the results using these new methods with conventional spectral estimates. As expected, the results are essentially the same for all methods until low signal to noise ratios are encountered (S/N = 2 for the test cases), where the new methods perform more reliably.

Computer programs necessary to obtain spectra for both individual stations and arrays using these methods have been written. Conventional and matched filter spectra are obtained individually and for the array sum. The program has many options which allow one to

use an observed signal as the reference filter, to generate a theoretical reference signal, to adjust a given reference signal for differences in epicentral distance, or to use a chirp filter as the matched filter. In addition, event spectra may be saved on tape so that eventually region-by-region comparisons of surface wave excitation as a function of magnitude, depth, etc. can be obtained routinely.

In the sections which follow we develop the methods, analyze several test cases and present results for actual teleseismic events observed at LASA to illustrate the techniques. An analysis of surface wave spectra for many events for different regions utilizing these techniques will be published in a separate report.

METHODS

The standard method of computation of a power spectral estimate for a signal immersed in noise is to compute the smoothed power spectrum of the time window containing the signal. From this smoothed power spectrum, a noise correction can be subtracted if the noise can be assumed to be random and stationary. This noise correction is obtained from the smoothed power spectrum of a noise sample $n_2(t)$ preceding the signal. That is, if

$$x(t) = s(t) + n_1(t)$$

then

$$\hat{P}_s(\omega) \cong P_x(\omega) - (T_x/T_{n_2})\, P_{n_2}(\omega)$$

or

$$\hat{P}_s(\omega) \approx |X(\omega)|^2 - (T_x/T_{n_2})|N_2(\omega)|^2 \tag{1}$$

$$= S^2(\omega) + 2\,\mathrm{Re}(S(\omega)N_1^*(\omega)) + |N_1(\omega)|^2 - (T_x/T_{n_2})|N_2(\omega)|^2$$

$$\equiv S^2(\omega) + \eta(\omega)$$

where

$x(t)$ = time series consisting of signal, $s(t)$ plus noise, $n_1(t)$

$S^2(\omega)$ = true power spectrum of $s(t)$

$\hat{P}_s(\omega)$ = estimated power spectrum of $s(t)$

$X(\omega)$ = Fourier transform of $x(t)$

$P_x(\omega)$ = power spectrum of $x(t)$

T_x = length of window for $x(t)$

$N_2(\omega)$ = Fourier transform of signal-free noise sample, $n_2(t)$

$P_{n_2}(\omega)$ = power spectrum of $n_2(t)$

T_{n_2} = length of $n_2(t)$ window

$n(\omega)$ = residual noise power representing errors in the noise correction.

If, however, the signal is dispersed and we have some knowledge of the dispersion, as is the case with teleseismic Rayleigh and Love waves, it is possible to make an alternate (improved) estimate of the signal spectrum. By matched filtering the seismogram $x(t)$ with a large reference surface wave signal $y_o(t)$ from the same source region, the signal dispersion is removed, i.e., the signal energy is compressed into a short autocorrelation-like pulse (Alexander and Rabenstine, 1967; Appendix A). The Fourier transform of a short window of this filter output containing the signal, divided by the amplitude response of the reference filter, will give a smoothed spectral estimate of the desired signal $s(t)$. Since the length of the window in the matched filtered output required to include the majority of the signal is significantly shorter than the original dispersed signal length, and since the mean and RMS level of stationary random noise is

unchanged by the matched filtering, the signal power spectrum estimated from this window T_m will have proportionally (T_m/T_x) less noise contamination than that computed directly from the signal window T_x (see Appendix A for discussion of these points). Consequently this approach results in a larger signal to noise ratio, hereafter denoted by $S(\omega)/N(\omega)$, for all frequencies.

The computational procedure used for obtaining the matched filter spectral estimates as well as the conventional estimates is described in Appendix C and shown in the flow chart in Figure 19. Briefly the procedure is as follows:

1. The filter and the time series are Fourier transformed:

$$y_o(t) \rightarrow Y_o(\omega)$$
$$x(t) \rightarrow X(\omega)$$

where $y_o(t)$, the filter, is the large reference surface wave signal (obtained empirically or generated from dispersion curves or a combination of these).

2. The Fourier transform of the time series is multiplied by the complex conjugate of the reference filter's Fourier transform to give the Fourier transform of the matched filtered output:

$$A(\omega) = X(\omega)Y_o^*(\omega)$$

3. This product is transformed back to the time domain:

$$A(\omega) \rightarrow a(t)$$

4. A suitable window of length T_m about the peak in $a(t)$ is selected and Fourier transformed:

$$a_m(t) \rightarrow A_m(\omega)$$

Note that $A_m(\omega)$ will automatically be a smoothed spectral estimate because of the truncation window T_m (Appendix A).

5. This final Fourier transform is corrected for the reference filter response, squared, and corrected for noise just as in the conventional method

$$\hat{P}_s(\omega) = \frac{|A_m(\omega)|^2}{|Y_o(\omega)|^2} - (T_m/T_{n_2})|N_2(\omega)|^2 \qquad (2)$$

In practice it is both convenient and advantageous to use a whitened reference filter such that $|Y_o(\omega)| = 1$ in the frequency band of interest since minima in $Y_o(\omega)$ were found to produce large fluctuations in $\hat{P}_s(\omega)$ by virtue of $A_m(\omega)$ being a smoothed spectral estimate with much less pronounced minima than $Y_o(\omega)$. Another advantage is that the matched filtered signal should be of shorter duration since it is a band-limited impulse rather than an autocorrelation; this property permits use of a shorter signal window. That is, for the whitened case

$$a_w(t) = \int_{-\infty}^{\infty} |S(\omega)| e^{i\omega t} d\omega$$

while for the unwhitened case

$$a(t) = \int_{-\infty}^{\infty} S^2(\omega) e^{i\omega t} d\omega = \int_{-\infty}^{\infty} a_w(\tau) a_w(t+\tau) d\tau.$$

Thus a(t) is approximately twice the duration of $a_w(t)$ since it is the autocorrelation of $a_w(t)$.

The only negative feature of the whitened matched filter is that as a detector it will be less satisfactory than the unwhitened filter. However we are not addressing the detection problem in this paper.

Note that the noise correction in (2) is only T_m/T_x as big as that in equation (1) so that spectra for smaller signals should be recoverable at lower levels than for the direct approach. Also by taking a finite window T_m about the peak we are automatically smoothing the signal spectral estimates. The noise power estimate in (2) will be the same as that in (1) if the noise is random and stationary (Papoulis, 1965 and Appendix A). As will be seen later, this assumption about the noise appears to be warranted for the noise samples encountered in this study.

For the multichannel (array) spectral estimates three different methods were employed each with optional weighting among channels. The first two methods (I and II) consist of summing with weights B_i the individual noise-corrected spectra obtained from equation (1) and from equation (2) respectively. This gives for K channels, suppressing the notation for frequency,

$$\sum_{i=1}^{K} B_i P_{si} / \sum_{i=1}^{K} B_i = \left[\sum_{i=1}^{K} B_i S_i^2 + \sum_{i=1}^{K} B_i \eta_i \right] / \sum_{i=1}^{K} B_i \qquad (3)$$

The weights are typically taken to be inversely proportional to the signal to noise ratio or simply inversely proportional to the noise RMS. If it is assumed that the signal spectrum at every station is the same, equation (3) becomes

$$\sum_{i=1}^{K} B_i P_{si} / \sum_{i=1}^{K} B_i = S^2 + \sum_{i=1}^{K} B_i \eta_i / \sum_{i=1}^{K} B_i = S^2 + \xi \qquad (4)$$

Provided the noise on each channel is random and stationary the expected value of the term $\xi(\omega)$ in equations (3) and (4) is zero since for each η_i we overcorrect for noise as often as we undercorrect in equations (1) and (2). Moreover the variance of $\xi(\omega)$ should decrease with the number of channels, K. Thus the summing will give an improved estimate of $|S(\omega)|^2$ with a variance in the case of uniform weighting given by

$$\frac{2|N(\omega)|^4}{K}\left[1 + \frac{|S(\omega)|^2}{|N(\omega)|^2}\right]$$

(see Appendix B).

The third technique (Method III) is to beam the individual matched filtered time series and compute the spectrum of the matched filtered signal on the sum trace using the same procedure for extracting signal spectra as used for the individual matched filtered traces (equation 2). In this case the S/N ratio on the sum trace (time domain) is approximately $(K^{1/2})$ greater than on individual channels, resulting directly in a better spectral estimate of $S^2(\omega)$ with a variance in the case of uniform weighting given by

$$\frac{2|N(\omega)|^4}{K^2}\left[1 + K\,\frac{|S(\omega)|^2}{|N(\omega)|^2}\right]$$

(see Appendix B).

Since this variance is always smaller than for the other two methods, especially at small signal to noise ratios, values from Method III should be best to use. As before, the window containing the signal remains short so the noise contribution is minimum even before a correction for it is made. Also, it is likely that the noise on the sum trace will be more nearly stationary than on individual channels so that the noise correction will be more reliable. This technique has the further advantage that only one spectral calculation is required whereas the first two methods each require determination of K individual spectra. This latter advantage represents a very significant saving in computer time and makes "on-line" spectral calculations feasible to consider in an operational system.

These methods described above were programmed for use on digital data. The computational procedures are discussed in Appendix C and the many options available are explained. The flow chart shown in Figure 19 summarizes the program. Basically the program incorporates the spectral methods (I, II, III) into a previously developed program (Alexander and Rabenstine, 1967) for matched filtering and array processing of matched filtered seismograms.

Note that if the signal is the same on each channel, Method III is equivalent to beaming with a constant velocity, and then match filtering the beam, windowing, and transforming to get the spectra. This would further reduce the calculations for Method III by a factor of 1/K. The size of error incurred at LASA by this approach is unknown and should be investigated before a real-time system is implemented.

Each of the above techniques should yield improved estimates of the signal spectrum as discussed in Appendix B, with the matched filter beam (Method III) preferred. However it is important to investigate which approach is the most effective in practice. We have attempted to do this empirically by analyzing test cases of actual noise where the signal spectrum is known exactly and by analyzing actual events recorded at LASA. The results of these tests are presented in the next sections.

TEST CASES

Test cases were generated by imbedding a set of synthetic Rayleigh waves into real noise at various signal-to-noise ratios.

The synthetic signals were constructed (Program NEWSYN) to correspond to surface wave signals that would be received at the nine LASA long period sites (A, E and F rings in Figure 1A) from an epicenter in the Greenland Sea (73.4N, 6.8E). With the instrument amplitude response (Figure 1B) included all had identical power spectra as shown in Figure 2A and phase spectra as determined from the appropriate epicentral distances (great circle path) and the dispersion curve shown in Figure 2B. These synthetic seismograms are shown in Figure 3.

The noise was real LP noise recorded digitally at 5 samples per second at the LASA on March 30, 1967 and reduced to 1 sample per second. Typical normalized power spectra of these noise samples are shown in Figure 4A.

In Appendix A it is shown that if the noise is random and stationary, matched filtering with a whitened reference filter should not change the noise spectrum on the matched filtered output. (It also follows that the mean and RMS in the time domain should remain the same.) Figure 4B shows a comparison of the noise power spectra before (solid line) and after (dashed line) matched filtering at LASA stations. A 30 minute noise window was used throughout. It is clear that for frequencies lower than about .05 Hz the power spectra are essentially unchanged in both level and shape. The shape remains similar at the shorter periods but the level may differ by up to a factor of 2. The results shown in Figure 4B are typical of the other LASA channels and other noise cases tested. We conclude, therefore, that at LASA the noise on each channel is sufficiently random and stationary for frequencies below .05 Hz that matched filtering does not appreciably change the noise spectrum. However for higher

frequencies the stationarity assumption appears to be only approximately valid.

Also shown in Figure 4B is the sum trace noise spectrum for the 3 channels shown; its power spectral level is approximately 3 times smaller than the individual channel levels. This result implies that most of the LP noise is not correlated from station to station at LASA. Alexander and Rabenstine, (1967), reached a similar conclusion, and all the results in this study using more stations give noise reductions on summing appropriate to uncorrelated noise, provided the stations are 20-25 km or more apart.

Figure 4C shows the effect of window length on the matched filter spectral estimates for the signal spectrum in the synthetic test cases. The window lengths are shown at the top centered on the matched filtered signal (whitened reference) which has a true normalized spectrum given by the dashed curve in the power spectrum plots in the same Figure. It is evident that a window of 300 seconds length or more does not significantly distort the signal spectrum in this case, whereas the 50 and 100 second windows result in over-smoothing. Thus the shortest window consistent with suitably undistorted signal spectra is 300 seconds; this window length was used throughout the analysis of test cases.

Test case seismograms

The signal to noise ratio used in preparing the test cases were defined as 1/2 the peak to peak value of the detrended signal to the RMS amplitude of the detrended noise. This gave a value of input signal to noise which was probably conservative (too high) by 3 db since the 1/2 peak to peak value is typically about 1.4 times the RMS amplitude of the signal (assuming a long dispersed signal waveform). However, this definition of S/N allows comparison with

previous studies (Alexander and Rabenstine, SDL Report Nos. 175 and 194, 1967) where a similar definition has been used. Figure 5A shows a synthetic case where the signal is mixed with the noise at S/N = 8. The signal, the noise, signal + noise, and the matched filtered traces are plotted with a common vertical scale to illuustrate graphically the meaning of S/N = 8 as defined above and to show that the matched filtering does not change the RMS noise level. The whitened matched filter option was used in this case and throughout the remainder of this study, because as discussed earlier it generally produces signals of shorter duration than the autocorrelation resulting from standard matched filtering (i.e. direct cross-correlation of reference signal with the seismogram), and because we found that minima in the reference signal spectrum caused fluctuations in the estimate of the weak signal spectrum. These spurious fluctuations are due both to noise "filling up" any actual holes in the weak signal spectrum and to the inherent smoothing from using a short signal window on the matched filter output (Figure 4C).

Figures 5B and 5C show the individual input traces for S/N=8 and the corresponding matched filtered outputs. The measured S/N on each matched filtered trace is indicated. Figure 5C also shows the phased sum (beam) of nine individual matched filtered outputs. Note that the matched filtering results in individual S/N ratio gains in the time domain of slightly over two while the sum of nine elements results in a factor of over seven S/N ratio gain above the original individual inputs. These results are consistent with the earlier results of Alexander and Rabenstine, (1967) for LASA.

Figure 6A shows the test case synthesis for S/N = 4 again with all traces plotted with a common amplitude scale. Figures 6B and 6C show the individual input traces and matched filtered outputs.

Figure 6C shows the sum of nine matched filtered outputs. As expected we achieve somewhat over a factor of 2 S/N gain on matched filtered outputs and about a factor of seven on the sum.

Figure 7A shows the test case synthesis for S/N = 2. Here the original signal is not evident in the noise whereas it is in the matched filtered output. Figures 7B and 7C show the input traces and matched filtered traces for this case. In most instances the signal is evident on the individual matched filtered traces but is nearly at the threshold where many false alarms would occur in a search for signals at this level. The array sum of nine elements, however, has an unmistakeable signal present (bottom trace on 7C).

Figure 8A shows the test case synthesis for S/N = 1. In this case the signal is not evident on the signal-to-noise trace nor is it evident on the matched filtered output. Thus, the threshhold for single channel detection (assuming identical signals) is between that shown in Figure 7A and that shown in 8A. Figures 8B and 8C verify this conclusion but show that the threshold for detection is below S/N = 1 for nine LASA channels since the signal on the sum trace in Figure 8C is unmistakeable. We further verified this empirical result by imbedding the signal at various positions and repeating the analysis.

In principle one expects individual (time domain) gains in S/N resulting from matched filtering to be proportional to the time-bandwidth product of the original signal and the gain on summing to be $\sqrt{K}$ where K is the number of sensors, so the reader is cautioned to generalize the above results to other signals and numbers of stations with these constraints in mind.

Test case spectra

We now turn to a discussion of the various spectral estimates obtained from analyzing these test cases. By comparing typical single

station spectral estimates and their sums with the test seismograms discussed above one can begin to get a feel for what spectral estimates to believe vis à vis the actual seismograms from which they were derived.

Figure 9 shows spectra for five of nine individual LASA stations as indicated for the S/N = 8 case (see corresponding seismograms in Figures 5B and 5C). The dashed black line is the input spectrum, the black line is the noise-corrected spectrum obtained by conventional analysis (equation (1)), and the red line is the noise-corrected matched filter signal spectrum (equation (2)). For the sum the dashed line shows the actual spectrum, the black line the sum of nine conventionally computed spectra (equation (3)), the solid red line the sum of the nine individual matched filter spectra, and the dashed red line the noise-corrected spectrum from the matched filtered sum trace shown in Figure 5C. The corresponding noise power spectra for these individual channels are shown in Figure 4A. It is clear that the conventional and matched filter estimates are very similar to one another and that the sums all give much better representation of the actual spectrum than do individual ones even for this relatively large S/N case. As indicated earlier the matched filter spectrum should be a smoothed version of the actual signal spectrum and this effect can be seen by comparing the solid red and black lines in Figure 9. The signal window used was 300 seconds. The conclusion is that at this S/N level the methods are all comparable in performance and give good spectral estimates, especially the sums.

Figure 10 shows the same display as does Figure 9 but for S/N=4 (see Figures 6B and 6C for corresponding seismograms). In this case the individual matched filter spectra (solid red lines) are as good or better than the conventional ones (solid black lines) and the summed spectra are better than any individual spectral estimate. Again, the spectrum from the matched filter sum (Figure 6C) is the best in this case as is expected theoretically (Appendix B). Thus at about

S/N = 4 the matched filter spectra begin to give more reliable spectral estimates than do the conventional ones, although the conventional sum is still quite acceptable in level and shape.

Figure 11 shows the same display as Figures 9 and 10 but for S/N = 2 (see Figures 7B and 7C for corresponding seismograms). In this case the individual spectra are all significantly in error, although the matched filter spectra define the location of the actual spectral peak somewhat more reliably than do the conventional estimates. However, sums of the individual matched filter spectra and the spectrum from the matched filter sum trace (Figure 7C) give reliable spectral values and shape around the peak and give reasonably accurate signal levels at the higher frequencies. The sum of conventional spectra (solid black line) is significantly in error. Again, the best result comes from the matched filter sum trace.

Finally Figure 12 shows the results for S/N = 1 (see Figures 8B and 8C for the corresponding seismograms). In this case none of the individual spectra comes close to representing the actual spectrum. Only the sum of individual matched filter spectra (solid red line) and the spectrum of the matched filter sum trace (Figure 8C) produce reasonable spectral estimates, and even then the spectral shape is significantly distorted, except at the peak.

The performance of the various methods can be assessed by comparing quantitatively the array estimates obtained in the test cases with the actual signal power in the array sums. Figure 13A shows the variance i.e. (estimate - actual)^2 as a function of frequency for S/N = 4 using nine LASA elements (see Figure 10 for the corresponding spectral estimates). Clearly the most accurate result (smallest variance) overall is given by Method III and the least accurate by Method I, with Method II between them but still much better than Method I. Figure 13B shows the variance with frequency for S/N = 2. (See Figure 11 for the corresponding spectral estimates.) Finally Figure 13C shows the variance with frequency

for S/N = 1. (See Figure 12 for the corresponding spectral estimates.) Method III is consistently the most accurate in each instance. However, as expected, Method II is also much better than Method I because the noise power is smaller by the ratio of the respective window lengths taken. These results are in accord with what is expected from the simplified theory given in Appendix B. There it is shown that Method III is the most accurate and should get progressively better than the other sums as the S/N decreases.

Since the slowly varying signal power spectrum was normalized to its maximum and kept fixed for all S/N cases the square root of the variance values times 100 represents approximately the percentage error in the spectral estimates in each case. Thus from Figures 13A, B, C it is clear that Method I breaks down (i.e. errors of over 100 percent at some frequencies) between S/N = 4 and S/N = 2; Method II breaks down between S/N = 2 and S/N = 1; on the other hand Method III at S/N = 1 has a maximum error for the entire frequency band of about 70 percent and an error at the peak of the signal of only 10 percent (variance of 1 percent). It must be cautioned that these numerical results apply only to the particular test case signals and noise samples used with sums over nine LASA elements. Therefore, they cannot be taken as representative of the errors expected in general from applying these techniques, although by design the test cases should be realistic for signals from the Greenland Sea area observed at LASA.

Thus the practical threshhold for the spectral methods considered here is between S/N of 1 and 2 for nine LASA channels. The best estimator both theoretically and observationally seems to be the noise-corrected spectrum of the matched filter sum trace signal (Method III). Certainly it is consistently at least

as good as either of the other sums. This is an important finding, because arrays such as LASA or even larger continental sized arrays can be used to obtain reliable spectra for weak events without having to compute the individual station spectra.

Again it must be stressed that this particular threshhold S/N applies for LASA (nine elements) for a particular signal duration and bandwidth. While this case may be roughly representative of teleseismic Rayleigh waves received at LASA an empirical threshhold test similar to that described above should be carried out for reference events from each source region of interest. However, we still can conclude that this experiment has demonstrated that reliable spectra for realistic weak surface wave signals can be obtained using the array methods discussed above, and that Method III is prefererable to use from the standpoint of both accuracy and economy in processing.

APPLICATION TO ACTUAL EVENTS

Using the methods presented earlier and the results of the test cases, actual events were analyzed and the three spectral estimates compared. We will discuss only two events in detail here because a separate report will be published presenting many observed spectra for various regions.

Epicenter data for the events used are given in Table 1.

For the Greenland Sea region Figures 14A, 14B, and 14C show the reference event, the input trace, and the matched filtered output respectively for each of nine LASA stations (Z component) in the D, E, and F rings. Figure 14C also shows the sum trace. Each trace is normalized to its maximum value in Figures 14A-C. Because the noise RMS is unchanged by matched filtering, the apparent reduction in noise level shown for individual stations in this figure is a measure of the minimum S/N gain achieved in each case. The matched filtered traces' S/N levels are between those for the test cases at S/N = 4 and S/N = 2 (Figures 6C and 7C respectively) or approximately at S/N = 3. Thus the spectra obtained by each of the three methods should be comparable in accuracy to those for the test cases at S/N = 4 and S/N = 2 (Figures 10 and 11).

Figures 15A, 15B, and 15C show spectral results for three of the nine individual LASA channels. Figures 14A, 14B, and 14C show the corresponding time series. In each case we show the reference event spectrum, the conventional S + N spectrum, the noise spectrum, the MF spectrum (S + N), and the noise-corrected conventional and MF spectra. Since the instrument responses are nominally the same for all the LASA sites (Figure 1B) and unchanged from event to event we do not need to make instrument corrections to obtain valid comparisons of the spectral estimates. Both the conventional and matched filtered results at the single stations give very similar spectra in both level and shape, with the matched filtered spectra smoother, as

expected. Note the similarity in spectral shape between the reference event spectrum and the smaller event spectrum even though the signal power everywhere differs by a factor of over 100 (and surface wave magnitude by more than 1 unit as compared with the USC&GS body-wave magnitudes (Table I) which differ by only .3 units, at 4.9 vs 4.6. This remarkable similarity in spectral shape implies that the source mechanism for both events was essentially the same. This particular pair of events also illustrates the importance of using a rather broad frequency band for estimating surface wave magnitude. From Figures 15A, 15B, and 15C the signal power at 20 seconds period where conventional surface wave magnitudes are determined is almost an order of magnitude smaller than the peak power at around 30 seconds period. Also the noise contamination is greatest at around 20 seconds period (Figures 15A, B and C).

Figure 15D compares the different array summed spectra for the A, E, and F rings (nine elements) at LASA for the small Greenland Sea event just discussed. It is clear that all three methods give essentially the same signal power estimates. By analogy with the corresponding S/N test case (Figures 9 and 10) we conclude that these are reliable spectral determinations. Also the consistency among the three different estimates of the spectrum suggest that it is a reliable result.

It is important to note that for this real case the previous conclusion that Method III is the best to use is supported, because the single estimate from the matched filter beam trace is very nearly the same as that produced by the other two array methods, and requires less computing time.

For the Yunnan events in Table I we show in Figures 16A, 16B, and 16C the reference event (23 September 1966) the input trace for 29 March 1967 and the matched filtered output respectively for each of nine LASA stations in the AO, D, E, and F rings. Figure 16C also shows the matched filtered sum trace. Each trace is normalized to its maximum value in Figures 16A, B and C. Because the noise RMS is

unchanged by matched filtering the apparent reduction in noise level in each case is a measure of the minimum S/N gain achieved just as in the Greenland Sea event discussed above. The matched filtered traces S/N levels are between those for the test case at S/N = 4 and S/N = 2 (Figures 6C and 7C respectively) but somewhat closer to the S/N = 4 case. Thus the spectra obtained by each of the three methods should be comparable in accuracy to those for the test cases at S/N = 4 and S/N = 2 (Figures 10 and 11) but closer to the case in Figure 10.

Figures 17A, 17B, and 17C show the spectral results for three of the LASA stations used for the Yunnan event (refer to Figures 16A, 16B, and 16C for the corresponding time series). These are typical of the single-station results for this event. As before we show in each case the reference event spectrum, the conventional S + N spectrum, the noise spectrum, the MF spectrum S + N, and the noise-corrected conventional and MF spectra. Again the conventional and matched filtered results at the single stations are very similar in both level and shape, with the matched filter spectra somewhat smoother as expected from theory and the test cases at S/N = 4. In contrast to the Greenland Sea events discussed above the small event and the reference event spectra match only approximately in shape with the smaller event enriched in higher frequencies compared to the reference. Also there appears to be somewhat more variability in shape and level from station to station over LASA for the Yunnan pair as compared to the Greenland Sea pair (Figures 15A, B, and C); however the shapes and levels are still not greatly different from station to station.

Figures 17D compares the different array summed spectra using Methods I, II, and III on channels at LASA for the small Yunnan event (Table I). It is clear that all three methods give essentially the same signal power estimates. By analogy with the corresponding S/N

test case (Figure 9) we conclude that these are reliable spectral determinations comparable in accuracy or better than the estimates for the small Greenland sea event of 18 November 1966 (Table 1 and Figure 15D) discussed earlier. Again the consistency among all the estimates further suggests that the spectra are reliable. Also we emphasize that the single estimate from the matched filtered beam trace (Method III) is in excellent agreement with the other spectral estimates for this real case. This is to be expected theoretically and by analogy with results for the test cases at S/N ≈ 4. Therefore our conclusion that Method III is preferable to use operationally because of the computational savings seems to hold in practice.

While the two actual events discussed hardly allows us to generalize we have demonstrated that reliable spectra can readily be obtained teleseismically using any of the three methods (I, II, or III) for events of m_b approaching 4.5. By comparison with the test cases we can infer that Method III should give reasonably good spectral estimates at S/N ratios approaching 1 (assuming a nine element array) at LASA so a reasonable expected threshhold would be well below $m_b = 4.5$ if the examples used here are at all typical. Use of more than nine elements in the array will lower the threshhold still more. This question of threshhold for spectral determinations will be deferred to a following report now in preparation summarizing spectral results for many different events and different source regions.

CONCLUSIONS

Based on the findings of this investigation we conclude that:

1. Reliable signal spectra can be obtained down to values of S/N ratio approaching unity by combined use of matched filtering and array processing of 9 LASA channels. In principle the threshold can be further lowered simply by using more sensors.

2. The "best" spectral estimator both theoretically and experimentally consists of first beaming individual matched filtered seismograms and then computing a single noise-corrected spectrum from this beamed trace. This result is extremely important from a practical standpoint since signficant computing time is saved by having to compute only one noise-corrected spectrum.

3. It is feasible to consider "on line" spectral calculations since only the matched filtered beams are required using the techniques developed here.

4. A signal window of about 300 seconds on the matched filtered trace was shown to be a good practical length to use so as to preserve spectral detail of signals in the 15-50 second period range. At the same time the 300 second window reduces the total noise contamination compared to signal windows required for long, dispersed wave trains.

5. Using the techniques and computer programs developed in this study surface wave spectra can be routinely obtained and saved for many events from source regions of interest.

6. It is both desirable and convenient to use whitened reference signals because (a) the resulting time domain signals (band limited impulses) are of shorter duration than cross correlations resulting from standard matched filtering thus allowing use of shorter signal windows and (b) spurious peaks in the weak signal spectral estimates resulting from minima in the reference signal spectrum are avoided.

REFERENCES

Alexander, S.S. and Rabenstine, D.B., 1967, Detection of surface waves from small events at teleseismic distances, Seismic Data Laboratory Report No. 175, Teledyne Geotech.

Alexander, S.S. and Rabenstine, D.B., Rayleigh wave signal to noise enhancement for a small teleseism using LASA, LRSM, and observatory stations, Seismic Data Laboratory Report No. 194, Teledyne Geotech.

Papoulis, A., 1965, Probability, random variables and stochastic processes, McGraw-Hill Book Company.

ACKNOWLEDGEMENTS

The authors gratefully acknowledge the valuable help of Dr. Robert Shumway in the statistical aspects of this study. Discussions with various members of the Seismic Data Laboratory research staff aided us greatly in other aspects of this investigation. Also we especially thank Mr. D.B. Rabenstine who participated in the early phases of this work and contributed significantly to the computational programs presented in this report.

TABLE I

USC&GS Epicenter Data

DATE	ORIGIN TIME (GMT)	LATITUDE	LONGITUDE	AREA	DEPTH (KM)	MAGNITUDE
18 Nov 66	18:07:54.0	73.4N	6.8E	Greenland Sea	33	4.6
18 Nov 66	18:48:43.9	73.4N	6.8E	Greenland Sea	33	4.9*
28 Sep 66	14:00:22.9	27.4N	100.1E	Yunnan, China	33	6.2*
29 Mar 67	06:53:10.8	27.3N	100.1E	Yunnan, China	33	4.9

*Reference event used as matched filter

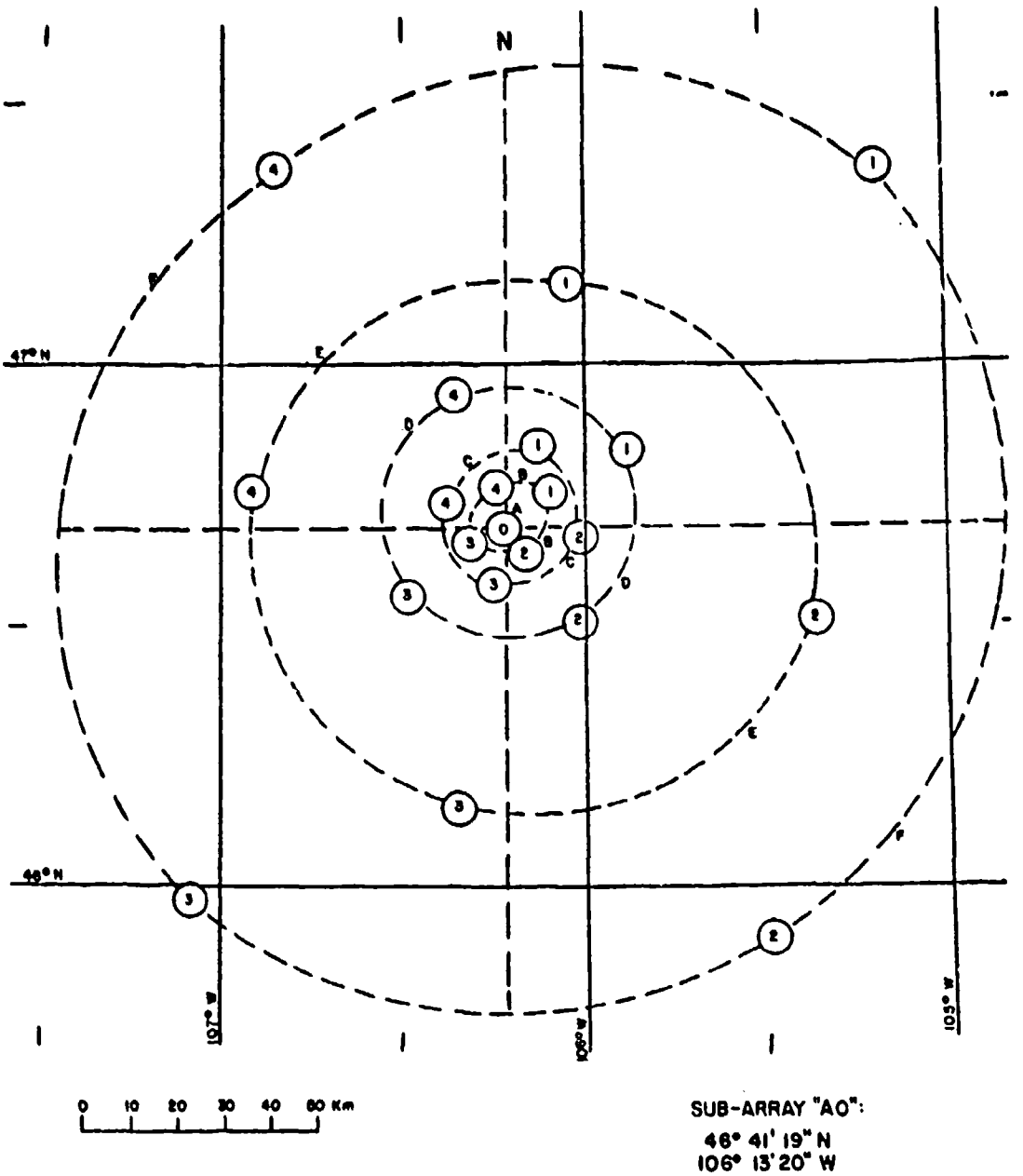

Figure 1A. Configuration of the Large Aperture Seismic Array in Montana.

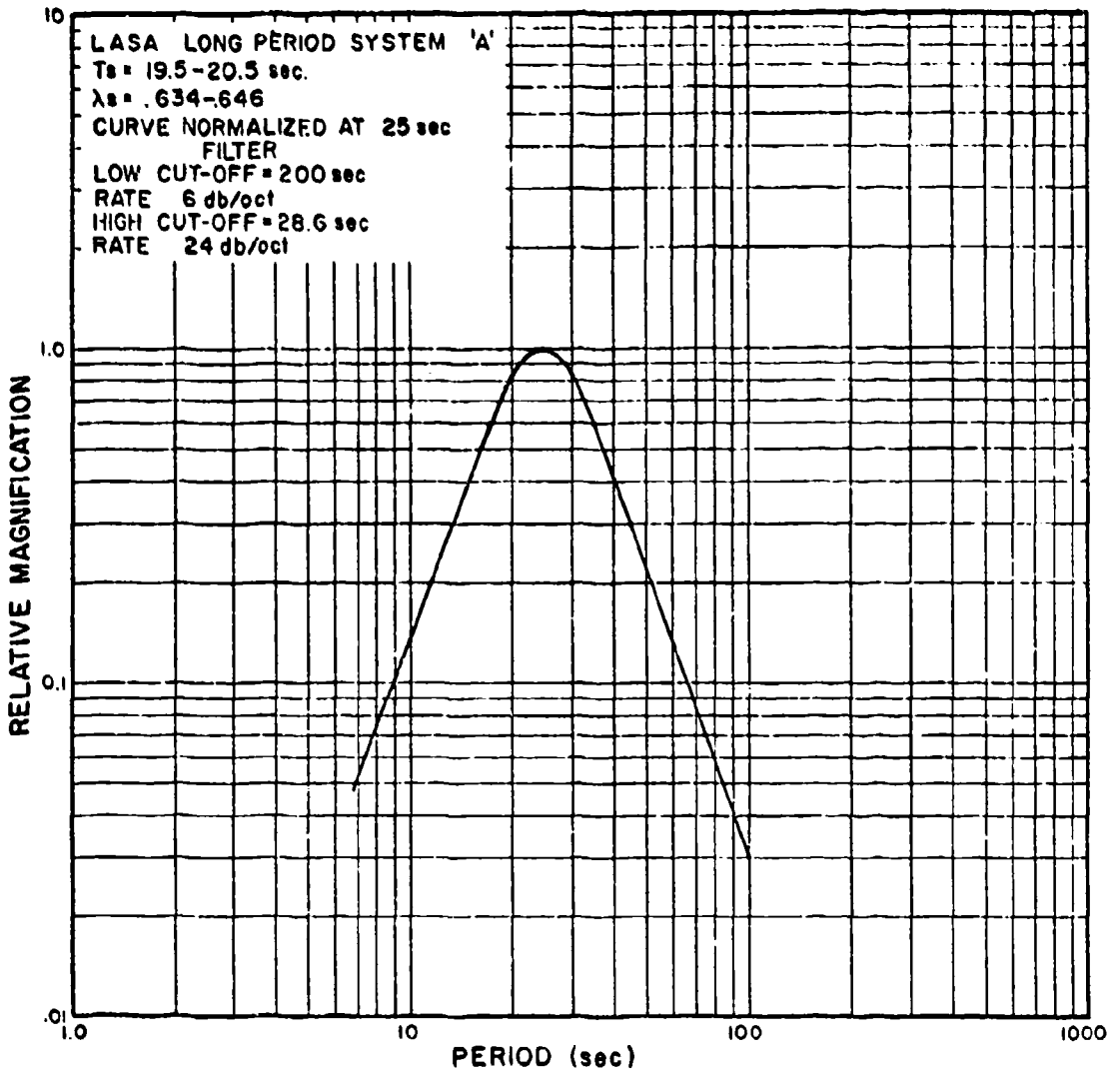

Figure 1B. LASA long period system "A" response.

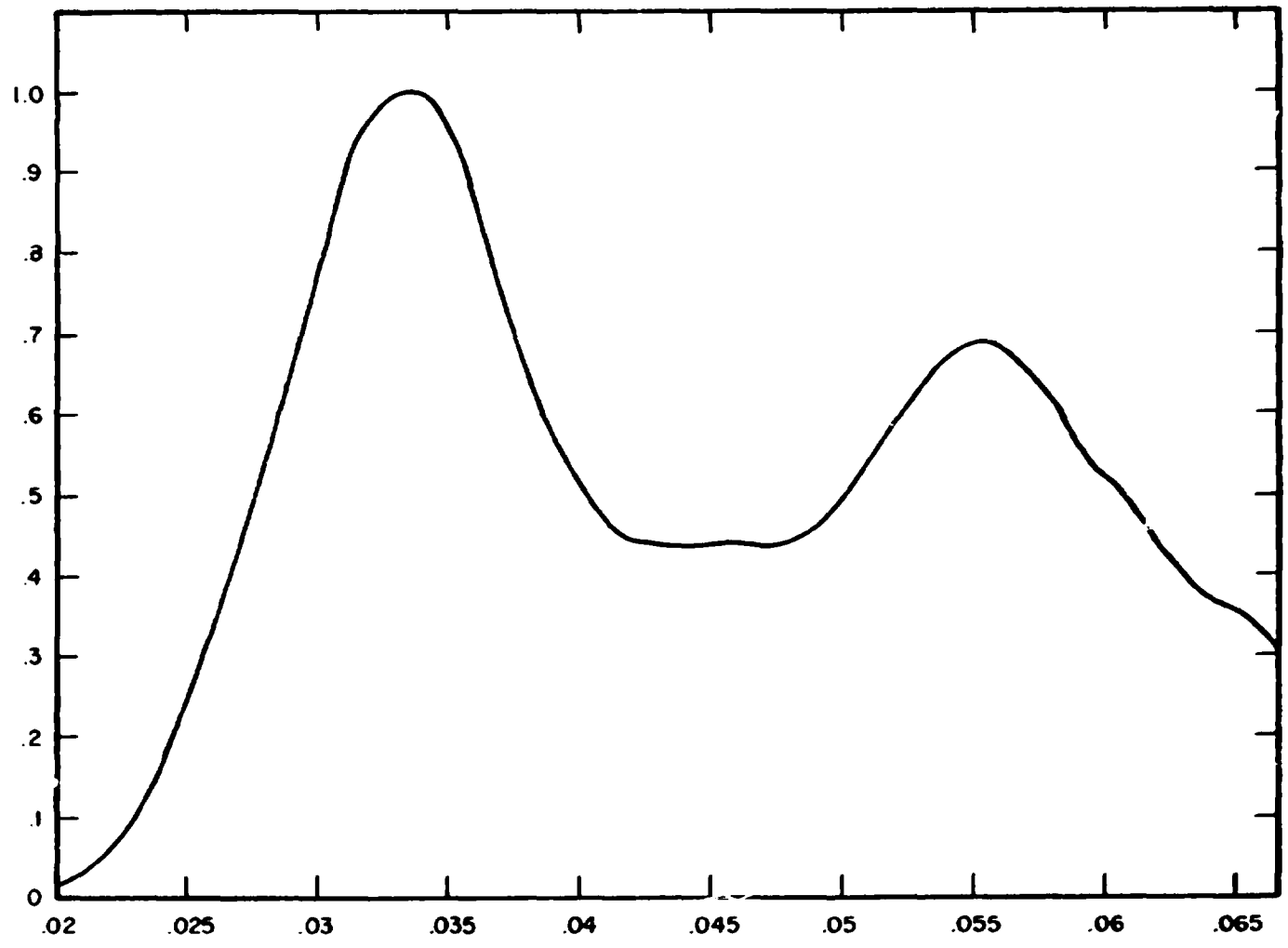

Figure 2A. Normalized power spectrum of synthetic signals computed for the LASA, A, E, and F rings.

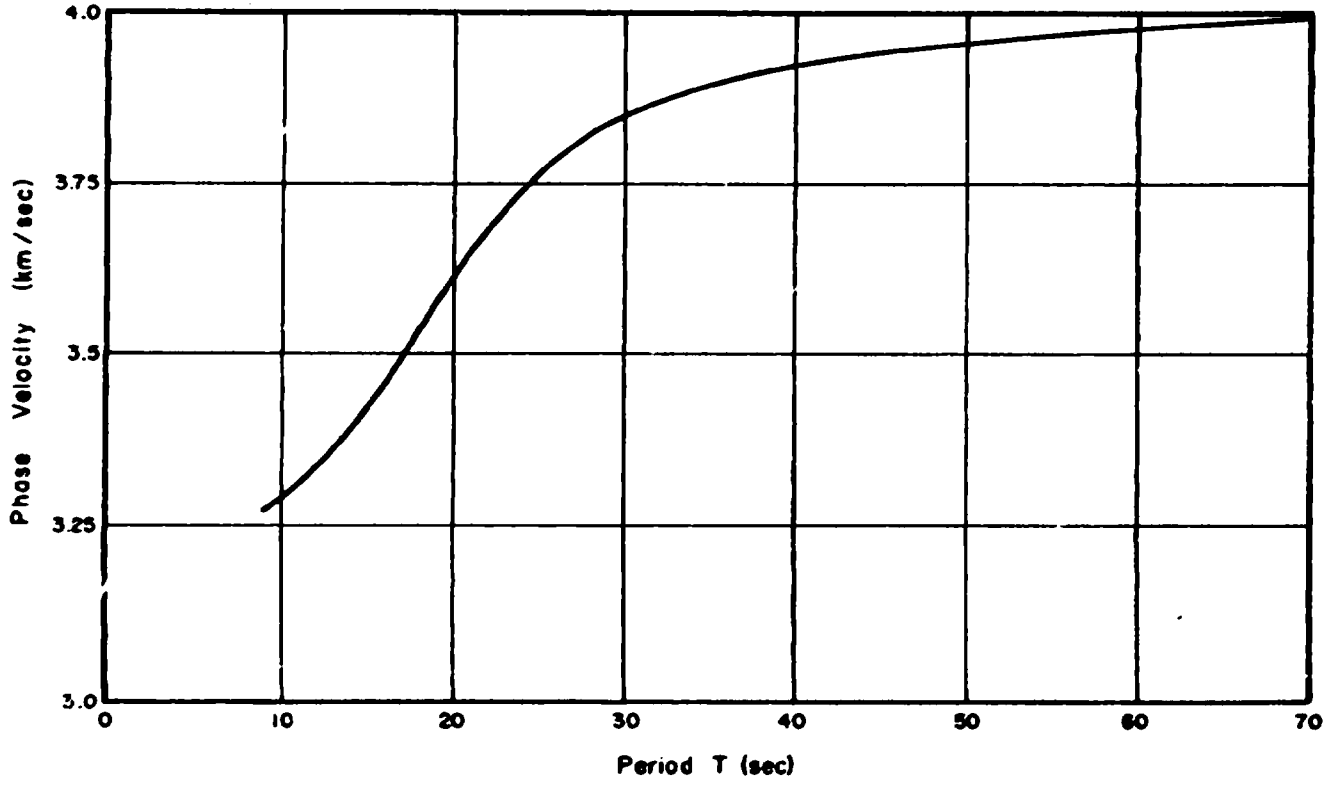

Figure 2B. Phase velocity dispersion used to compute synthetic seismograms for the LASA A, E, and F rings.

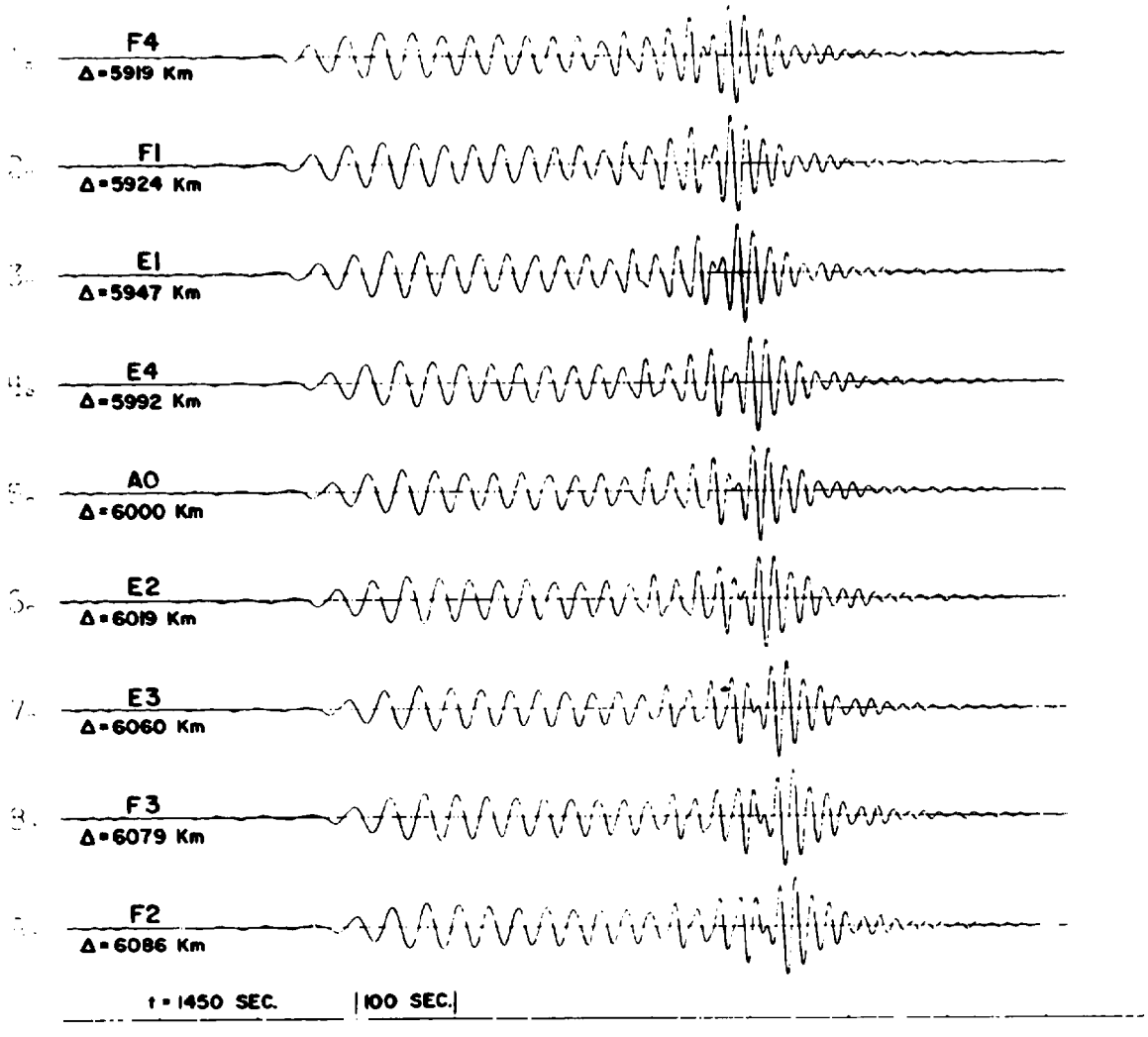

Figure 3. Synthetic signals used as reference filters for the LASA A, E, and F rings.

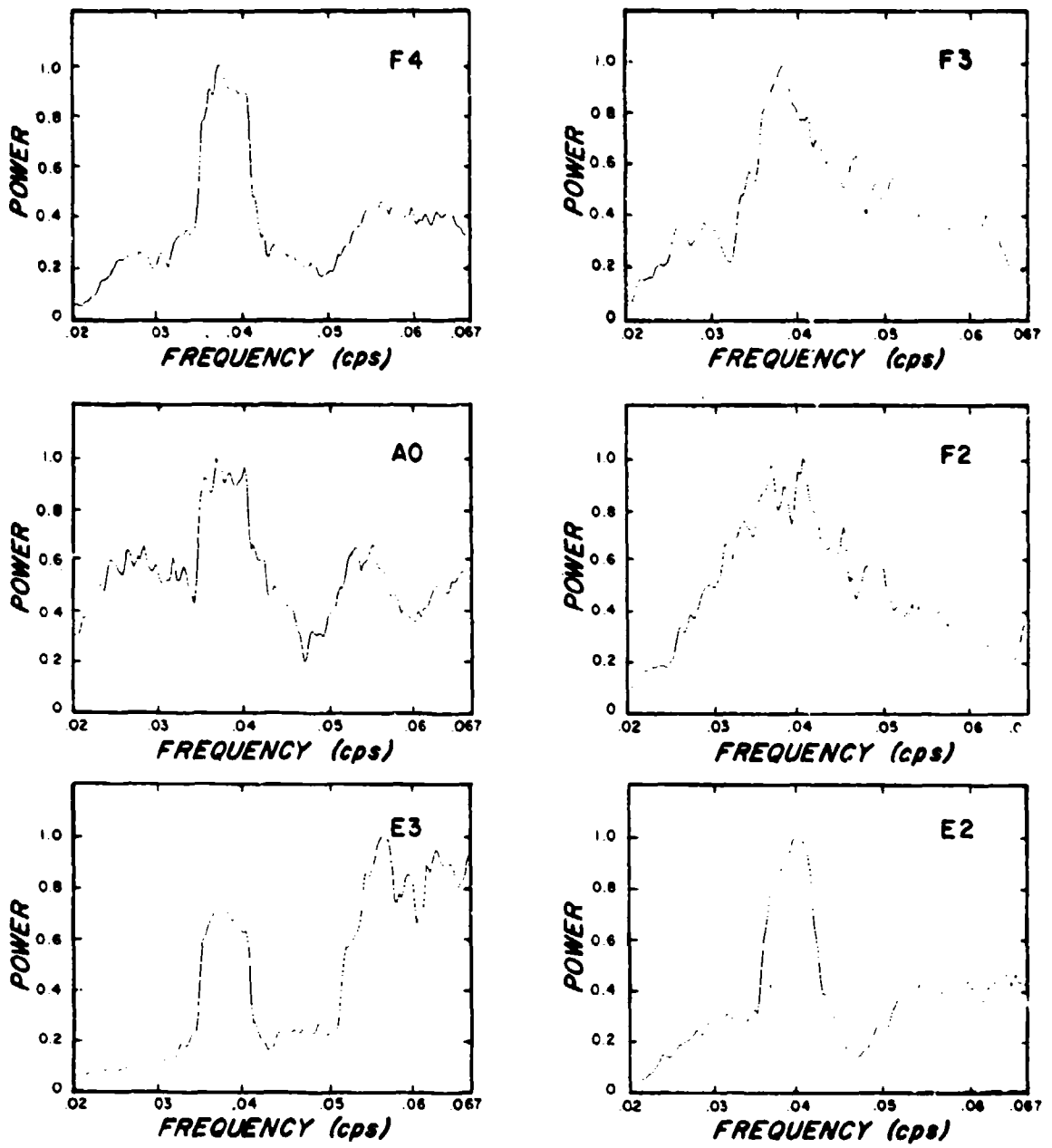

Figure 4A. Typical normalized noise power spectra at six LASA stations for a 30 minute noise sample on 30 March 1967.

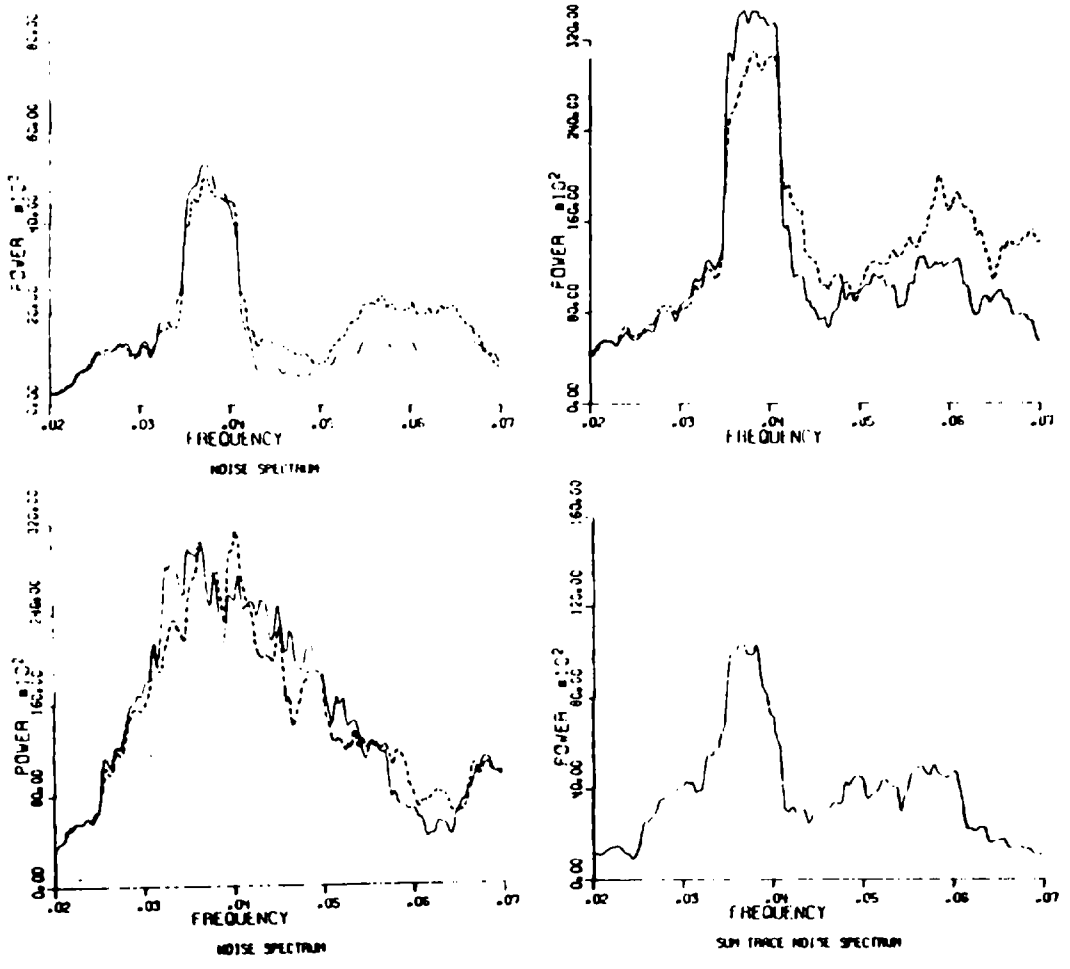

Figure 4B. Comparison of directly computed noise power spectra and noise power spectra from the matched filtered output at three LASA stations.

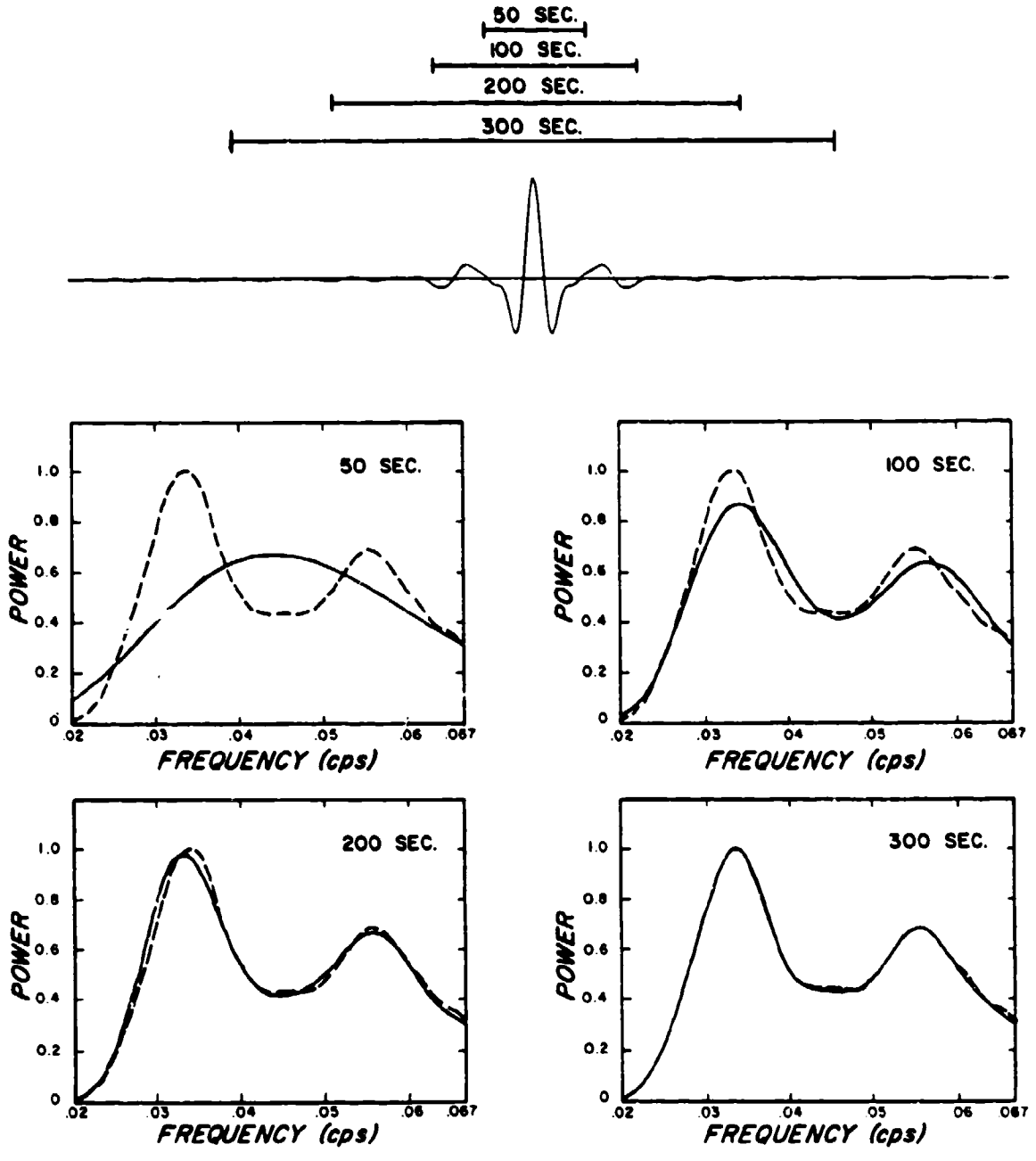

Figure 4C. Effect of window length on matched filtered signal spectral estimates.

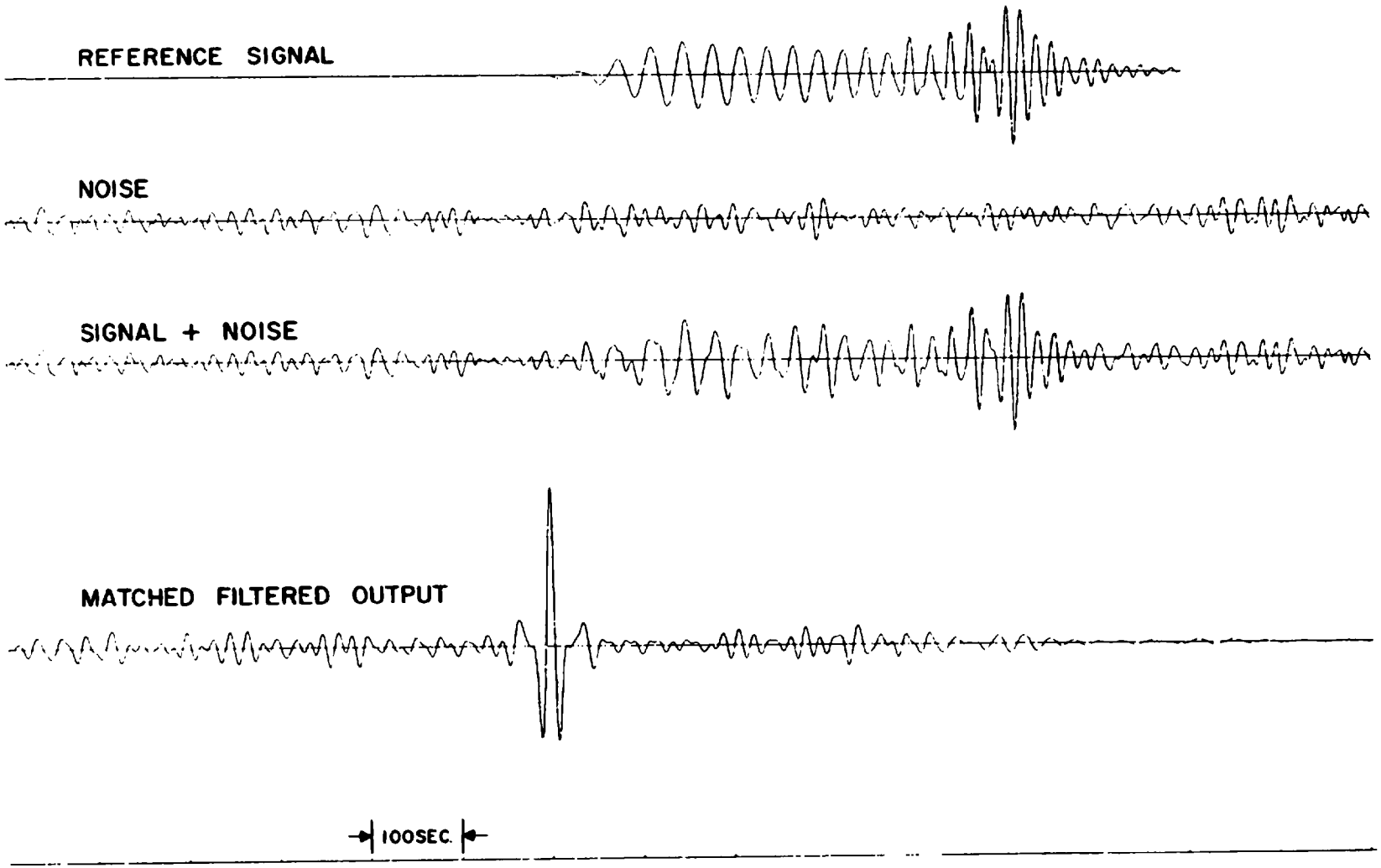

Figure 5A. Typical synthetic test case normalized to noise RMS showing to scale the mixing of signal and noise and the matched filtered output for S/N = 8.

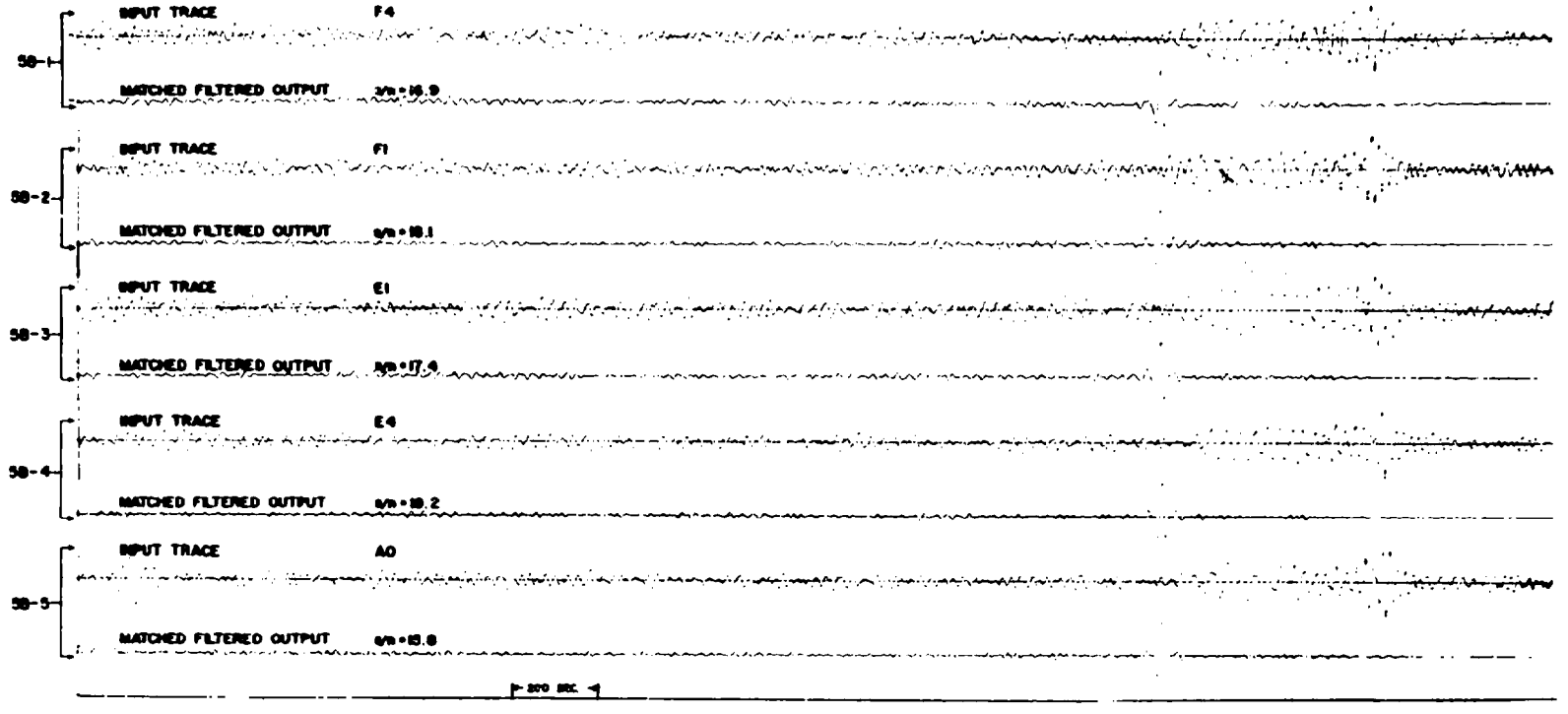

Figure 5B. Typical synthetic test case showing input traces and matched filtered outputs normalized to peak amplitude for four LASA stations. S/N = 8.

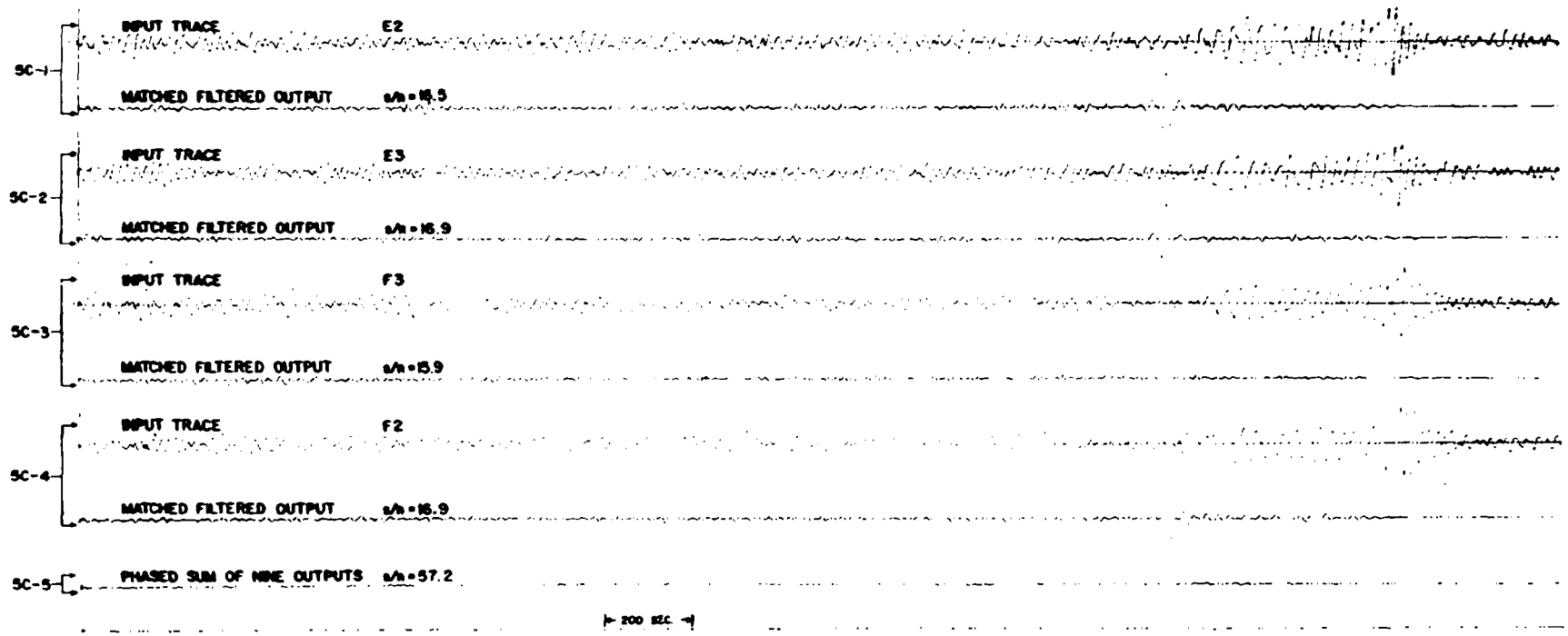

Figure 5C. Typical synthetic test case showing input traces and matched filtered outputs normalized to peak amplitude for four LASA stations and the phased sum trace of nine matched filtered outputs. S/N = 8.

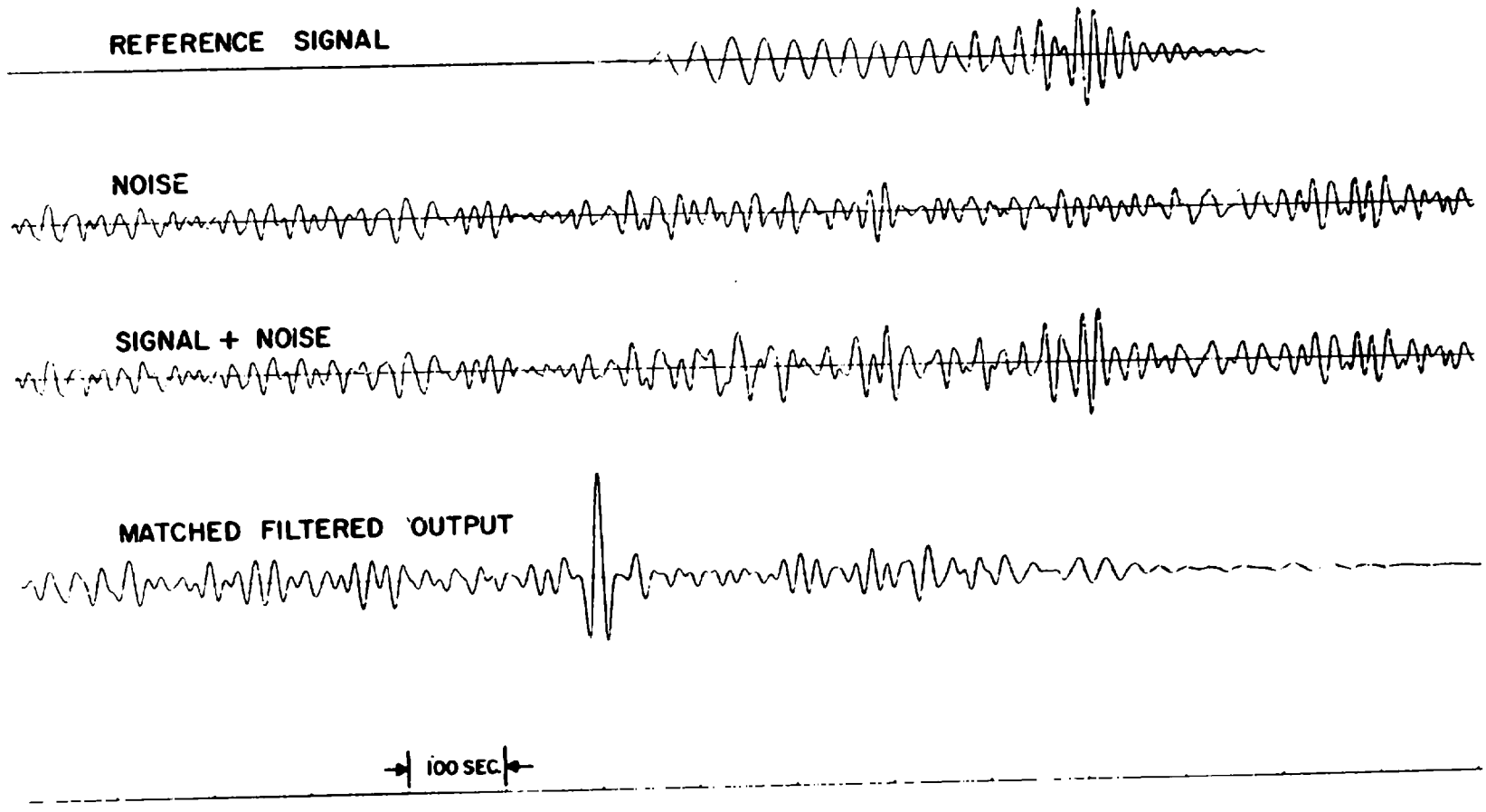

Figure 6A. Typical synthetic test case normalized to noise RMS showing to scale the mixing of signal and noise and the matched filtered output. Amplitude scales are the same on all traces. S/N = 4.

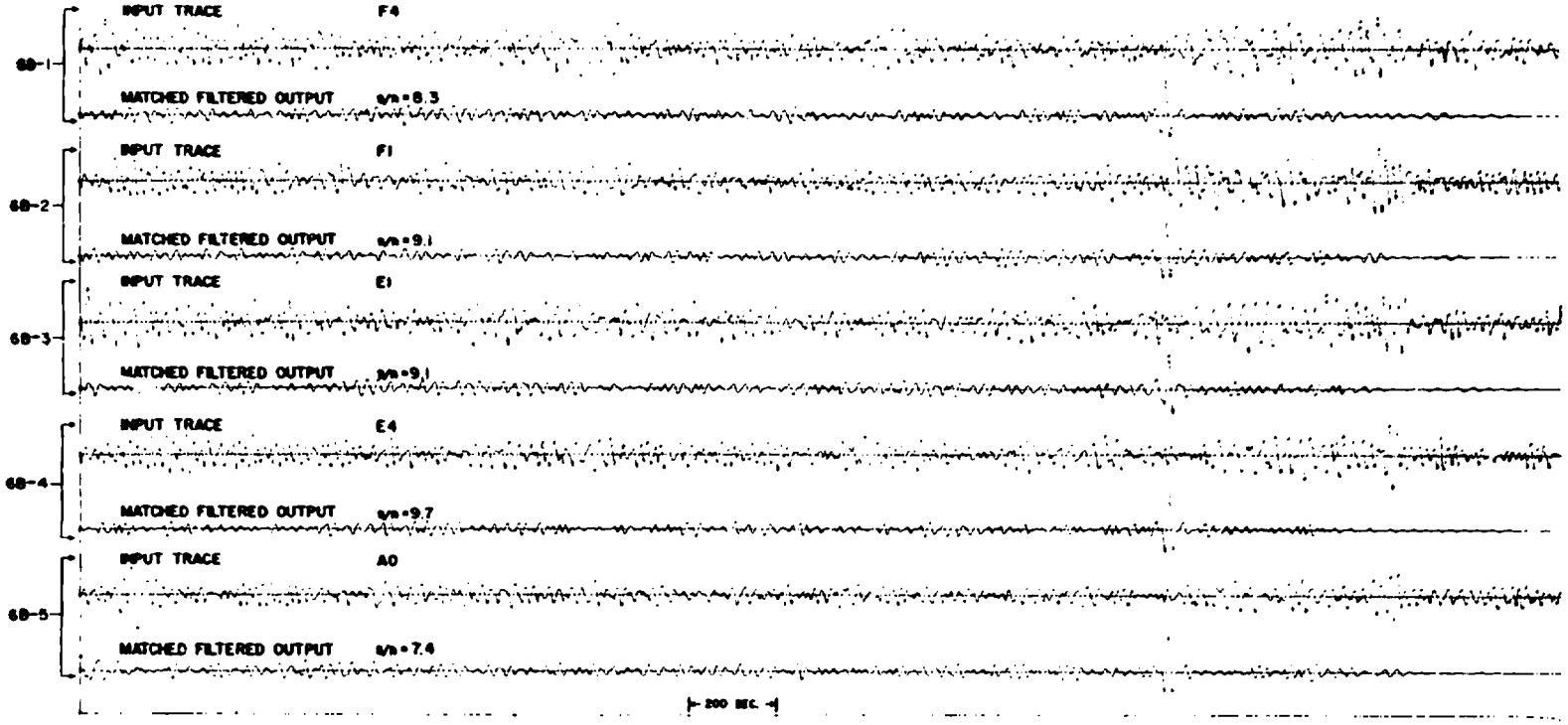

Figure 6B. Typical synthetic test case showing input traces and matched filtered outputs normalized to peak amplitude for four LASA stations. S/N = 4.

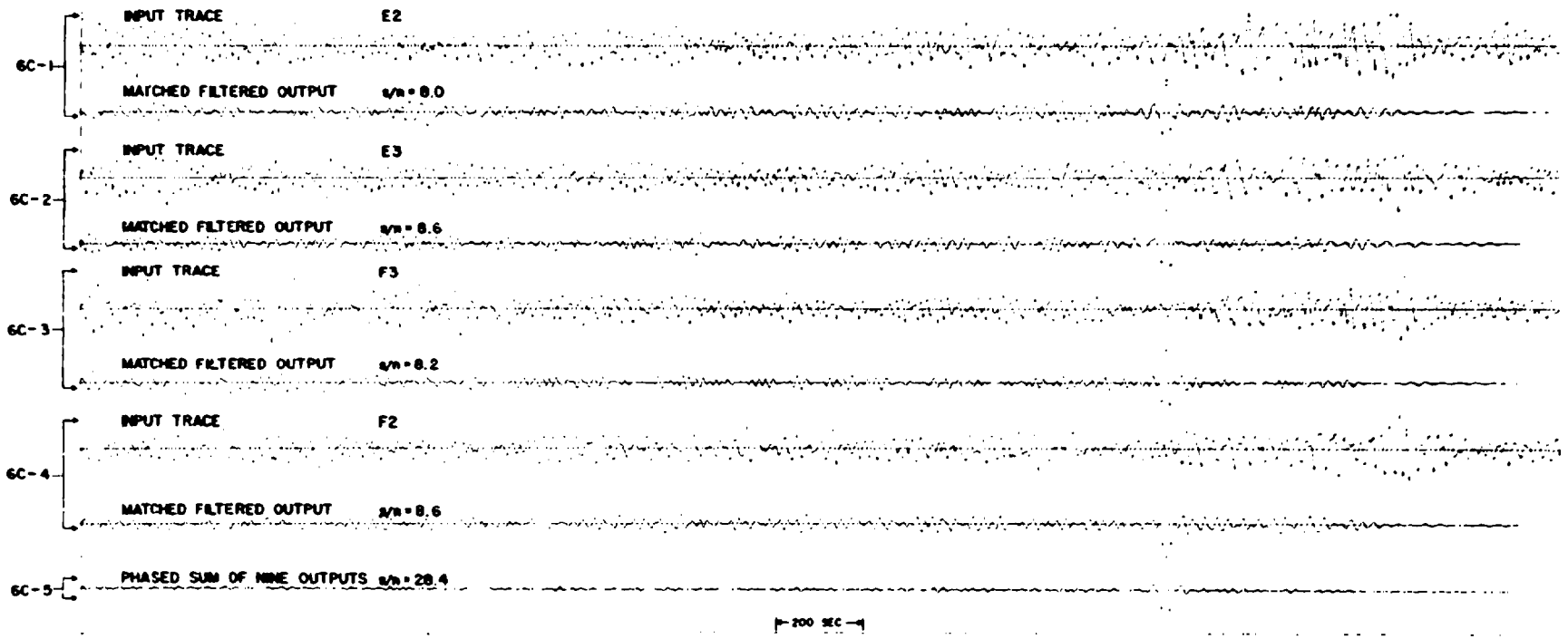

Figure 6C. Typical synthetic test case showing input traces and matched filtered outputs normalized to peak amplitude for four LASA stations and the phased sum trace of nine matched filtered outputs. S/N = 4.

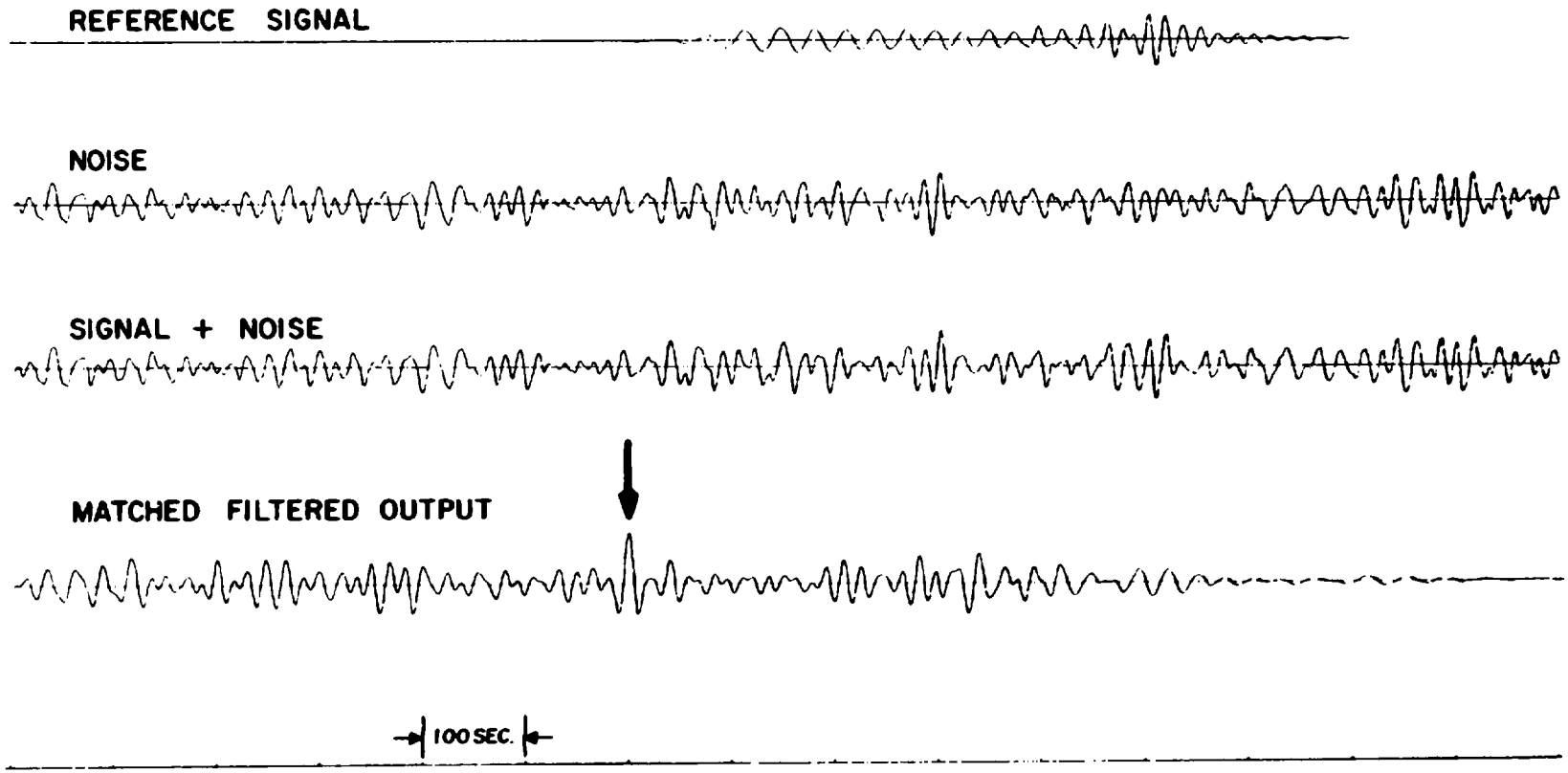

Figure 7A. Typical synthetic test case normalized to noise RMS showing to scale the mixing of signal and noise and the matched filtered output. Amplitude scales are the same on all traces. S/N = 2.

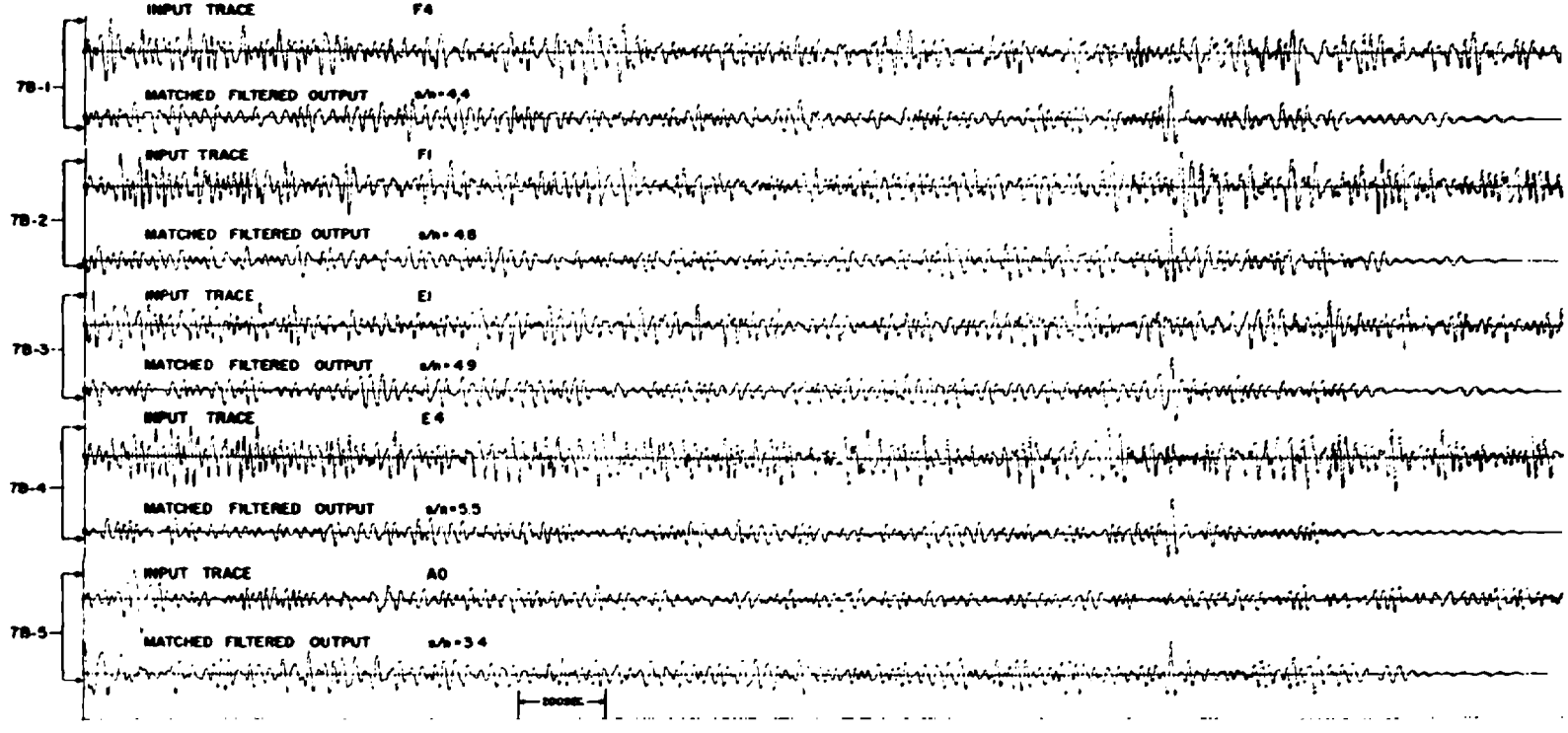

Figure 7B. Typical synthetic test case showing input traces and matched filtered outputs normalized to peak amplitude for four LASA stations. S/N = 2.

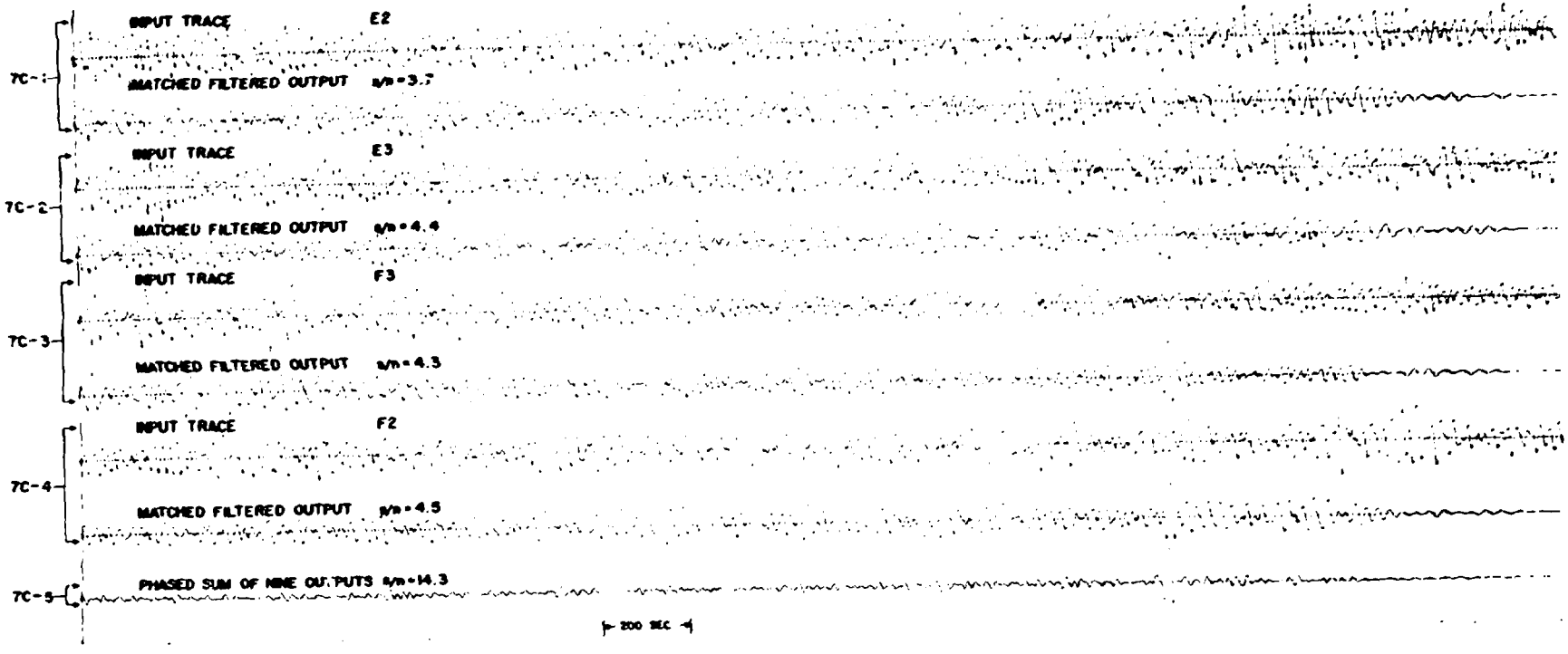

Figure 7C. Typical synthetic test case showing input traces and matched filtered outputs normalized to peak amplitude for four LASA stations and the phased sum trace of nine matched filtered outputs. S/N = 2.

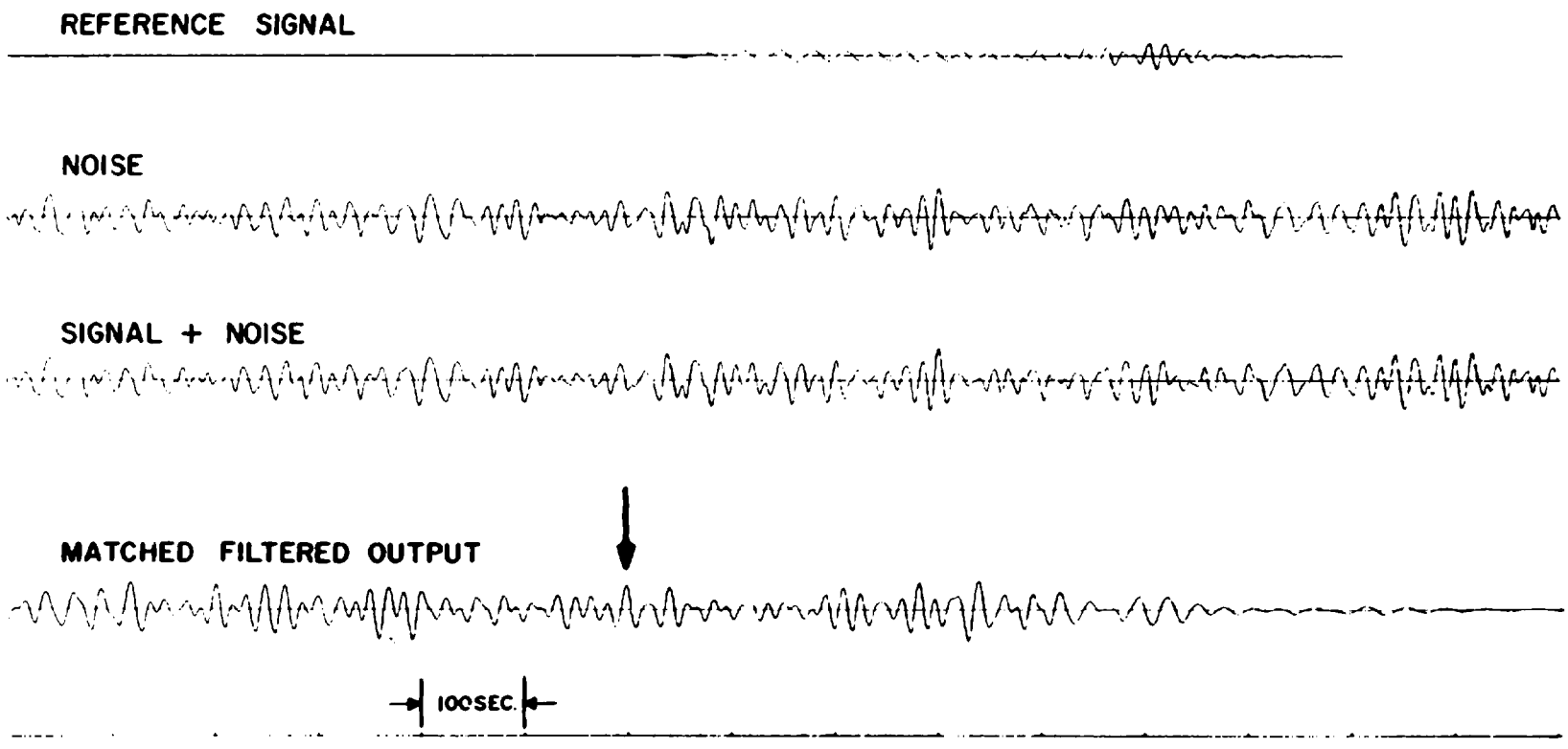

Figure 8A. Typical synthetic test case normalized to noise RMS showing to scale the mixing of signal and noise and the matched filtered output. Amplitude scales are the same on all traces. S/N = 1.

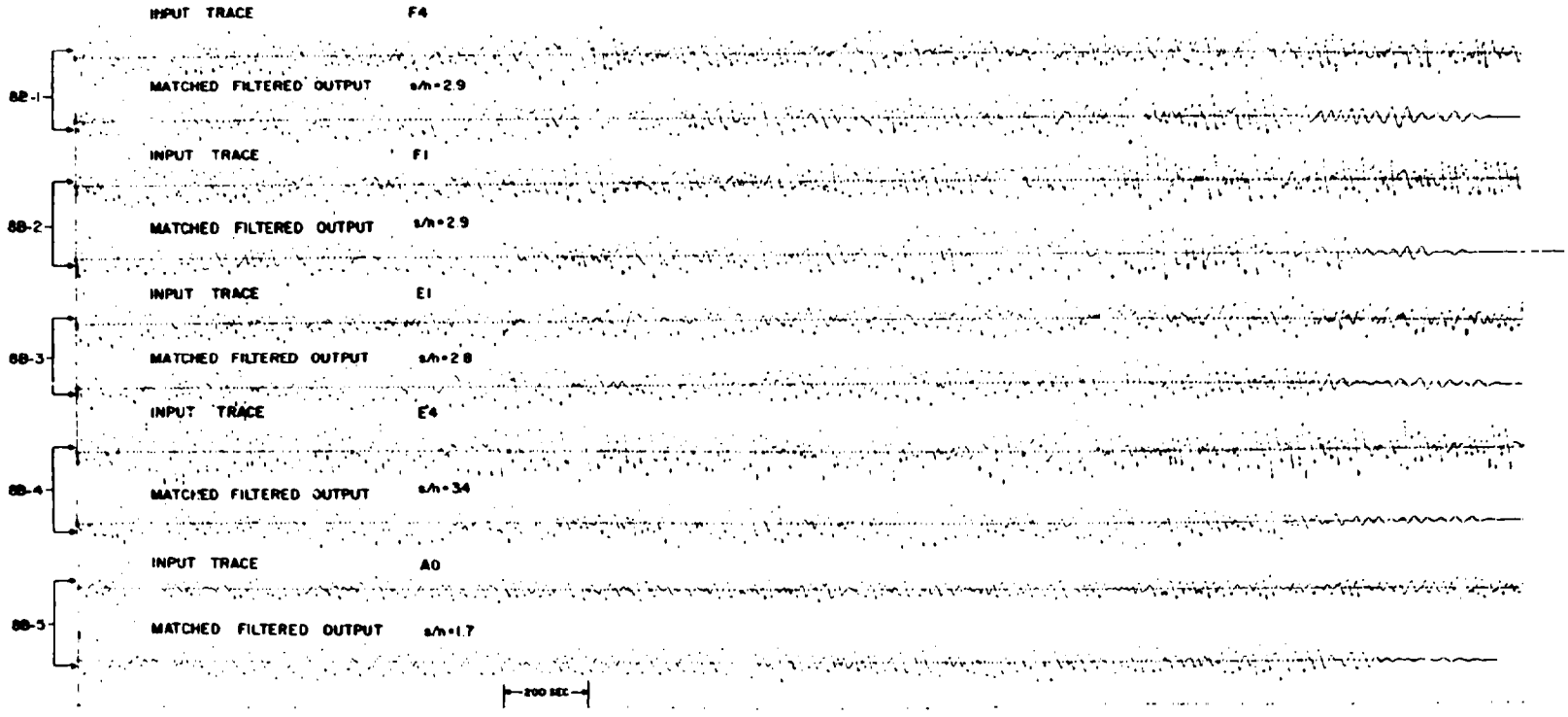

Figure 8B. Typical synthetic test case showing input traces and matched filtered outputs normalized to peak amplitude for four LASA stations. S/N = 1.

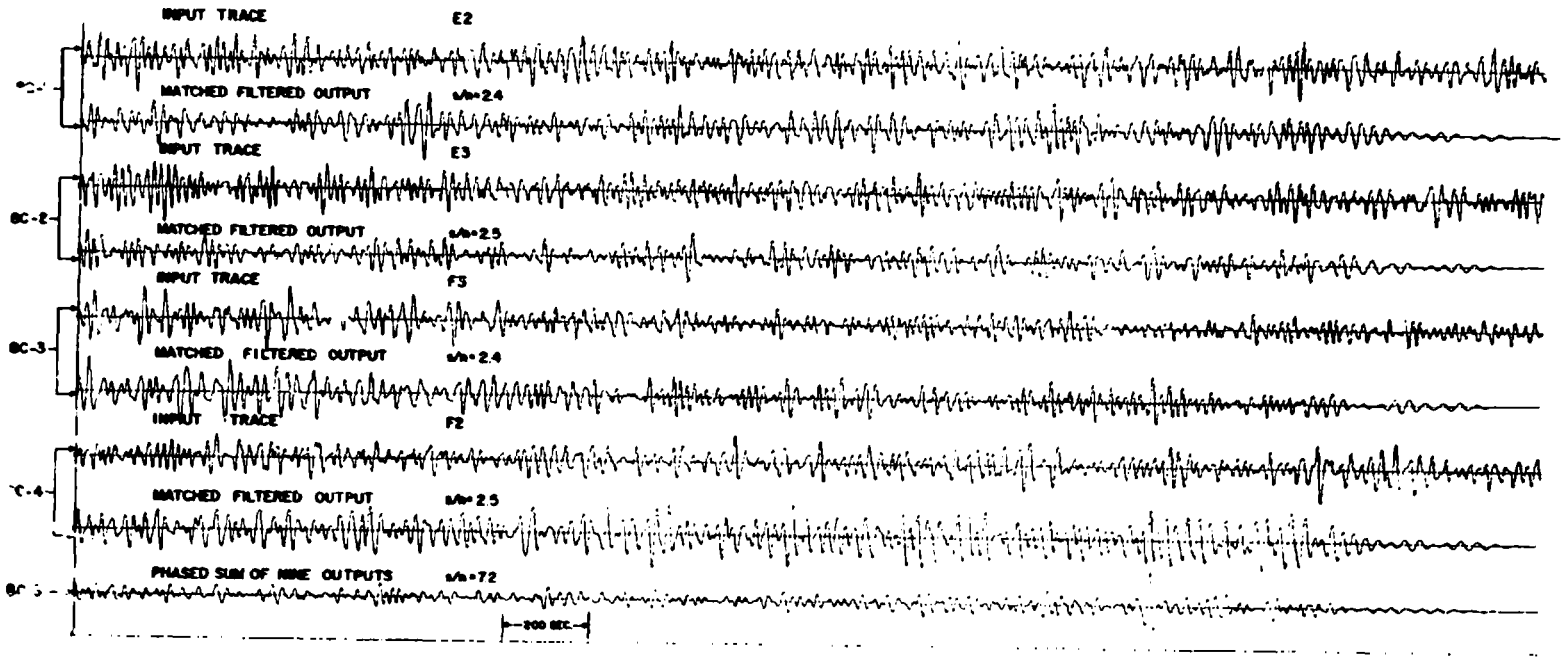

Figure 8C. Typical synthetic test case showing input traces and matched filtered outputs normalized to peak amplitude for four LASA stations and the phased sum trace of nine matched filtered outputs. S/N = 1.

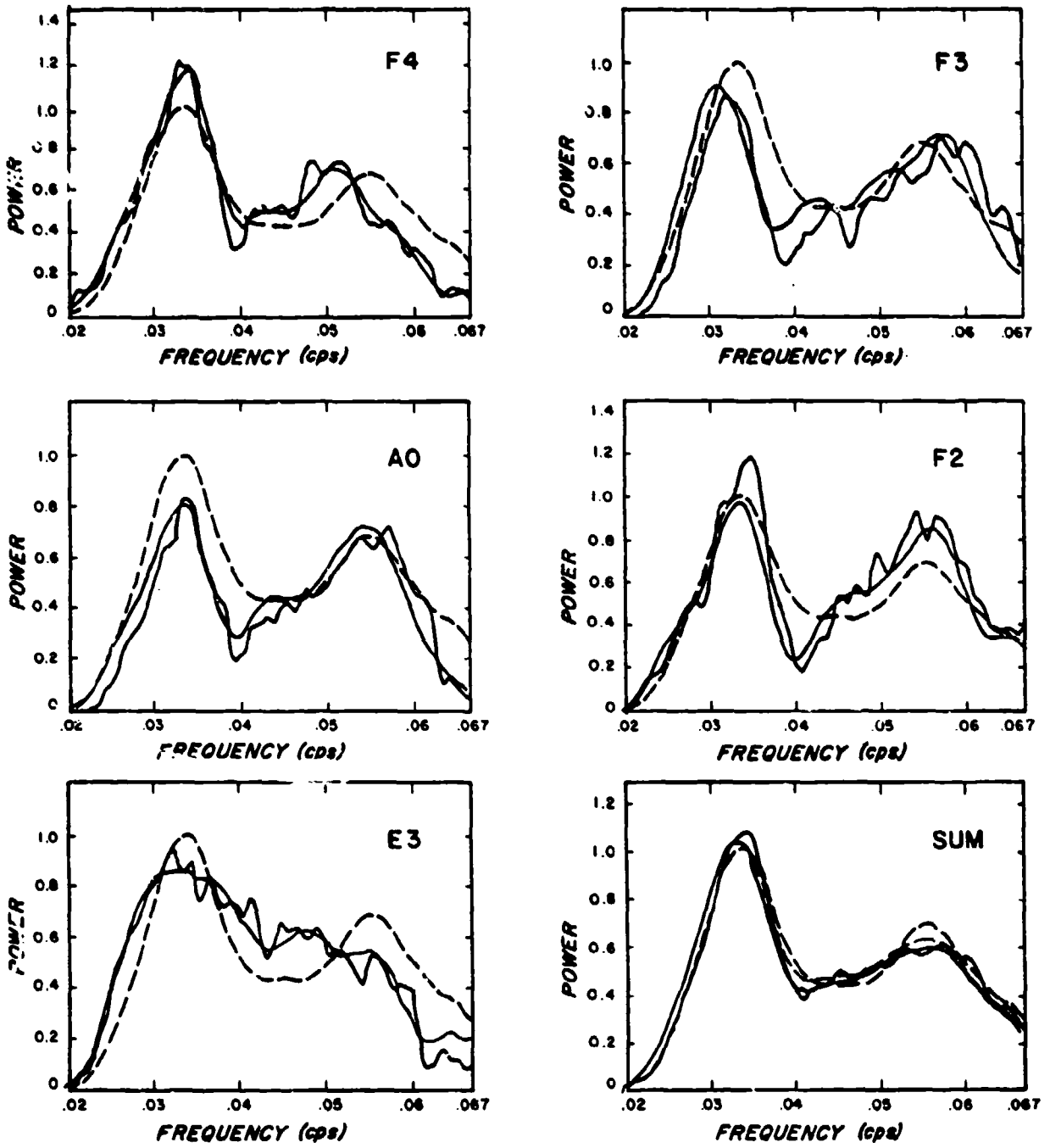

Figure 9. Synthetic test case spectra corrected for noise for five LASA stations and the sums of nine LASA station spectra compared with the original signal spectrum. S/N = 8.

Original Signal ____ Directly Computed _____

M.F. Computed —— Sum Trace Spectrum_ _ _ _

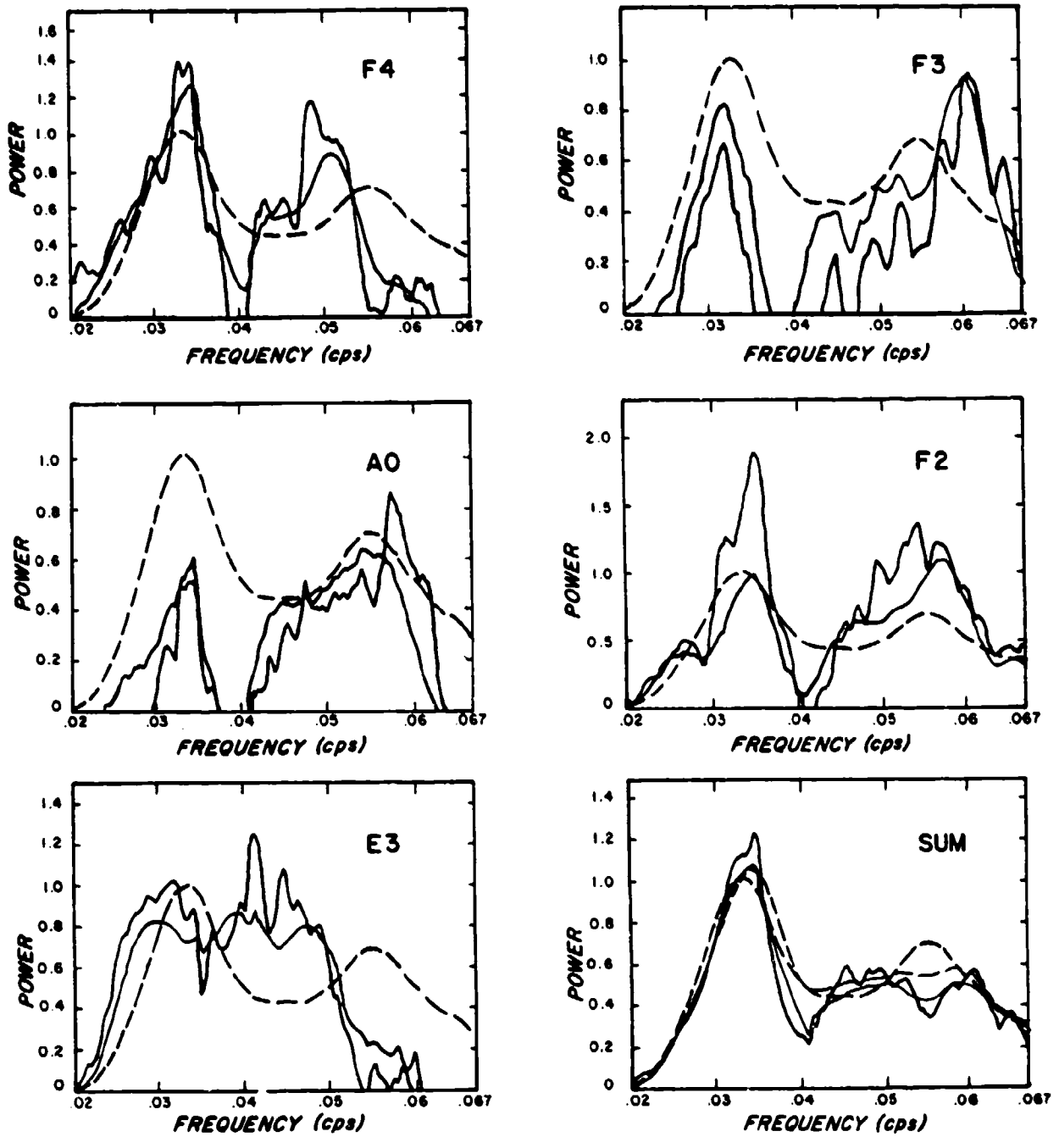

Figure 10. Synthetic test case spectra corrected for noise for five LASA stations and the sums of nine LASA station spectra compared with the original signal spectrum. S/N = 4.

Original Signal - - - - Directly Computed ——

M.F. Computed —— Sum Trace Spectrum - - - -

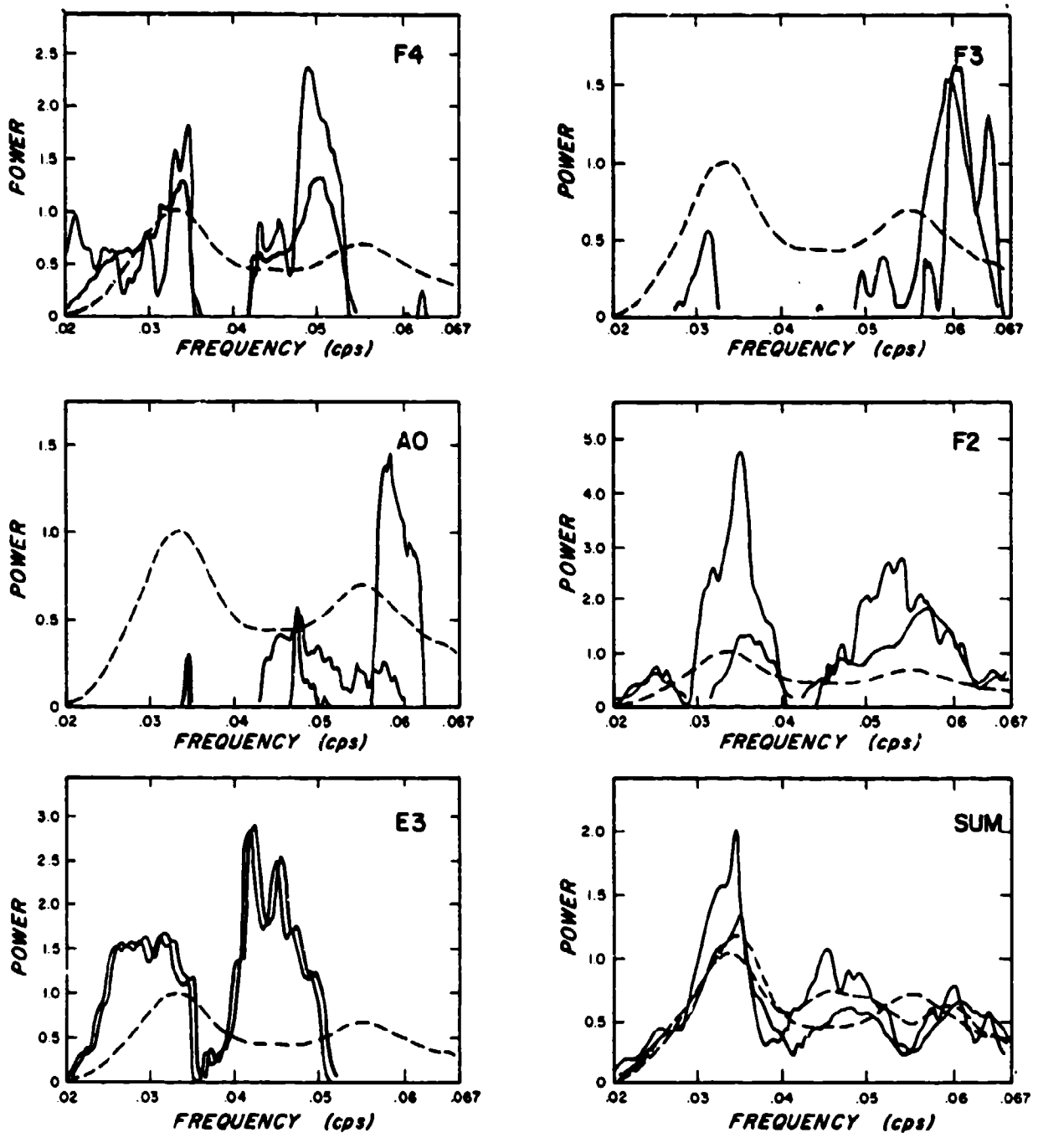

Figure 11. Synthetic test case spectra corrected for noise for five LASA stations and the sums of nine LASA station spectra compared with the original signal spectrum. S/N = 2.

Original Signal - - - - Directly Computed ——

M.F. Computed —— Sum Trace Spectrum - - - -

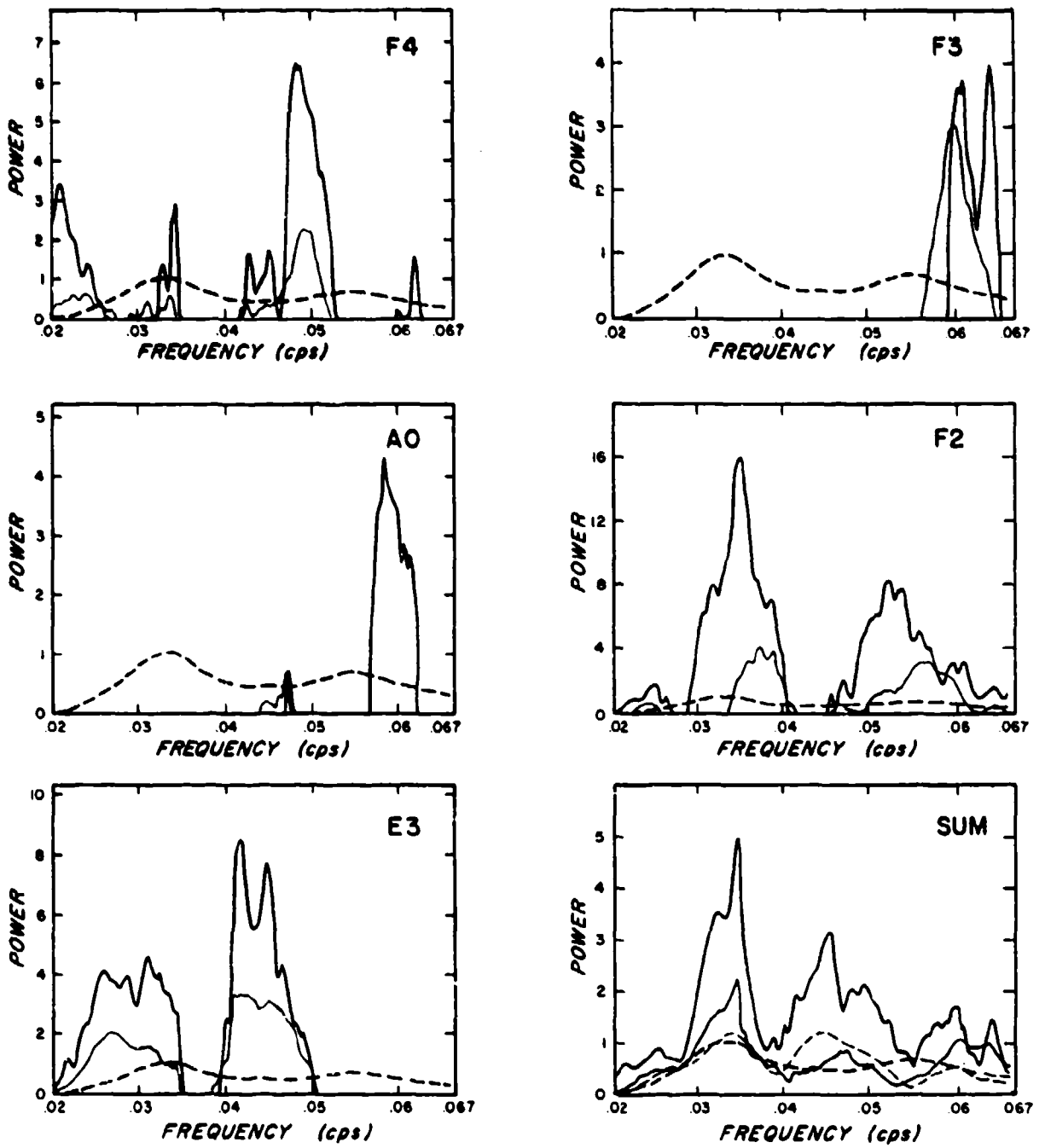

Figure 12. Synthetic test case spectra corrected for noise for five LASA stations and the sums of nine LASA station spectra compared with the original signal spectrum. S/N = 1.

Original Signal _ _ _ _ Directly Computed ——

M. F. Computed —— Sum Trace Spectrum - - - -

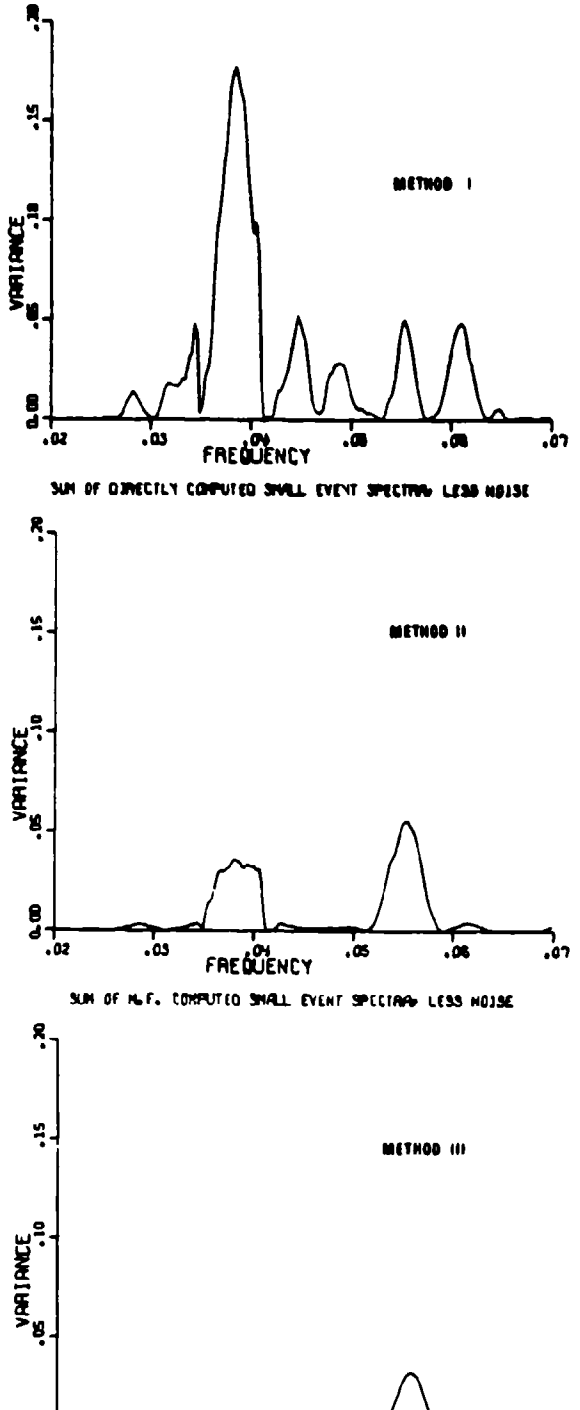

Figure 13A. Comparison of the performance of various spectral methods vs frequency for S/N = 4.

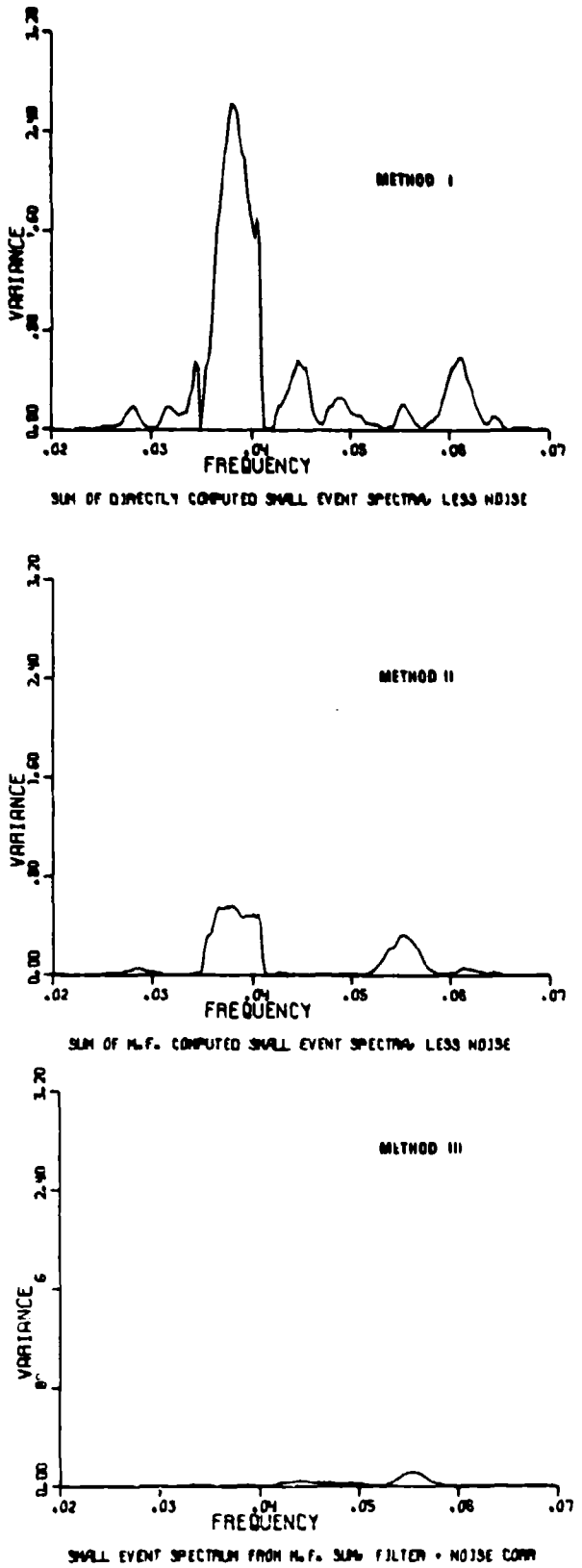

Figure 13E. Comparison of the performance of various spectral methods vs frequency for S/N = 2.

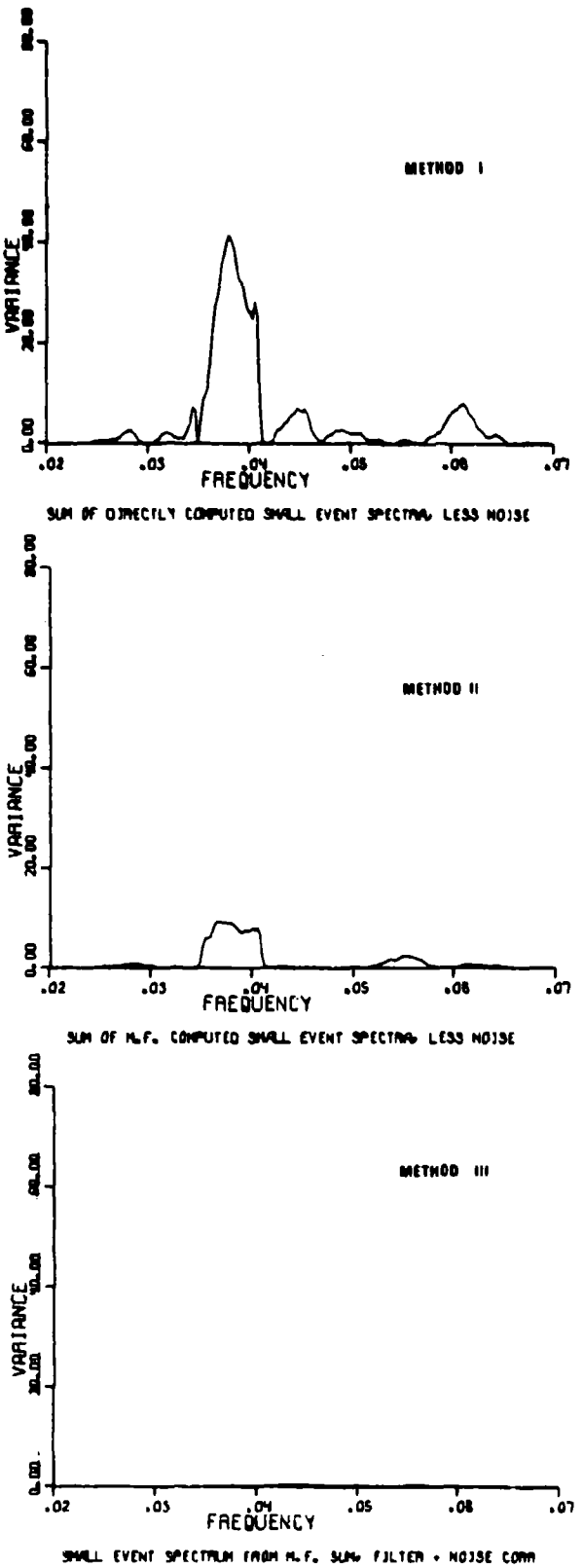

Figure 13C. Comparison of the performance of various spectral methods vs frequency for S/N = 1.

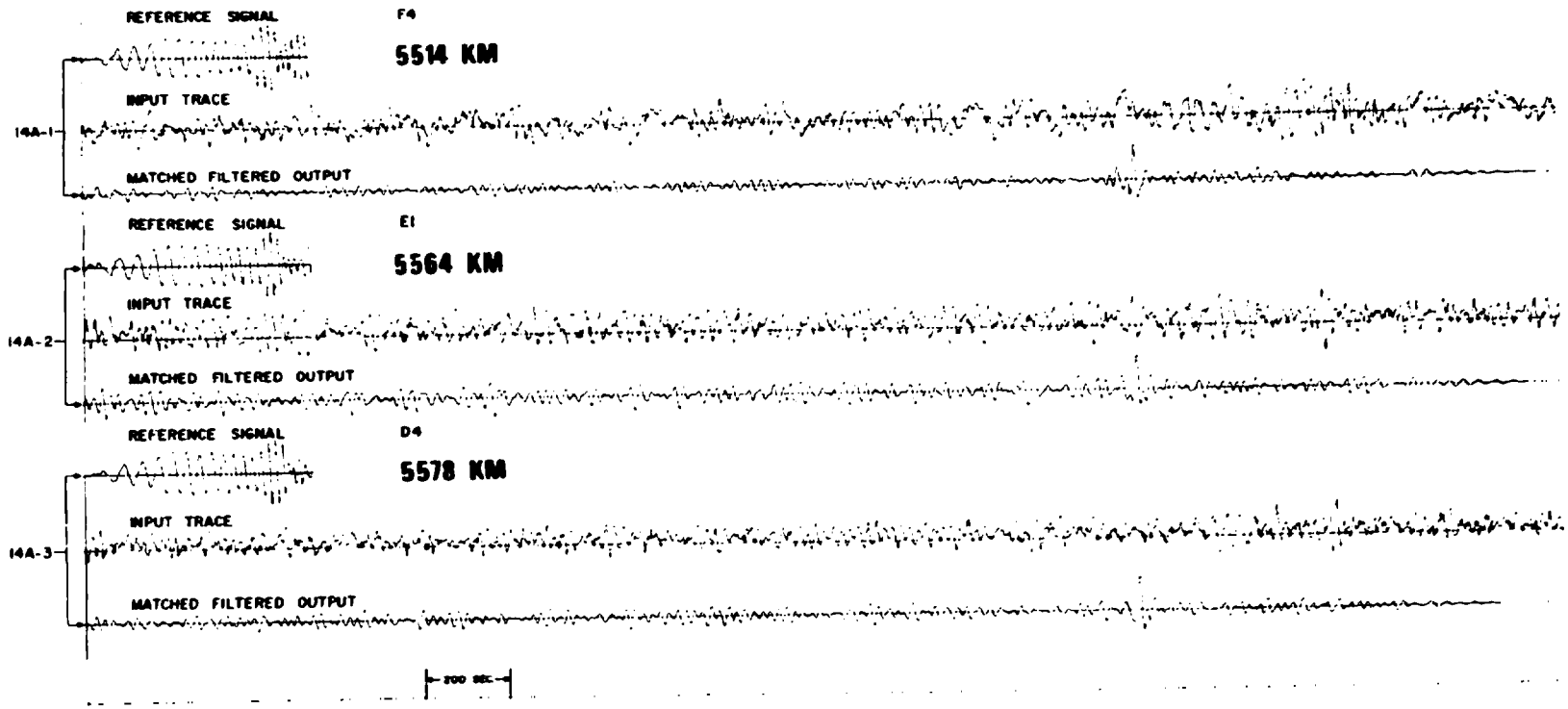

Figure 14A. Results of matched filter processing of Greenland Sea events at three LASA stations. Each trace is normalized to its maximum value.

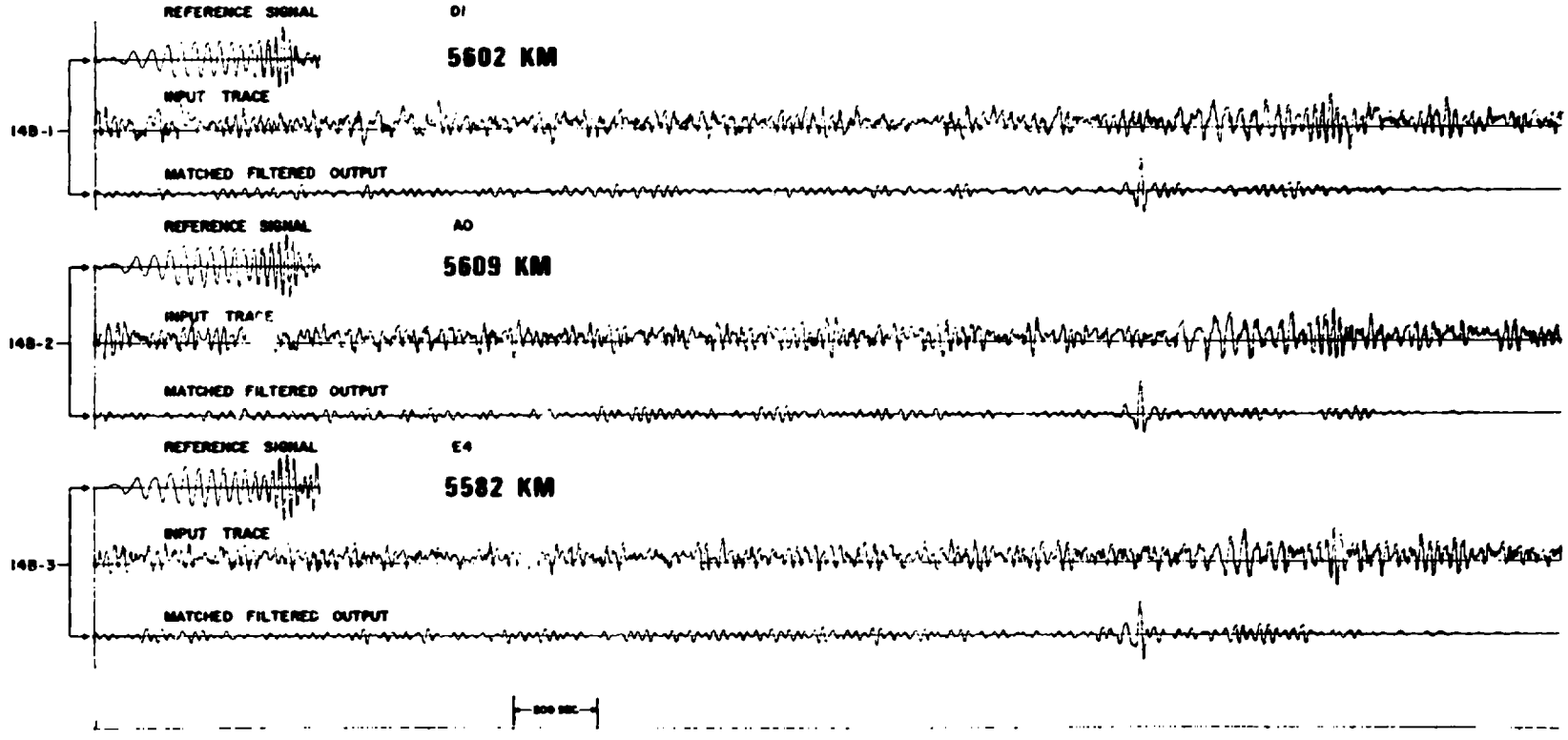

Figure 14B. Results of matched filter processing of Greenland Sea events at three LASA stations. Each trace is normalized to its maximum value.

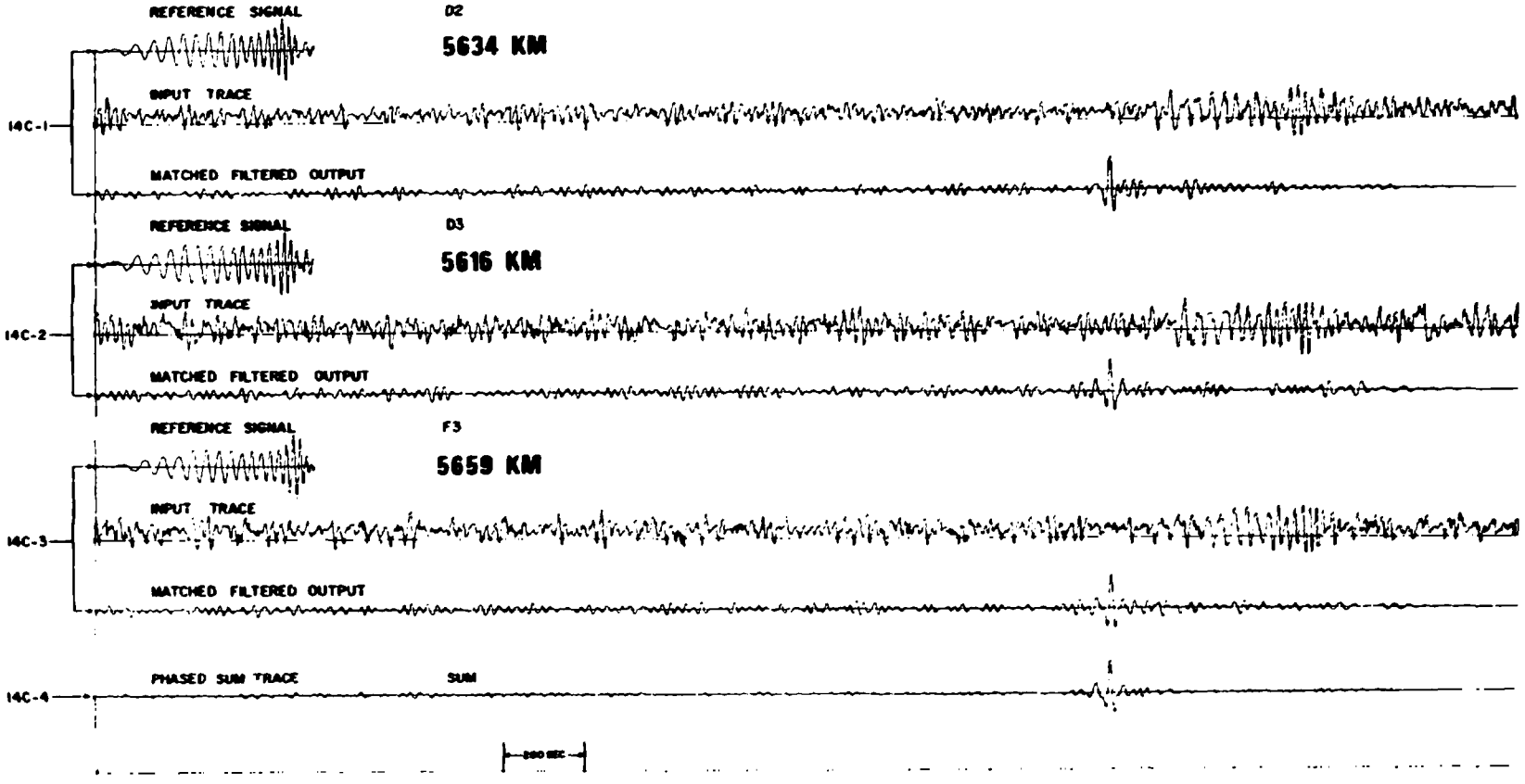

Figure 14C. Results of matched filter processing of Greenland Sea events at three LASA stations and the phased sum of nine matched filtered outputs. Each trace is normalized to its maximum value.

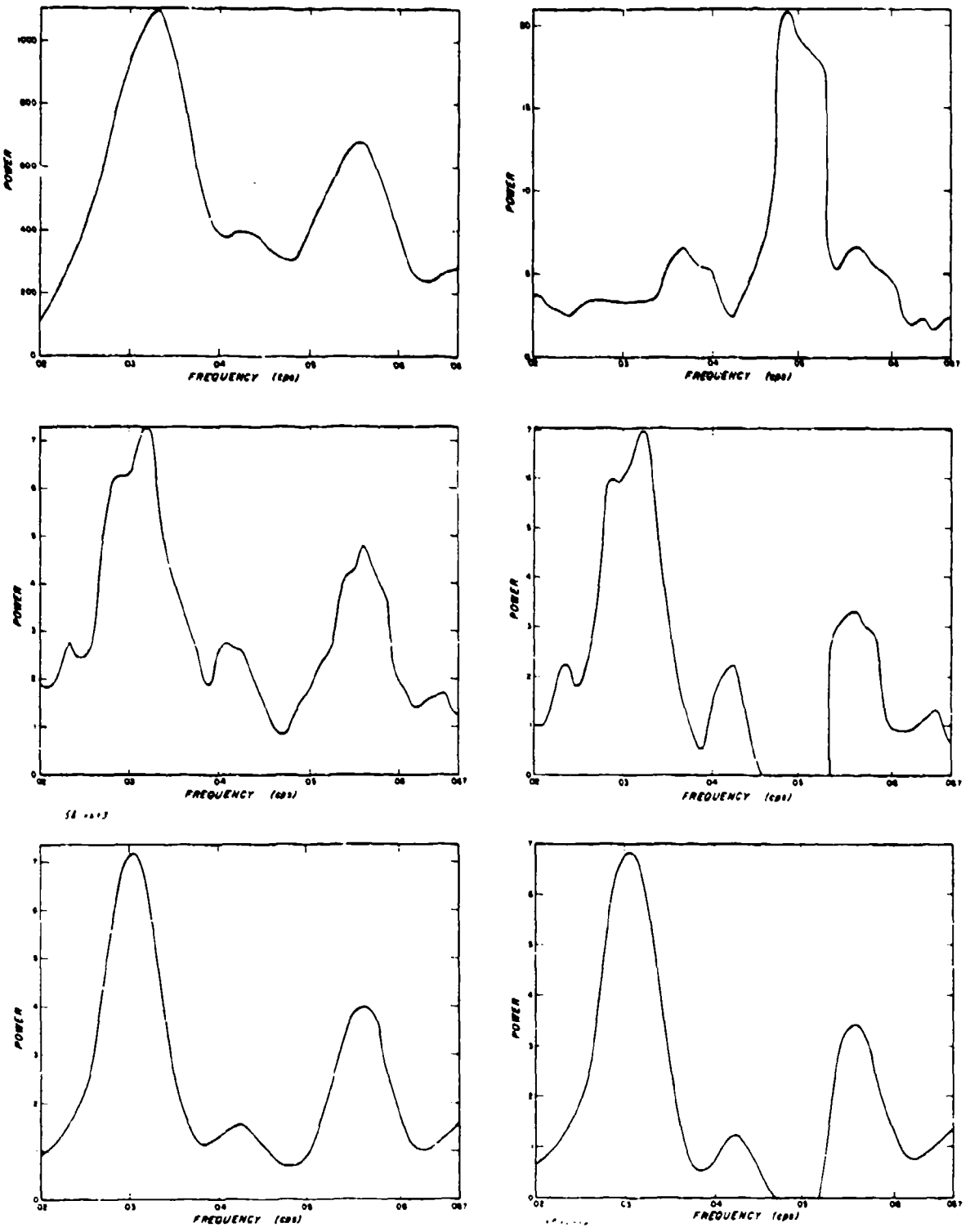

Figure 15A. Individual LASA station spectra for Greenland Sea events, trace D4Z uncorrected for instrument response.

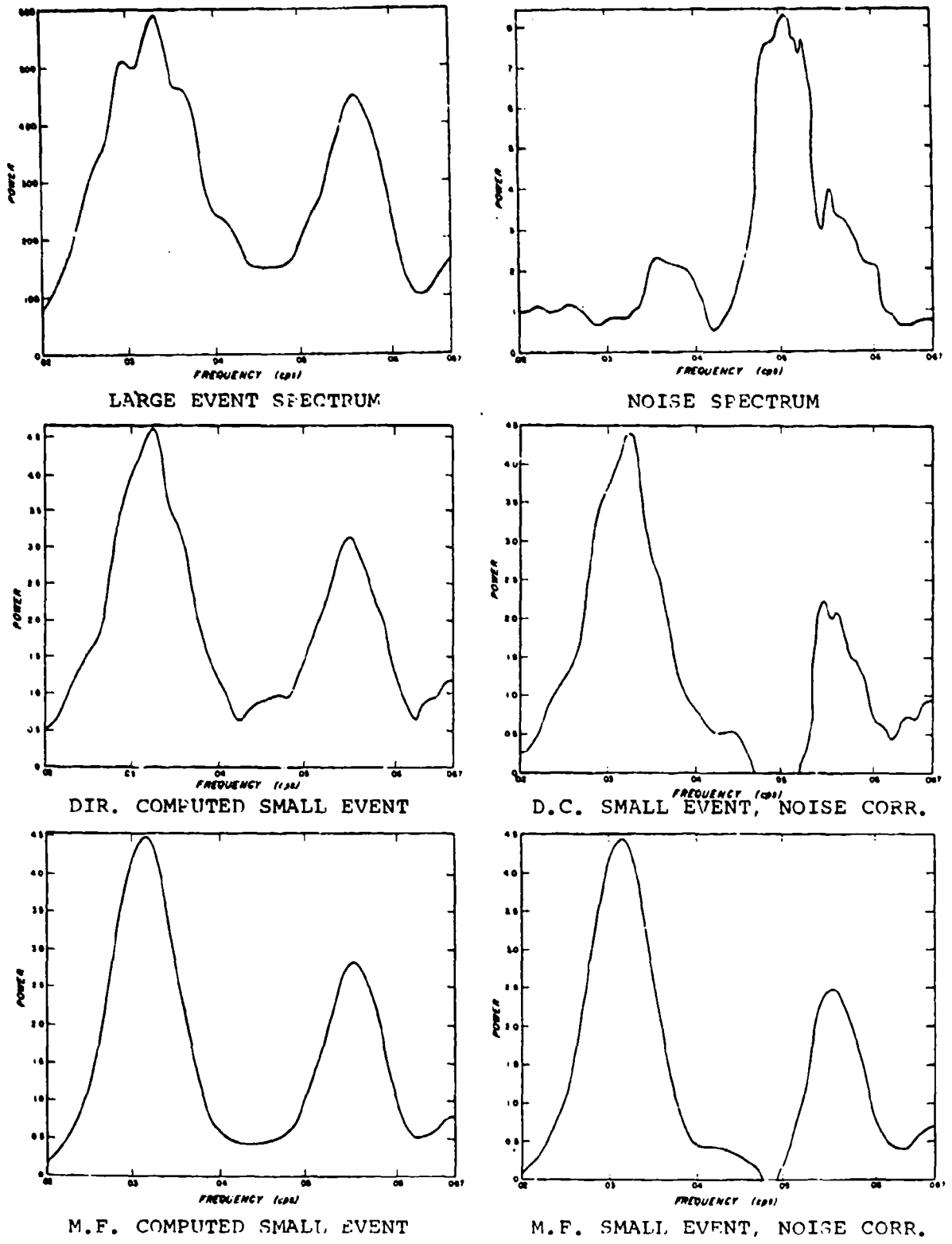

Figure 15B. Individual LASA station spectra for Greenland Sea events, trace E4Z uncorrected for instrument response.

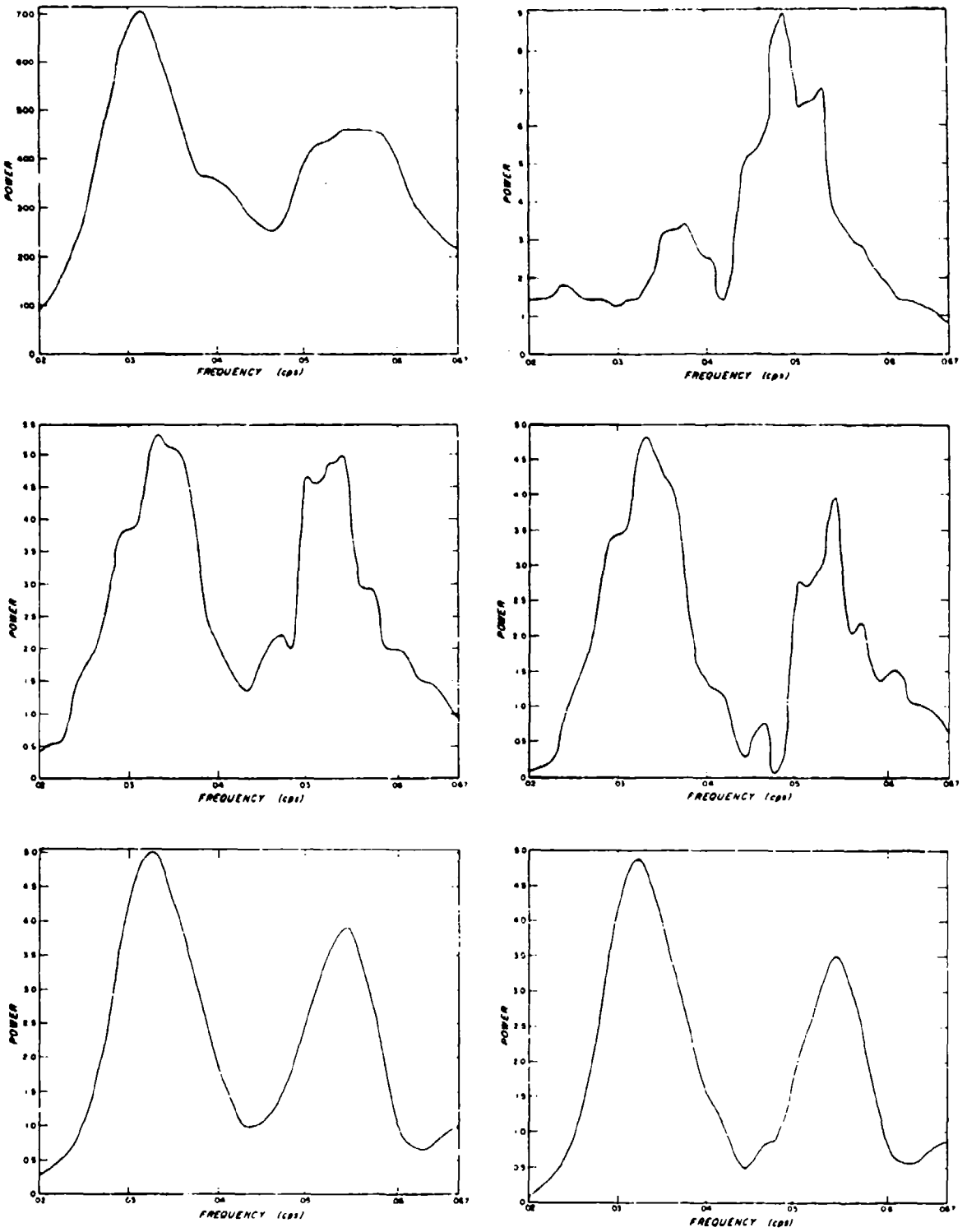

Figure 15C. Individual LASA station spectra for Greenland Sea events, trace F32 uncorrected for instrument response.

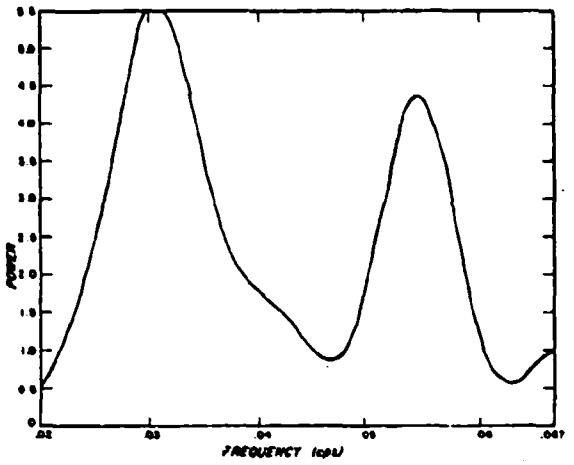

SUM TRACE SIGNAL, INCL. NOISE

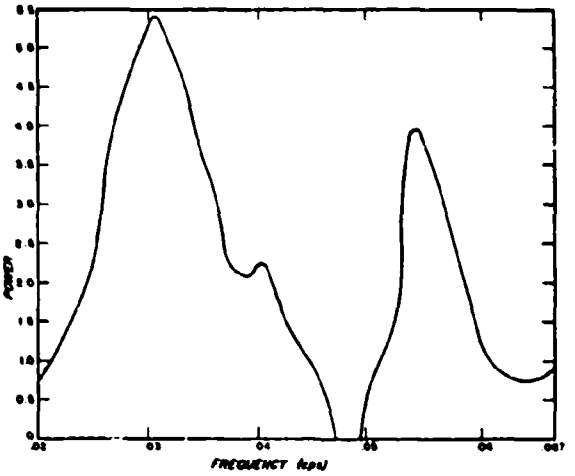

SUM OF DIR. COMPUTED SPECTRA

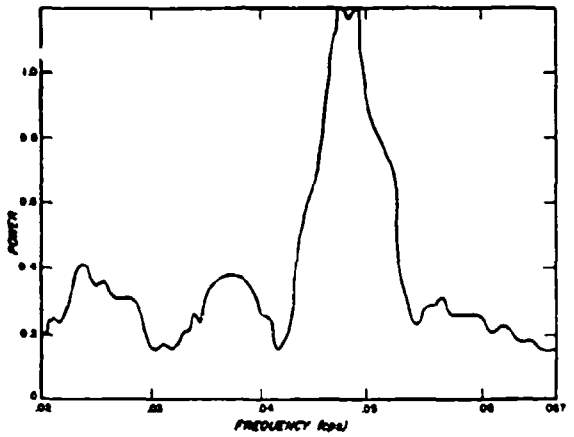

SUM TRACE NOISE

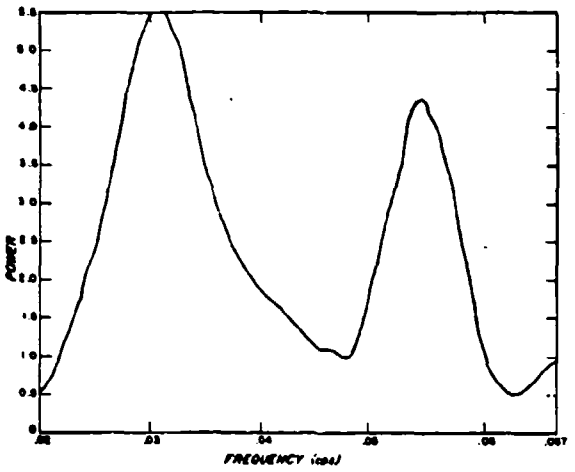

SUM OF M.F. SPECTRA

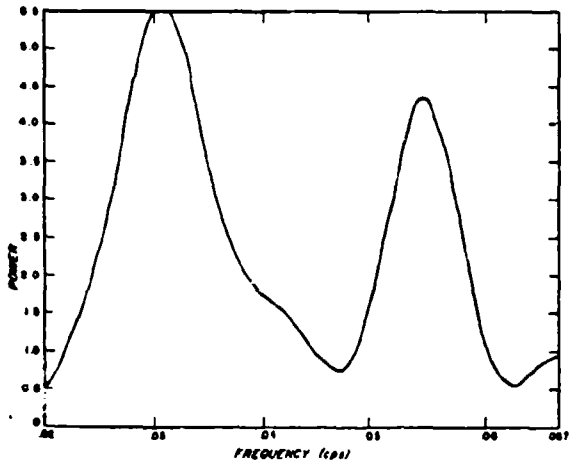

SUM TRACE SIGNAL, NOISE CORR.

EQ GREENLAND SEA
SUM SPECTRA

Figure 15D. Summed spectra and sum trace spectra of nine LASA stations for Greenland Sea events, uncorrected for instrument response.

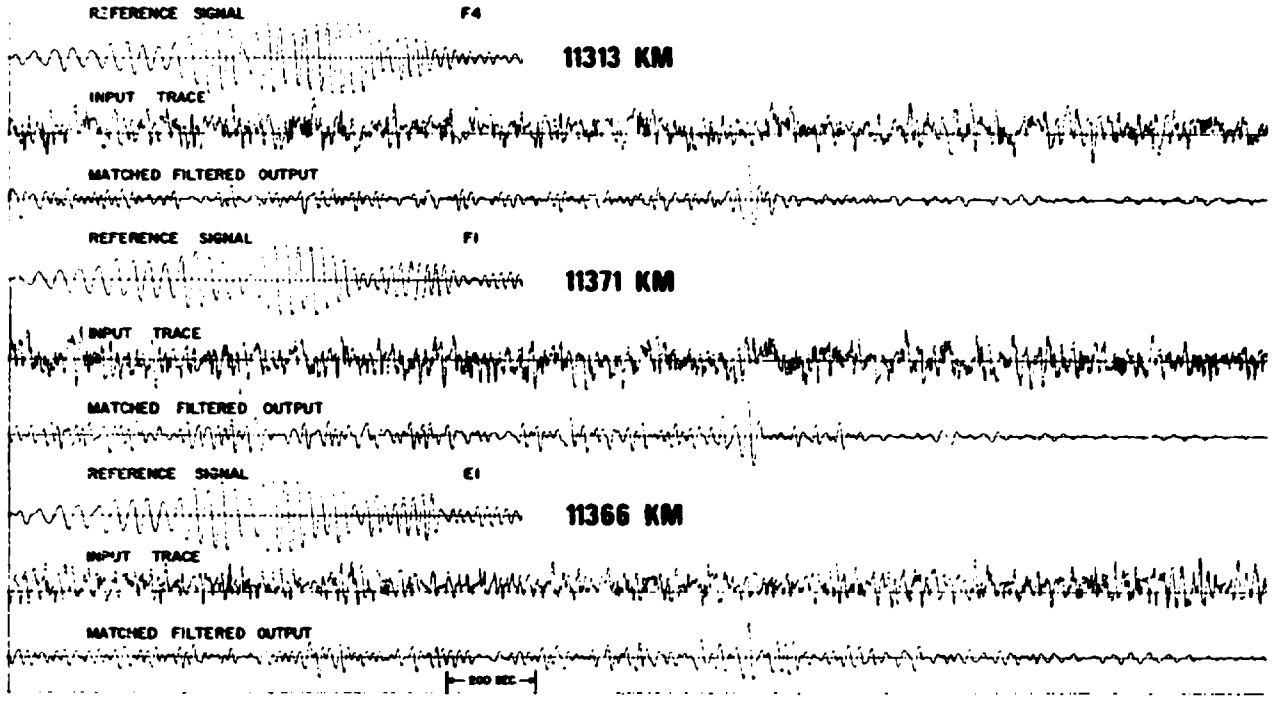

Figure 16A. Results of matched filter processing of Yunnan, China events at three LASA stations. Each trace is normalized to its maximum value.

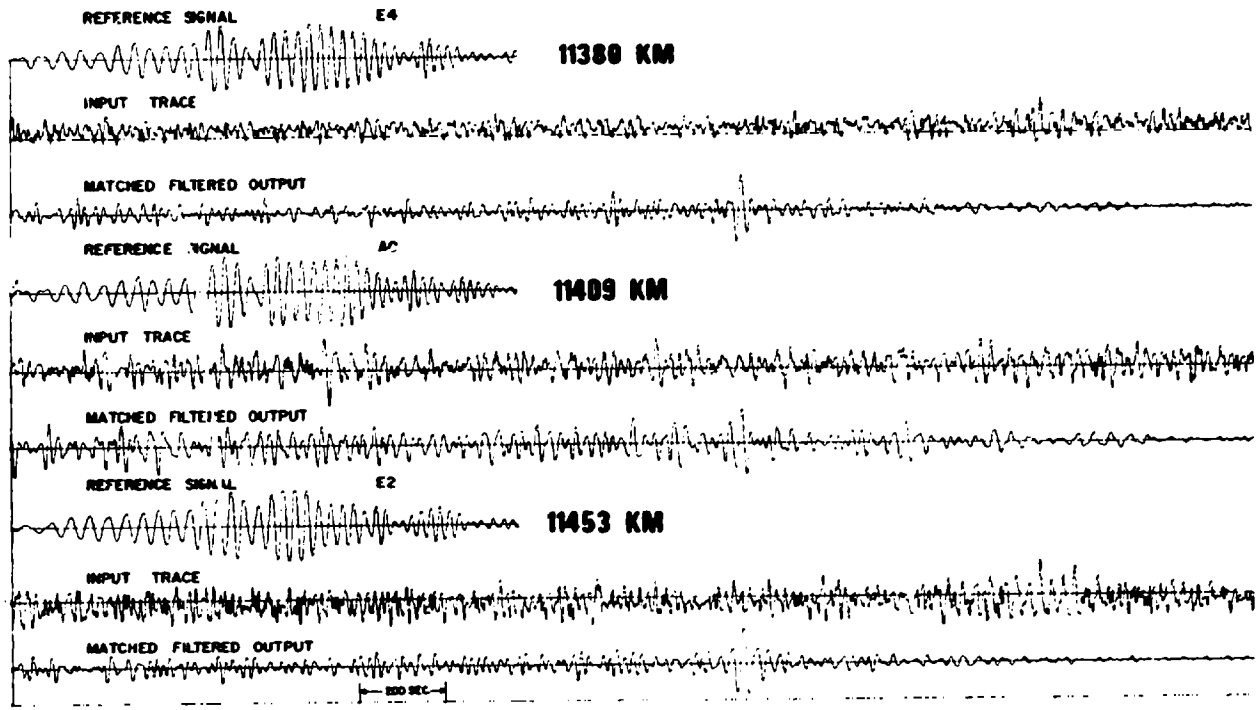

Figure 16B. Results of matched filter processing of Yunnan, China events at three LASA stations. Each trace is normalized to its maximum value.

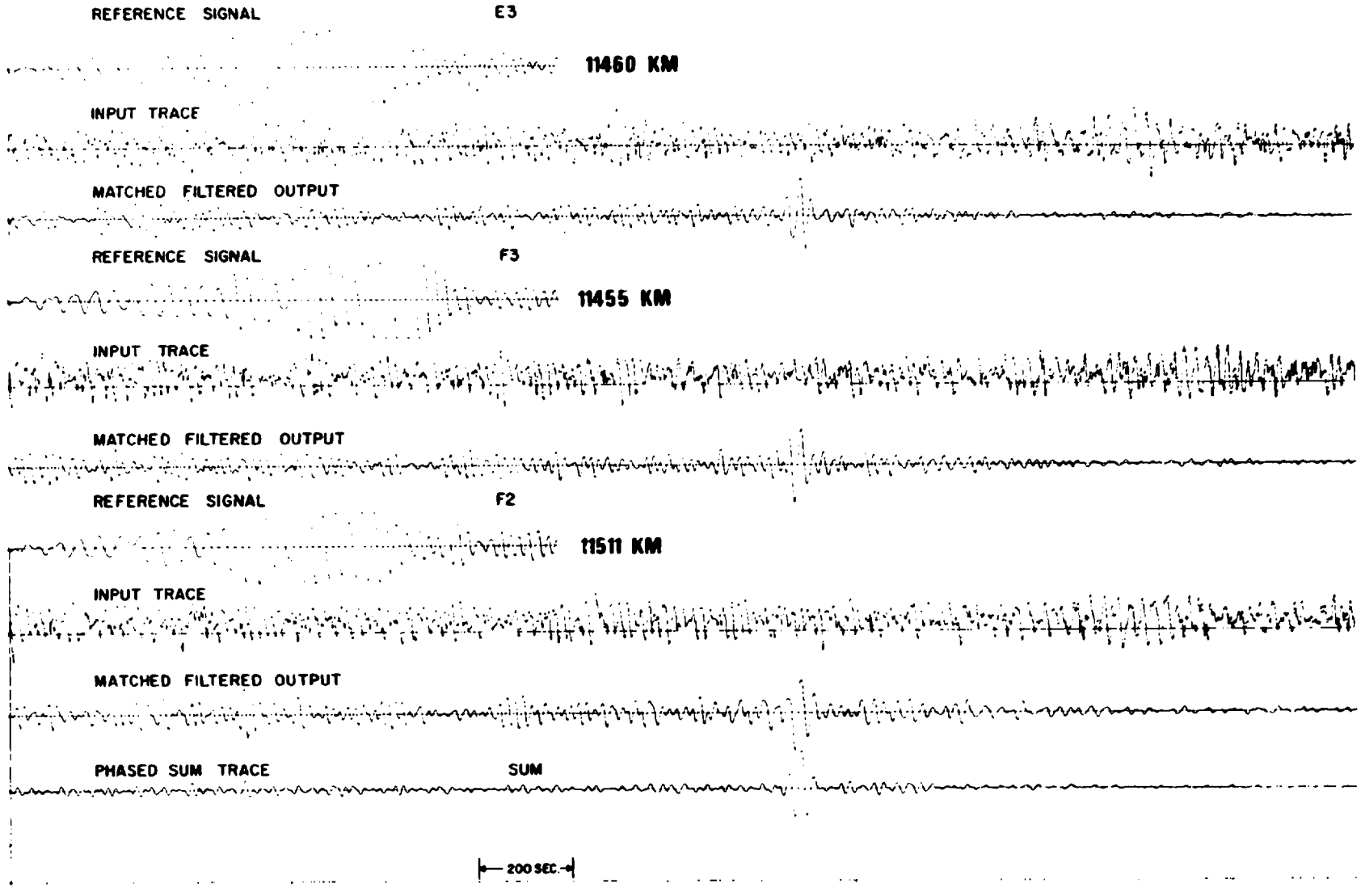

Figure 16C. Results of matched filter processing of Yunnan, China events at three LASA stations and the phased sum trace of 11 matched filtered outputs. Each trace is normalized to its maximum value.

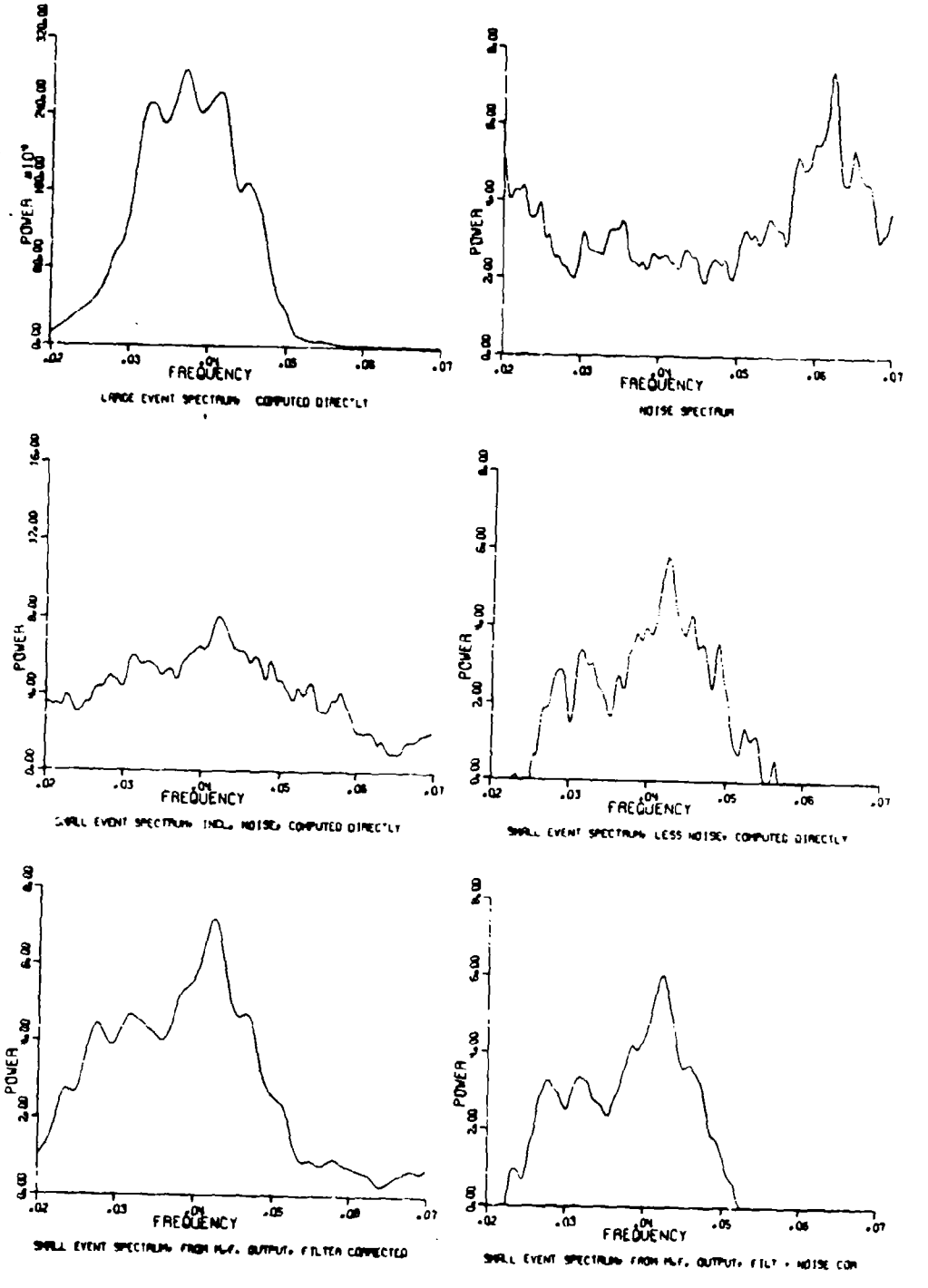

Figure 17A. Individual LASA station spectra for Yunnan, China events, trace F42 uncorrected for instrument response.

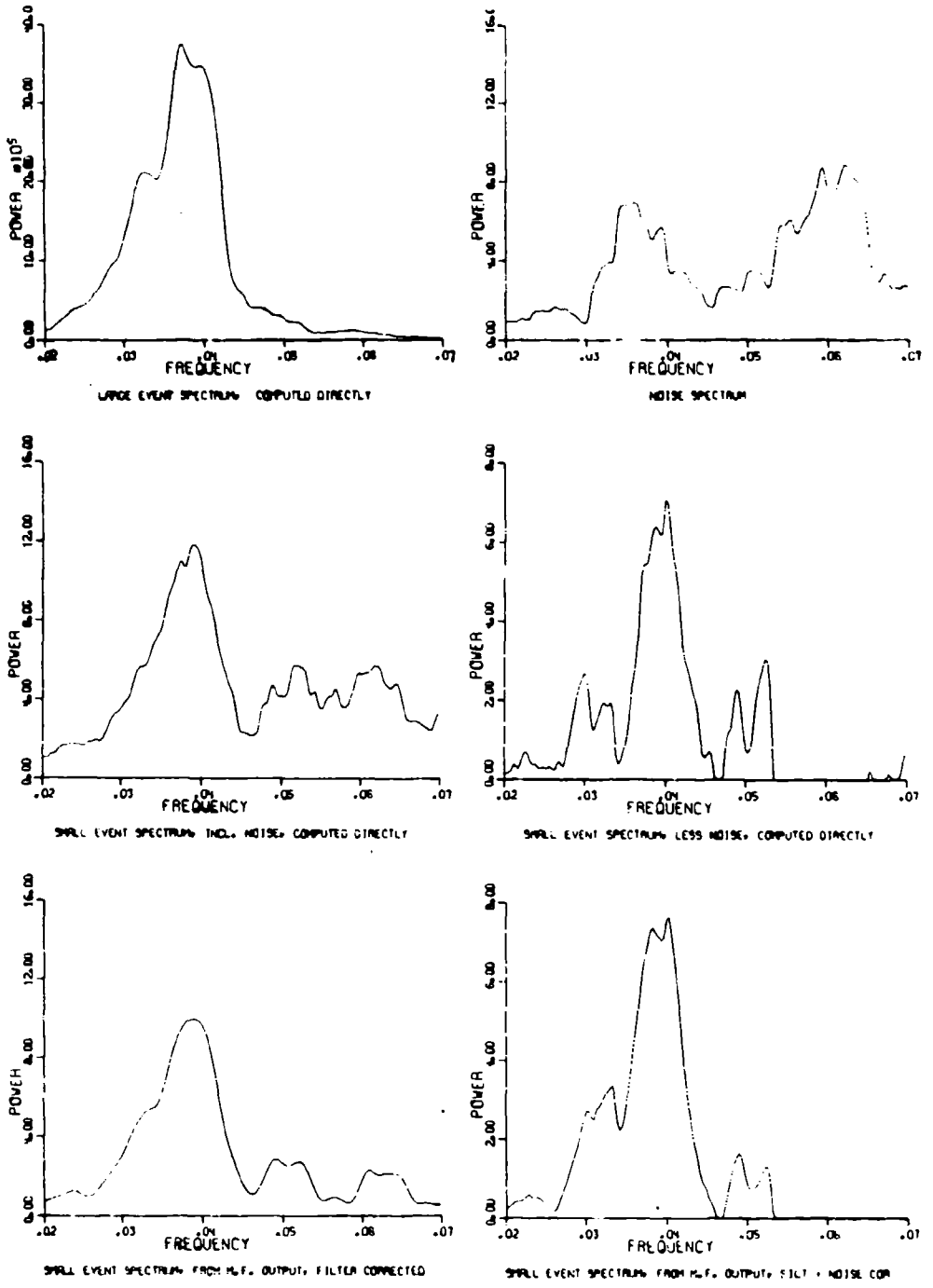

Figure 17B. Individual LASA station spectra for Yunnan, China events, trace E3Z uncorrected for instrument response.

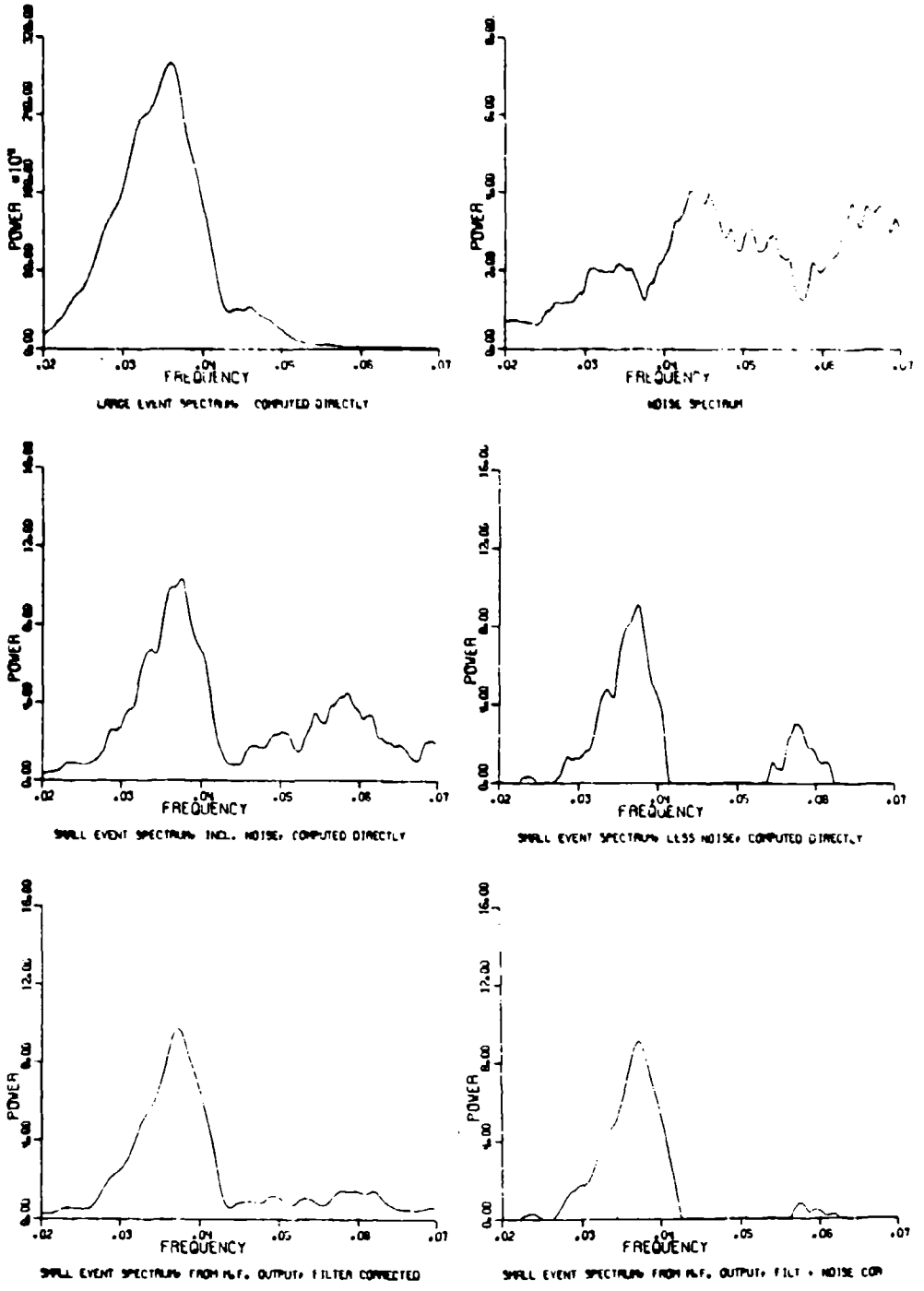

Figure 17C. Individual LASA station spectra for Yunnan, China events, trace E2Z uncorrected for instrument response.

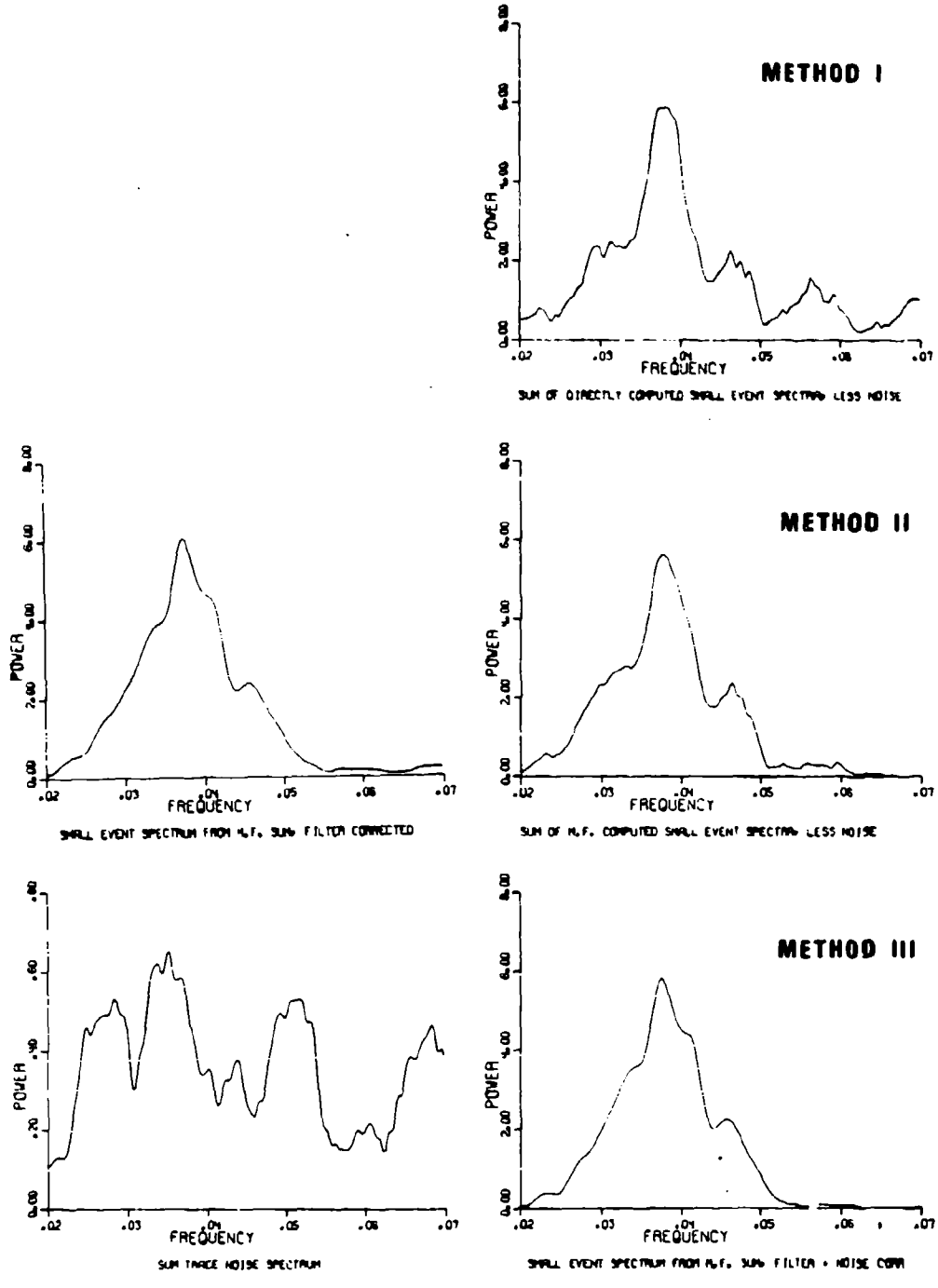

Figure 17D. Summed spectra and sum trace spectra of 11 LASA stations for Yunnan China events, uncorrected for instrument response.

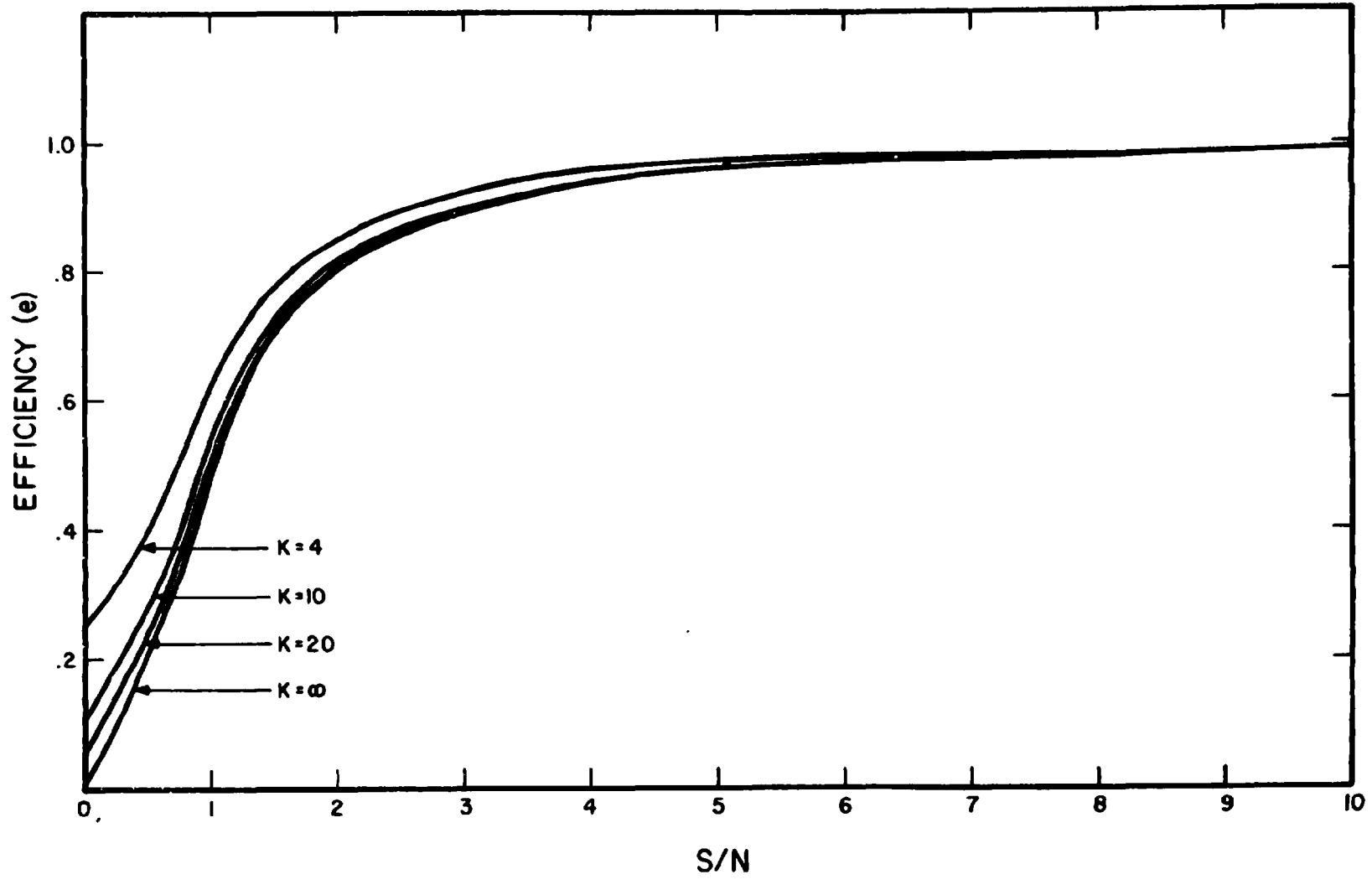

Figure 18. Efficiency vs signal to noise ratio comparing variances of array methods theoretically.

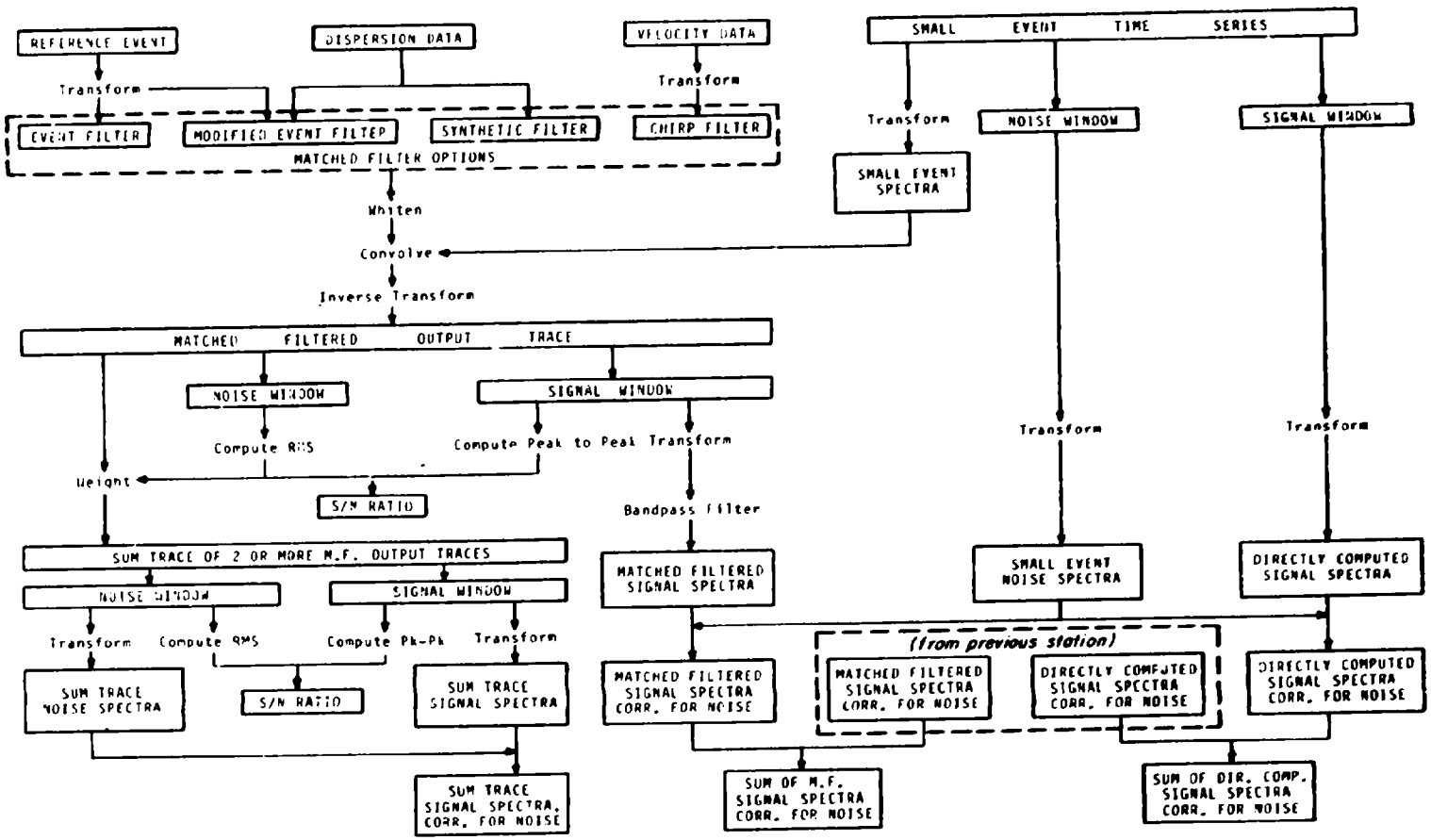

Figure 19. Data processing flow chart.

APPENDIX A
MATCHED FILTER METHOD AND ITS ASSOCIATED SIGNAL TO NOISE GAIN

We present here a discussion of the details of the matched filter operation which shows that because the signal is compressed in time while the noise is not, S/N is increased. Basically the presentation is the same as that in the Appendix (Alexander and Rabenstine, 1967) with some additions and revisions relevant to this study.

The test seismogram x(t) has the Fourier representation

$$x(t) = \int_{-\infty}^{\infty} X(\omega)\, e^{i\omega t} d\omega \qquad \text{(A-1)}$$

and energy (by Parseval's identity)

$$E_x = \int_{-\infty}^{\infty} |X(\omega)|^2 \, d\omega \qquad \text{(A-2)}$$

The matched filter has the Fourier representation

$$a(t) = \int_{-\infty}^{\infty} X(\omega) Y_o^*(\omega)\, e^{i\omega t} d\omega \qquad \text{(A-3)}$$

where $Y_o^*(\omega)$ is the complex conjugate of the Fourier transform of the reference signal y(t), $(Y_o(\omega) = |Y_o(\omega)| e^{i\theta(\omega)})$. The associated energy of the matched filter output is

$$E_a = \int_{-\infty}^{\infty} |X(\omega)|^2 |Y_o(\omega)|^2 \, d\omega \qquad \text{(A-4)}$$

This is equivalent to the energy in x(t) after it is filtered with a function whose spectrum is $Y_o(\omega)$. Note that if we whiten $Y_o(\omega)$ (i.e. divide by $|Y_o(\omega)|$) so that instead of $Y_o^*(\omega)$ we have $Y_o^*/|Y_o(\omega)| = e^{-i\theta(\omega)}$ in equation (A-3), this equation becomes

$$a_w(t) = \int_{-\infty}^{\infty} X(\omega) e^{-i\left[\theta(\omega) - \omega t\right]} d\omega \qquad \text{(A-5)}$$

with energy

$$E_{a_w} = \int_{-\infty}^{\infty} |X(\omega)|^2 d\omega \qquad \text{(A-6)}$$

Thus, if the reference signal is whitened before applying it as a matched filter the energy of x(t) is conserved in the operation since $E_{a_w} \equiv E_x$.

What is left to show is that the signal is compressed in time while the noise is not.

If we take x(t) = s(t) + n(t) (signal + random noise), then,

$$X(\omega) = |S(\omega)| \exp\left[i\left(\phi_{os}(\omega) - \frac{\omega\Delta}{C(\omega)} + \phi_i(\omega)\right)\right] + |N(\omega)| \exp\left[i(\Psi(\omega) + \phi_i(\omega))\right] \qquad \text{(A-7)}$$

$$Y_o(\omega) = |Y_o(\omega)| \exp\left[-i\left(\phi_{oy}(\omega) - \frac{\omega\Delta}{C(\omega)} + \phi_i(\omega)\right)\right] \equiv |Y_o(\omega)| \, e^{-i\theta(\omega)} \qquad \text{(A-8)}$$

and

where

$\phi_{os}(\omega)$ = phase spectrum at the source for s(t)

$\phi_{oy}(\omega)$ = phase spectrum at the source for y(t)

$\phi_i(\omega)$ = instrument phase spectrum (assumed identical for x and y)

$C(\omega)$ = phase velocity spectrum

Δ = epicentral distance

$|S(\omega)|$ = amplitude spectrum of s(t)

$|Y(\omega)|$ = amplitude spectrum of $y(t)$

$\theta(\omega)$ = total phase associated with $y(t)$

$\Psi(\omega)$ = random phase associated with $n(t)$

therefore,

$$XY^* = |S(\omega)|\ |Y_o(\omega)|\ \exp\left[i(\phi_{os}(\omega) - \phi_{oy}(\omega))\right] + |N(\omega)|\ |Y_o(\omega)|\ \exp\left[i(\Psi(\omega) - \theta(\omega))\right] \quad \text{(A-9)}$$

The first term on the right hand side of the equation (A-9) is the matched filter signal spectrum and the second term is the noise spectrum. We will discuss each term separately. From the first term, the signal on the matched filter seismogram is given by

$$s_f(t) = \int_{-\infty}^{\infty} |S(\omega)|\ |Y_o(\omega)|\ \exp\left[i(\phi_{os}(\omega) - \phi_{oy}(\omega) + \omega t)\right] d\omega \quad \text{(A-10)}$$

If both $s(t)$ and $y(t)$ have the same phase spectrum at the source then $\phi_{os} = \phi_{oy}$ and (A-10) reduces to

$$s_f(t) = \int_{-\infty}^{\infty} |S(\omega)|\ |Y_o(\omega)|\ e^{i\omega t}\, d\omega \quad \text{(A-11)}$$

or for the whitened reference signal case (i.e. $|Y_o(\omega)| = 1$)

$$s_{fw}(t) = \int_{-\infty}^{\infty} |S(\omega)| e^{i\omega t}\, d\omega \quad \text{(A-12)}$$

This is the band-limited impulse representing the signal of shortest duration which has the spectrum of the signal. Therefore this signal also has the largest possible energy density in the time domain. To demonstrate this we compare the energy density of $s_{fw}(t)$ with that

of the dispersed signal as recorded

$$s(t) = \int_{-\infty}^{\infty} |S(\omega)| \exp\left[i\left(\phi_{os}(\omega) - \frac{\omega\Delta}{C(\omega)} + \phi_i(\omega) + \omega t\right)\right] d\omega \qquad (A\text{-}13)$$

For $s_{fw}(t)$ the maximum energy density occurs at $t = 0$, since it is here that all the frequencies add together in phase (zero group delay for all frequencies) and

$$\int_{-\infty}^{\infty} |S(\omega)| d\omega \geq \int_{-\infty}^{\infty} |S(\omega)| e^{i\omega t} d\omega \text{ for all } t \neq 0.$$

Note that $s_{fw}(t)$ is not "causal" because it is non-zero earlier than $t = 0$. That is, $s_{fw}(t)$ is symmetric about $t = 0$ and represents what is obtained by band-pass filtering a delta function with a phaseless filter of spectrum $|S(\omega)|$. To make it causal we would construct the minimum phase wavelet with the spectrum $|S(\omega)|$. For $s(t)$ the energy is spread over a longer time window because the group delays (energy arrival times) are frequency-dependent; that is, the energy arrival at frequency ω occurs at a value of t such that

$$\frac{d}{d\omega}\left[\phi_{os}(\omega) - \frac{\omega\Delta}{C(\omega)} + \phi_i(\omega) + \omega t\right] = \phi'_{os}(\omega) - \frac{\Delta}{U(\omega)} + \phi'_i(\omega) + t = 0$$

or (A-14)

$$t = \frac{\Delta}{U(\omega)} - \phi'_{os}(\omega) - \phi'_i(\omega)$$

where

$U(\omega)$ = group velocity with frequency

$\phi'_{os}(\omega)$ = group delay time at the source

$\phi'_i(\omega)$ = group delay time through the instrument

Since this total group delay time (A-14) is frequency dependent, energy at different frequencies arrives at different times on the seismogram. Given that the total energy of s(t) is equal to that of $s_{fw}(t)$ by the same arguments presented earlier, this means that the maximum energy density of s(t) will always be less than that for $s_{fw}(t)$ (the case where the energy for every frequency arrives at the same time). Thus, the signal is compressed in time without loss of energy.

We now show how the noise is affected by the matched filter operation. What we compare is the noise

$$N(t) = \int_{-\infty}^{\infty} |N(\omega)| \exp\left[i(\Psi(\omega) + \phi_i(\omega) + \omega t)\right] d\omega \qquad \text{(A-15)}$$

with the matched filtered noise

$$n_f(t) = \int_{-\infty}^{\infty} N(\omega)\, Y^*(\omega) e^{i\omega t}\, d\omega \qquad \text{(A-16)}$$

or for the whitened reference signal case

$$n_{fw}(t) = \int_{-\infty}^{\infty} |N(\omega)| \exp\left[i\left(-\phi_{oy}(\omega) + \frac{\omega\Delta}{C(\omega)} + \Psi(\omega) + \omega t\right)\right] d\omega$$

The group delay at frequency ω in (A-17) is given by

$$t_d(\omega) = -\Psi'(\omega) - \frac{\Delta}{U(\omega)} + \phi'_{oy}(\omega) \qquad \text{(A-18)}$$

Since $\Psi(\omega)$ is random, its derivatives $\Psi'(\omega)$ are also random. The second two terms on the right side of (A-18) introduce a systematic shift in group delay time with frequency, but because $\Psi(\omega)$ is random, $t_d(\omega)$ is still random and consequently the noise is not compressed. Since the matched filter operating on n(t) in the whitened, reference signal case conserves energy by the earlier arguments) and is a linear filter with a flat amplitude spectrum, the noise

has the same mean (zero) and the same variance (RMS amplitude) as before, so that the mean energy density in $n_{fw}(t)$ is the same as the mean energy density in n(t). See Papoulis, 1965, p. 345-347 for a proof of this point (stationarity is assumed).

Thus we conclude that the matched filter operation increases the signal energy density while not increasing the noise energy density. This means an enhancement in any conventional time domain S/N estimate. As discussed in the text we can take further advantage of this effect in terms of higher $S(\omega)/N(\omega)$ in calculations of spectra. The gain results from having essentially all the signal power but less total noise power at all frequencies contained in a time window short compared to the dispersed signal duration. The procedure is to compute the spectrum of a window of length T centered on the peak of the matched filtered output. Mathematically this amounts to multiplying in the time domain by a unit amplitude box-car function of length T; the corresponding operation in the frequency domain is a convolution with a function of the form $\frac{\sin\pi fT}{\pi fT}$. This results in a smoothed spectrum; the distortion produced due to smoothing depends both on T and the shape of the signal spectrum. Figure 4C illustrates this effect for the signal spectrum used in the test cases of this study. Generally speaking the signal bandwidth controls the acceptable minimum values of T because the approximate form of the matched filtered signal is $\frac{\sin\pi\Delta ft}{\pi\Delta ft}$ as can be seen from setting $S(\omega) = 1$ over a finite frequency band $2\pi\Delta f$ in equation (A-12). Other well known types of time domain windows could be employed which would produce different smoothing operators, but the general effects on the spectra would be similar to the case discussed here.

Since the case where the reference signal spectrum of the matched filter is not whitened is equivalent to prefiltering x(t) with a phaseless filter whose spectrum is $|Y_o(\omega)|$ and then using the whitened

reference signal, all the arguments above with respect to increasing signal energy density relative to the noise energy density hold for this case as well.

As a final note it should be pointed out that all the analysis done in this Appendix assumes infinite limits in both time and frequency, while in practice we must work with finite times and finite frequency bands. However, it can easily be shown that the results of this section apply equally well to the actual situations involving finite intervals, provided the proper care is taken to avoid aliasing and wrap-around in computing the Fourier transforms.

APPENDIX B

STATISTICAL ANALYSIS OF SPECTRAL METHODS

Consider the spectral representation of the operations involved in the array estimates of spectra; namely if $x_i(t) = s_i(t) + n_{1i}(t)$ is of length T_1, and $n_{2i}(t)$ is a noise sample of length T_2 ahead of the signal on the i^{th} channel then, denoting e.g., $|A(\omega)|^2$ by $A^2(\omega)$,

$$\left[\hat{S}^2(\omega)\right]_{I,II} = \frac{1}{K} \sum_{i=1}^{K} \left\{\left[S(\omega) + N_1(\omega)\right]^2 - \frac{T_1}{T_2} N_2^2(\omega)\right\}_i \qquad \text{(B-1)}$$

$$= \text{sum of individual station spectra} \quad \text{(Methods I and II)}$$

$$\left[\hat{S}^2(\omega)\right]_{III} = \left[\frac{1}{K} \sum_{i=1}^{K} (S(\omega) + N_1(\omega)_i\right]^2 - \left[\frac{1}{K} \sum_{i=1}^{K} \left(\frac{T_1}{T_2} N_2(\omega)\right)_i\right]^2 \qquad \text{(B-2)}$$

$$= \text{spectrum from beamed trace (Method III)}$$

We will show that both approaches give valid estimates of the signal spectrum but that the latter (Method III) is preferable because it always has a smaller variance. The presentation below follows the analysis of this problem by R. Shumway (personal communication).

To simplify the statistical analysis let us assume that $T_1 = T_2$ on each channel; that the true noise power spectrum is the same for all channels; that the noise is uncorrelated across channels and on each channel it is random and stationary; and finally that the signal spectrum is identical on all channels. Any of these except the assumption that the noise is random, stationary and uncorrelated can be relaxed without altering the basic results concerning the performance of the two approaches. Under the conditions just stated:

$$x_i(t) = s(t) + n_{1i}(t) \qquad i = 1,K \qquad \text{(B-3)}$$

so

$$X_i(\omega) = S(\omega) + N_{1i}(\omega) \qquad i = 1,K \qquad \text{(B-4)}$$

and

$$n_{2i}(t) \rightarrow N_{2i}(\omega)$$

where $N_{1i}(\omega)$ and $N_{2i}(\omega)$ are the finite Fourier transforms of each of the realizations of the random noise process.

$$E\left\{|N_{1i}(\omega)|^2\right\} = E\left\{|N_{2i}(\omega)|^2\right\} = N^2(\omega) \qquad \text{for all } i \qquad \text{(B-5)}$$

$$|X_i(\omega)|^2 = |S(\omega) + N_{1i}(\omega)|^2 = S^2(\omega) + 2\,\mathrm{Re}\left[S^*(\omega)N_{1i}(\omega)\right] + N_{1i}^2(\omega) \qquad \text{(B-6)}$$

so

$$E\left\{|X(\omega)|^2\right\} = S^2(\omega) + N^2(\omega) \qquad \text{(B-7)}$$

since

$$E\left\{\mathrm{Re}\ (S^*N)\right\} = 0$$

Using (B7) and (B5) we find that if the noise is time stationary

$$E\left\{|X_i|^2 - |N_{2i}|^2\right\} = |S(\omega)|^2 \qquad \text{single station signal power estimate} \qquad \text{(B-8)}$$

and for an array estimate of $S^2(\omega)$ we get

$$\frac{1}{K}\sum_{i=1}^{K}\left\{|X_i|^2 - |N_{2i}|^2\right\} = |\hat{S}(\omega)|^2 \qquad \text{(Methods I and II} \qquad \text{(B-9)}$$

The variance is given by

$$\text{var}\ |\hat{S}(\omega)|^2 = \frac{1}{K^2}\sum_{i=1}^{K}\left[\text{var}|X_i(\omega)|^2 + \text{var}\ |N_{2i}(\omega)|^2\right] \qquad \text{(B-10)}$$

If we assume that $X_i(\omega)$ (complex) is distributed normally then it is represented as

$$X_i(\omega) \sim N(\hat{S}(\omega),\ N^2(\omega))$$

or

$$(\text{Re}\ X_i,\ \text{Im}X_i) = N\left[\begin{matrix}\text{Re}\ S \\ \text{Im}\ S,\end{matrix}\begin{pmatrix} N^2/2 & 0 \\ 0 & N^2/2 \end{pmatrix}\right] \qquad \text{(B-11)}$$

Then $|X_i|^2$ is distributed as chi square with two degrees of freedom and non-centrality parameter δ^2 where $\delta^2(\omega) = 2\,\frac{|S(\omega)|^2}{|N(\omega)|^2}$

$$\frac{|X_i(\omega)|^2}{N^2(\omega)/_2} \sim \chi^2_{2,\ \delta^2(\omega)} \qquad \text{(B-12)}$$

so that

$$\text{var}\ \frac{|X_i(\omega)|^2}{N^2(\omega)/2} = 4 + 4\delta^2(\omega) \qquad \text{(B-13)}$$

or

$$\text{var}\ |X_i(\omega)|^2 = N^4(\omega)\left[1 + \delta^2(\omega)\right] = N^4(\omega)\left[1 + 2S^2(\omega)/N^2(\omega)\right] \qquad \text{(B-13)}$$

likewise

$$\text{var}\ |N_{2i}(\omega)|^2 = N^4(\omega) \qquad \text{(same as above with } \delta=0\text{)}$$

Thus, from these results and (B10)

$$\text{var}\ |\hat{S}(\omega)|^2_{I,II} = \frac{1}{K^2}\sum_{i=1}^{K} 2N^4(\omega)\left[1 + \frac{S^2(\omega)}{N^2(\omega)}\right] \qquad \text{(B-14)}$$

$$= \frac{2}{K}N^4(\omega)\left[1 + \frac{S^2(\omega)}{N^2(\omega)}\right] \qquad \text{(Methods I and II)}$$

Now consider Method III where

$$|\hat{S}(\omega)|^2_{III} = \left|\frac{1}{K}\sum_{i=1}^{K} X_i(\omega)\right|^2 - \left|\frac{1}{K}\sum N_{2i}(\omega)\right|^2 \qquad \text{(B-15)}$$

$$\equiv |\overline{X(\omega)}|^2 - |\overline{N_2(\omega)}|^2 \quad \text{(difference of squares of means)}$$

Then

$$E\left\{|\overline{X(\omega)}|^2\right\} = E\left\{|S(\omega) + \overline{N_1(\omega)}|^2\right\}$$

$$= S^2(\omega) + 2E\left\{\text{Re}\left(S^*(\omega)\overline{N_1(\omega)}\right)\right\} + E\left\{|\overline{N_1(\omega)}|^2\right\} \qquad \text{(B-16)}$$

$$= S^2(\omega) + \frac{|N(\omega)|^2}{K}$$

and

$$E\left\{|\overline{N_2(\omega)}|^2\right\} = \frac{|N(\omega)|^2}{K}$$

so

$$E\left\{|\overline{X(\omega)}|^2 - |\overline{N_2(\omega)}|^2\right\} = |S(\omega)|^2 \qquad \text{(B-17)}$$

To find the variance first note that

$$\overline{X(\omega)} \sim N\left(S(\omega),\ N^2(\omega)/K\right)$$

$$\text{or} \quad (\text{Re } X,\ \text{Im } X) \sim N\left\{\begin{matrix}\text{ReS} \\ \text{ImS},\end{matrix}\begin{pmatrix} N^2/2K & 0 \\ 0 & N^2/2K \end{pmatrix}\right\} \qquad \text{(B-18)}$$

so

$$\frac{|\overline{X(\omega)}|^2}{N^2/2K} \sim \chi^2_{2,\nu^2(\omega)} \qquad \begin{matrix}\text{chi square with 2 degrees} \\ \text{of freedom and noncentrality} \\ \text{parameter } \nu^2(\omega)\end{matrix} \qquad \text{(B-19)}$$

where

$$\nu^2(\omega) = 2K\,\frac{S^2(\omega)}{N^2(\omega)}$$

thus

$$\text{var}\left\{\frac{|\bar{X}(\omega)|^2}{N^2/2K}\right\} = 4 + 4\,\nu^2 \qquad \text{(B-20)}$$

or

$$\text{var}\,|\bar{X}(\omega)|^2 = \frac{N^4(\omega)}{K^2}\,(1 + \nu^2(\omega))$$

$$= \frac{N^4(\omega)}{K^2}\,\left(1 + 2K\,\frac{S^2(\omega)}{N^2(\omega)}\right) \qquad \text{(B-21)}$$

and similarly

$$\text{var}\,|\overline{N_2}(\omega)| = \frac{N^4(\omega)}{K^2}$$

same as above with $\nu^2 = 0$

so

$$\text{var}\left\{|\bar{X}(\omega)|^2 - |\overline{N_2}(\omega)|^2\right\} = \text{var}\,|\bar{X}|^2 + \text{var}\,|\bar{N}_2|^2$$

or

$$\text{var}\left\{|\hat{S}(\omega)|^2\right\} = \frac{2N^4(\omega)}{K^2}\left[1 + K\,\frac{S^2(\omega)}{N^2(\omega)}\right] \qquad \text{(Method III)} \qquad \text{(B-22)}$$

Then we can summarize these results in the following table:

TABLE B-1

METHOD	STATISTIC	MEAN	VARIANCE
I, II	$\frac{1}{K}\sum_{i=1}^{K}\left\{\lvert X_i(\omega)\rvert^2 - \lvert N_{2i}(\omega)\rvert^2\right\}$	$S^2(\omega)$	$\frac{2N^4(\omega)}{K}\left[1 + \frac{S^2(\omega)}{N^2(\omega)}\right]$
III	$\lvert\frac{1}{K}\sum_{i=1}^{K} X_i(\omega)\rvert^2 - \lvert\frac{1}{K}\sum_{j=1}^{K} N_{2i}(\omega)\rvert^2$ or $N_{2i}(\omega)\rvert^2\lvert\overline{X}(\omega)\rvert^2 - \lvert\overline{N_2}(\omega)\rvert^2$	$S^2(\omega)$	$\frac{2N^4(\omega)}{K^2}\left[1 + \frac{KS^2(\omega)}{N^2(\omega)}\right]$

The variances can be compared by computing the efficiency

$$e \equiv \frac{\text{var III}}{\text{var I,II}} = \frac{1}{K}\left[\frac{1+K\,S^2/N^2}{1+\,S^2/N^2}\right] = \frac{S^2/N^2 + \frac{1}{K}}{1 + S^2/N^2} \qquad \text{(B-23)}$$

This quantity is bounded by $0 < e < 1$ which shows that it is always better to use Method III, that is, beam before calculating spectra. We can further note that the performance depends on the signal to noise ratio such that for large signal to noise ratios the methods have almost equivalent variances whereas for small S/N values Method III has a variance approaching $\frac{1}{K}$ smaller and becomes highly preferable to employ. As an example take K = 4, 10, 20, and ∞ and see how the efficiency varies with S/N. This is shown in Figure 18. It is evident in all cases that for S/N values below about 2 Method III gives much better results (i.e. smaller variance).

The result that Method III always gives better (smaller variance) signal power estimates is of great practical importance

because only one pair (signal window, noise window) of spectral computations is needed whereas K pairs of spectra are required in Methods I and II; using Method III clearly results in a very great savings in computing time.

APPENDIX C
COMPUTATIONAL DETAILS

Program COLLAPSE, whose basic structure and computational procedures are shown in Figure 19, was developed for use in the present study. This program was used to process the actual events discussed and the test cases in which synthetic signals generated by Program NEWSYN had been imbedded in noise, and to calculate all the spectral estimates. Options are available for matched filtering by a large reference event which can be adjusted for additional or less dispersion, a synthetic filter generated from dispersion data, and a chirp filter transformed from velocity data. The synthetic signals themselves were used as matched filters for the test cases.

Fourier spectra were estimated for the first 3400 seconds on the test seismograms, convolved with the Fourier spectra estimated from 700 seconds of the synthetic signal for each station, and inverse transformed to produce the matched filtered outputs. The RMS value of an 1800 second noise sample on the test seismograms was computed for each station, and the matched filtered outputs were weighted by 1/RMS and added together to produce the sum trace. The spectrum of a 300 second sample about the peak output of the sum trace was then corrected for noise with the spectrum of an 1800 second noise sample (Method III). At each station power spectra were estimated for a 700 second signal sample on the test seismograms and a 300 second sample about the peak of the matched filtered outputs and were corrected for noise with the power spectra of the 1800 second noise samples on the test seismograms. The program was modified so that the power spectra from the test seismograms (Method I), the power spectra from the matched filtered outputs (Method II), and the power spectra of the synthetic signals were weighted by 1/(noise RMS) and then summed. The 1/2 peak to peak/RMS Signal to Noise Ratios on the matched filtered outputs and the sum trace were computed and are shown on Figures 5B, 5C, 6B, 6C, 7B, 7C, 8B, and 8C.

Analogous procedures were used on the actual events but with appropriate signal windows on the input traces.

PROGRAM DESCRIPTION

SEISMIC DATA LABORATORY
Alexandria, Virginia

DIGITAL COMPUTING SECTION

A. IDENTIFICATION

Title: COLLAPSE

COOP Identification: Z COLLAPSE

Category:

Programmer: D.B. Rabenstine and J.W. Lambert

Date: July 1969

B. PURPOSE

This program processes time series data from magnetic tapes in SDL subset format. The processes (each optional) which can be performed on the data include (1) time shift, (2) demagnify, (3) band pass filter, (4) matched, phase-equalization or chirp filter, (5) weighted summation, and (6) signal-to-noise computation. There is also an option to do a spectral analysis of signals both before and after filtering.

Matched filters may be read from magnetic tape in subset format or constructed from dispersion data from cards. Matched filters read from tape may be modified by data read from cards.

C. USAGE

1. Operational Procedure: This is a Fortran-63 main program which calls the following subroutines: SYSLIMIT, LIBDATE, PI, ERASE, FETCH, SPLØT, FACTER, CØØLER, SMUTHE, PØLYE1 CØØLBACK, BPFILT, PEAKTØPK, ABML, TAPER, and PLAT.

2. Parameters:

Card 1 (Repeated for each set, see ISUM, card 10)

Col.	Format	Name	Description of Usage
1-5	I5	MTYPE	= 1,2,3, or 4, matched filter, read filter from tape.
			= 11,12,13, or 14, read matched filer from tape and modify with dispersion data from cards.
			= 21,22,23, or 24, construct chirp filter.

Col.	Format	Name	Description of Usage
			= -1,-2,-3, or -4 construct synthetic filter (matched or phase equalize) from dispersion data from cards. units digit = 1, "normal" filter types as indicated above, no spectra. units digit = 2, "normal" filter types, compute and plot power spectra (of signal in, noise in, signal out; see IWHITE below). units digit = 3, filter response (type as indicated above) divided by noise power spectrum, no spectra output. units digit = 4, filter response divided by noise power spectrum, compute and plot power spectra, (see IWHITE below)
6-10	I5	IWHITE	= 0 normal filter response; = 1 white filter response
11-15	I5	IPOP	= 1 plot all traces; filters, inputs, outputs, sum. = 0 plot only outputs and sum. = -1 plot only sum
16-20	I5	L	The number of time points in both the filter and input series is extended with zero's to 2^L.
21-25	I5	NA	Number across on Calcomp plots (see IPOP).
26-30	I5	NCODE	Calcomp plot time scale increment in hundredths of an inch per point.
31-40	F10.0	RANGE	Calcomp plot amplitude in hundredths of an inch.
41-50	F10.0	DT	Time series sampling interval in seconds (after decimation, if any).
51-55	I5	INØRM	= -1 summation (if any) unweighted = 0 summation with weights equal to 1.0/noise RMS). = 1 summation with weights equal to (signal peak amplitude)/(noise RMS)^2

Col.	Format	Name	Description of Usage
50-55	I5	IFILT	= 0 no band pass filtering >0 number of points to be specified on bandpass filter response (must be specified from D.C. to folding frequency)
61-65	I5	ISMØØN	All power spectra are smoothed by a running average (boxcar) of 2xISMOON + 1 points.

Card 2 (Repeated for each set)

Col.	Format	Name	Description
1-80	10A8	IDENT	Arbitrary identification for printer and Calcomp outputs.

Card (s) 3 (For each set if IFILT >0)

Col.	Format	Name	Description
1-10,	8F10.0	AMP(I),FREQ	Points (4 per card) on response curve of bandpass filter. Must be specified in order of increasing frequency from D.C. to folding frequency (Hz). Response value at frequencies between those specified ar linearly interpolated.

Card 4 (For each case, if MTYPE = 21-24: chirp filter)

Col.	Format	Name	Description
1-10	F10.0	DI	Distance (epicenter-station) for which filter is to be designed.
11-20	F10.0	DO	Distance for closest station in this set (=DI if single case set).
21-30	F10.0	CH	Highest group velocity of this filter.
31-40	F10.0	TL	Longest period (i.e. period corresponding to CH) of this filter.
41-50	F10.0	CL	Lowest velocity of this filter.
51-60	F10.0	TS	Shortest period (i.e. period corresponding to CL) of this filter.
61-70	F10.0	DT	Sampling interval of filter (should be same as data after decimation).

Card 5 (For each case, if MTYPE = 1-14: matched filter from subset tape)

Col.	Format	Name	Description
1-5	I5	ISEIS	Seismogram number of filter.
6	A1	ISTAR	*if operator is to mount new tape, otherwise blank.
7-10	I4	IC	Channel number (order) of filter seismogram.
11-15	I5	IS	Starting point of filter relative to first point of on tape (before decimation). If IS<0, |IS| zero's are inserted in front of filter.
16-20	I5	IP	Number of points in filter (after decimation).
21-25	I5	NDEC	Decimator; $1 \leq NDEC \leq 5$.
26-30	F5.1	SCALEF	Scale factor (counts/μ) applied to filter. (Set to 1.0 if left blank).

Card 6 (For each case, if MTYPE = -1 to -4: synthetic matched filter; or 11-14: filter from tape to be modified).

Col.	Format	Name	Description
1-5	I5	KC	>0, order of polynomial fit of phase velocity. = 0, use filter from previous case (synthetic M.F. only) <0, new distance, but use polynomial from previous case.
6-10	I5	KI	>0, order of polynomial fit of instrument phase $\leq$0, no instrument phase correction
11-20	F10.0	DELTA	distance 1: for filter modification = path length increment; for synthetic filter = total length of single segment path or first segment length of two part path.
21-30	F10.0	cø	Highest velocity of interest in filter.
31-40	I10	KC2	>0, order of polynomial fit of phase velocity for second segment of two part path.
41-50	F10.0	DELTA2	If KC2>0, = length of second segment of two part path.

Card(s) 7 (If KC>0)

Col.	Format	Name	Description
1-10, 11-20 ...	8F10.0	CC(I),I=1, KC	Polynomial coefficients of first segment phas velocity as a function of frequency (Hz).

Card(s) 8 (If KC2>0)

Col.	Format	Name	Description
1-10, 11-20 ...	8F10.0	CC2(I),I=1, KC2	Polynomial coefficients of second segment pha velocity as a function of frequency (Hz)

Card (s) 9 (If KI>0)

Col.	Format	Name	Description
1-10, 11-20 ...	8F10.0	CI(I),I=1,IT	Polynomial coefficients of instrument phase shift as a function of frequency (Hz).

Card 10 (For each case)

Col.	Format	Name	Description
1-5	I5	ISEIS	Seismogram number of time series to be filtered.
6	A1	ISTAR	* if operator is to mount new tape, otherwise blank.
7-10	I4	IC	Channel number (order) of time series to be filtered.
11-15	I5	IS	Starting point of time series relative to first point on tape (before decimation). If IS<0, |IS| zeros are inserted in front of time series.
16-20	I5	IP	Number of points to be filtered (after decimation)
21-25	I5	NDEC	Decimator; $1 \leq NDEC \leq 5$

Col.	Format	Name	Description
26-30	I5	ISUMT	= 0, do not put sum trace on save tape. >0, put sum trace on save tape. <0, read save tape label from cards (11-13), write label on save tape put sum trace on save tape.
31-35	I5	ISAVT	= 0, do not put this filter output on save tape. <0, put this filter output on save tape <0, read save tape label from cards (11-13), write label on save tape, put this filter output on save tape.
36-40	I5	ISUM	= 0, do not add this filter output into sum. <0, clear sum, then add this filter output. >0, add this filter output to sum. >1, add this filter output to sum, this is the last case in set.
41-45,	2I5	KN1,KN2	Noise window taken from point KN1 to point KN2 (relative to point IS) for computing signal-to-noise ratio and also noise power spectrum.
51-55,	2I5	KS1,KS2	Signal window in filter output taken from point KS1 to point KS2 (relative to point IS) for computing signal-to-noise ratio and signal power spectrum.
61-65,	2I5	KE1,KE2	Signal window in input time series taken from point KE1 to point KE2 for computing input signal power spectrum.
71-75	I5	IHILB	= 0, normal output. >0, Hilbert transform.
76-80	F5.0	SCALEX	Scale factor (counts/μ) applied to time series.

Card 11 (If ISUMT or ISAVT <0, Cards 11-13 are save tape label)

Col.	Format	Name	Description
1-10	I10	K1	Seismogram number
11-20	I10	K2	Number of channels
21-30	I10	K3	Number of points per channel
31-40	F10.2	S4	Sampling rate

Col.	Format	Name	Description
41-50	F10.2	T5	Hour of first point
51-60	F10.2	T6	Minute of first point
61-70	F10.2	T7	Second of first point

Card 12 (If, ISUMT or ISAVT <0)

Col.	Format	Name	Description
1-3, 4-6, ...	25A3	ICH(K),K=1,K2	Channel identifiers

Card 13 (If, ISUMT or ISAVT<0)

Col.	Format	Name	Description
1-72	9A8	ID(K),K=1,9	Event Identification

3. Space Required:

4. Temporary Space: Tape only

5. Alarms: If problems are encountered retrieving a seismogram tape, an alarm message will be printed:

***** NE = XY *****

where

X = logical unit (1 or 2).

Y = 1 if seismogram not on tape.
= 2 channel number requested <1.
= 3 channel number requested > number of channels available.
= 4 decimator >5.

6. Error Returns: See Alarms

7. Error Stops: See Alarms

8. Tape Mountings:

a). Input:
Unit 1: If MTYPE = 1-14, mount subset tape containing matched filter, else BY unit 1.

Unit 2: Mount subset tape containing time series to be filtered.

b). Output:
Unit 3: If ISUMT ≠ 0, or ISAVT ≠ 0, mount blank tape for save tape, else BY unit 3.

Unit 4: If plots are desired, mount plot tape, else BY unit 4.

Unit 5: If units digit of MTYPE is 2 or 4, mount, tape for printer plots, else By unit 5.

d). Equivalences:
/E/7=50/6=51

9. Formats:

a). Input:
Card: See Parameters
Tape: Units 1 and 2 are subset format.

b). Output:
Card: None
Tape: Unit 3 is subset format if user provides label cards (see Parameters).

Unit 4 is Calcomp plot tape from SPLOT.

Tape: Unit 5 is special format for use interval to program.

10. Selective jumps: None

11. Timing: About one minute/case for matched filtering; two minutes/case for spectra.